Heat Transfer Model of Horizontal Air Gaps in Bench Top Testing of Thermal Protective Fabrics

A Thesis Submitted to the College of

Graduate Studies and Research

in Partial Fulfillment of the Requirements

for the Degree of Master of Science in the

Department of Mechanical Engineering at the

University of Saskatchewan

Saskatoon, Saskatchewan

By

Chris Michael John Sawcyn

PERMISSION TO USE

In presenting this thesis in partial fulfillment of the requirements for a Postgraduate degree from the University of Saskatchewan, I agree that the Libraries of this University may make it freely available for inspection. I further agree that permission for copying of this thesis in any manner, in whole or in part, for scholarly purposes may be granted by the professor or professors who supervised my thesis work or, in their absence, by the Head of the Department or the Dean of the College in which my thesis work was done. It is understood that any copying or publication or use of this thesis or parts thereof for financial gain shall not be allowed without my written permission. It is also understood that due recognition shall be given to me and to the University of Saskatchewan in any scholarly use which may be made of any material in my thesis.

Requests for permission to copy or to make other use of material in this thesis in whole or part should be addressed to:

Head of the Department of Mechanical Engineering
57 Campus Drive
University of Saskatchewan
Saskatoon, Saskatchewan
S7N 5A9

ABSTRACT

Standard bench top tests are used to evaluate the performance of thermal protective clothing when exposed to fire. Previously, a model was developed to predict the heat transfer within a protective fabric, air gap and test sensor during an ASTM D 4108 bench top test. The performance of the previous model was excellent when using a standard air gap of 6.4 mm (1/4 in.). However, the previous model did not predict the heat transfer as accurately when using other air gap sizes. Therefore, a new model was developed to model heat transfer in the air gap between heated fabrics and the copper disc test sensor.

A number of experiments including temperature measurements and flow visualization were performed in order to ascertain the boundary conditions for the new model. The information gathered was used to create a more sophisticated treatment of both radiation and convection heat transfer within the bench top testing apparatus.

A computer program was written to implement a quasi-steady state method in the new model. The predicted heat transfer across the finite air gap was used to calculate predicted times to second-degree burns using the Stoll criterion. The results of this new model were compared to those of the previous model and with the results obtained experimentally for air gap widths of up to 19.0 mm (3/4 in.). This comparison demonstrated that the new model more accurately predicts the heat transfer over the entire range of air gaps tested.

"It was a pleasure to burn"

- Fahrenheit 451 – Ray Bradbury

ACKNOWLEDGMENTS

The author would like to take this opportunity to thank the following people and organizations. Through their support, involvement, and financial assistance, this research was made possible.

- Dr. D.A. Torvi for his supervision and dedication to this project.
- Dr. D.J. Bergstrom and Dr. J.D. Bugg for their direction as part of the author's supervisory committee.
- Mr. Dave Deutscher and Mr. Darren Braun for their excellence in the engineering thermo-fluids laboratory and for assisting mechanical engineering graduate students in their experiments.
- Jonathan Heseltine for his photographic expertise and assistance during the flow visualization experiments.
- Todd Threlfall for designing all of the data acquisition programs and for his assistance during many of the experiments in this project.
- The Mechanical Engineering secretaries: Sherri Haberman, April Wettig, and Michelle Howe for their dedication to making everyone's lives easier.
- The College of Graduate Studies and Research, the Department of Mechanical Engineering and President's NSERC Fund at the University of Saskatchewan, and the Natural Sciences and Engineering Research Council of Canada for their funding of this research.
- My grandparents for their unconditional love and support of everything I strive to achieve.
- My parents and sister for their ability to inspire me to achieve higher aspirations and of course for their unconditional love and support.
- My fiancé Valerie, for her never-ending patience and strength during my post-secondary education. Without your love, I would not have known how magnificent life could be.

TABLE OF CONTENTS

LIST OF FIGURES

NOMENCLATURE

Notation

A	area (m^2)
A.W.G.	American Wire Gauge
c_p	specific heat (J/kg·˚C)
dt	time step (s)
F	radiation view factor
G	energy generation due to chemical reaction (J/m^3)
g	gravitational acceleration (9.81 m/s^2)
h	convection heat transfer coefficient (W/m^2·˚C)
i	time step number (dimensionless)
k	thermal conductivity (W/m·˚C)
L	length of enclosure (m)
Nu	Nusselt number (dimensionless)
P	pre-exponential factor (1/s)
Pr	Prandtl number (dimensionless)
q	heat rate (W)
q”	heat flux (W/m^2)
R	ideal gas constant (8.314 J/mole·K)
Ra	Rayleigh number (dimensionless)
T	temperature (˚C, K)
t	time (s)
w	size of air gap spacing, width (m)

Greek Symbols

α	thermal diffusivity (m^2/s)
β	coefficient of thermal expansion (1/K)
ΔE	activation energy (J/mole)
Δt	time step (s)
ε	emissivity (dimensionless)
υ	kinematic viscosity (m^2/s)
ρ	density (kg/m^3)
σ	Stefan Boltzmann constant (5.67×10^{-8} $W/m^2 \cdot K^4$)
Ω	Henriques' burn integral value (dimensionless)

Subscripts

amb	ambient
conv	convection
rad	radiation
losses	losses

CHAPTER 1 INTRODUCTION

Every year people are injured by fire as a result of industrial accidents. For this reason, workers in many industries and the fire service wear thermal protective garments made of specialized fabrics. The performance of these garments must be tested by some standardized means in order to assess their thermal protective value. For this reason, various full scale and bench top tests have been implemented (e.g., [1]).

In these tests, convective and radiative heat sources simulate an industrial accident using a heat flux of approximately 80 kW/m^2. A test sensor is placed behind the fabric to measure the heat flux transferred through the fabric in order to estimate the time required to produce second degree burns in human skin located in the same position as the test sensor. Realistically, the clothing a person wears is not always in direct contact with their skin. This phenomenon is reflected in various tests by either the presence or absence of a finite air gap between the test sensor and the protective fabric. The location of the sensor, either directly in contact with the fabric or with a finite air gap between the sensor and the fabric, will have a large impact on the heat transfer between the fabric and sensor, and hence the predicted skin burn damage.

Previously, Torvi developed a finite element model of the heat transfer in thermal protective fabrics under high heat flux conditions [2]. The purpose of the model was to predict the thermal response of a thermal protective fabric as it is exposed to a high heat flux. The model was also used to estimate the energy transfer between the fabric and the bench top test sensor. As will be shown, the model performed extremely well for smaller air gap values. However, the accuracy of the model decreased as the width of the air gap increased.

This work is intended to produce a new model that will more accurately predict the energy transfer that occurs in the horizontal air gap present in these standard bench top tests. This thesis contains experimental results obtained using a bench top test apparatus as well as numerical results generated by the new model. The two sets of data are compared and the performance characteristics and implications of the new model are discussed.

A description of the bench top testing apparatus is given in this chapter. The insulating properties of the air gap are discussed as well as the need for a refined model. Previous work involving numerical simulations and the investigation of the heat transfer within enclosures is discussed and the uniqueness of this work is established.

1.1 Protective Clothing Tests

When testing a thermal protective fabric under high heat flux conditions, various aspects of the performance of the garment can be evaluated, such as the ability to resist charring, tearing and shrinking during exposures to extreme temperatures. The ability to reduce the transmission of energy to the skin and the corresponding reduction in the extent of an injury can also be tested. In order to test these various aspects of the fabric performance, standardized tests have been developed. In this thesis, the emphasis is on tests used to evaluate the thermal protection that these fabrics provide the end user.

1.1.1 Full Scale Testing

Figure 1.1 Full Scale Mannequin Testing, “Harry Burns” (Reprinted With Permission of Mark Ackerman, University of Alberta)

A comprehensive method of testing protective clothing is to outfit a mannequin with a fire protective garment and expose the mannequin to a laboratory fire estimated to simulate an industrial accident as seen in Figure 1.1 (e.g., ASTM F 1930 [3]). The nominal heat flux of these simulated conditions is approximately 80 kW/m^2. A discussion of whether this heat flux magnitude is appropriate appears in Torvi [2]. By means of various test sensors placed on the mannequin’s skin, the time required to receive second and third-degree burns for human skin in the same location as the sensor can be predicted. The major advantage of these full scale tests is that the behavior of the whole garment during a high heat flux exposure can be investigated.

Since some thermal protective fabrics experience extreme shrinkage during an exposure, areas such as the lower arms and legs may become exposed to the fire. This type of behavior is more easily witnessed during a full scale test. However, there is a large cost, in terms of time and money, associated with conducting this type of test. Consequently, there are limited facilities in existence to conduct full scale thermal protective garment testing. A few examples of full scale testing mannequins are: Thermo-man®, which was developed for the U.S. military by the Acurex Corporation for testing flight suits [4], Pyro-man®, which was developed by North Carolina State University, and Harry Burns, which was developed by the University of Alberta [5].

1.1.2 Bench Top Testing

A more accessible, affordable, and easy method of evaluating thermal protective fabrics is the bench top test. The bench top test allows a small sample of the thermal protective fabric to be tested instead of an entire garment. Also, the need for multiple burners and test sensors is eliminated. One of the first bench top tests was developed by Behnke [6]. This test was used to evaluate fabrics under high heat flux exposures for short durations. Today, similar tests are used that are based on this earlier platform.

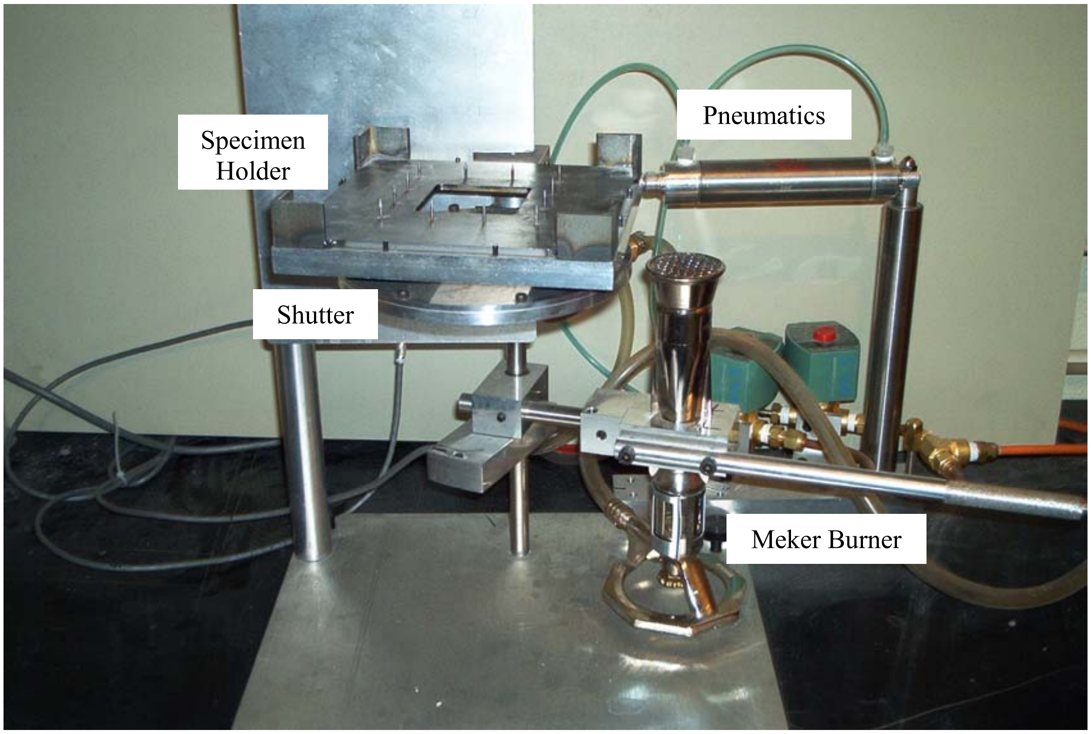

Figure 1.2 Photograph of the Bench Top Testing Apparatus

In Figure 1.2, a photograph of the bench top testing apparatus is shown. A more detailed description and the procedure for using this apparatus is given in Chapter 2. The apparatus consists of a fabric specimen holder, a Meker Burner, a water-cooled pneumatically-actuated computer-controlled shutter, and a copper calorimeter test sensor (not shown). This and similar equipment can be used to comply with various test standards, namely ASTM D 4108 [7], ISO 9151 [1], and CGSB 155.1 [8]. A schematic representation of the fundamental parts of the apparatus appears in Figure 1.3.

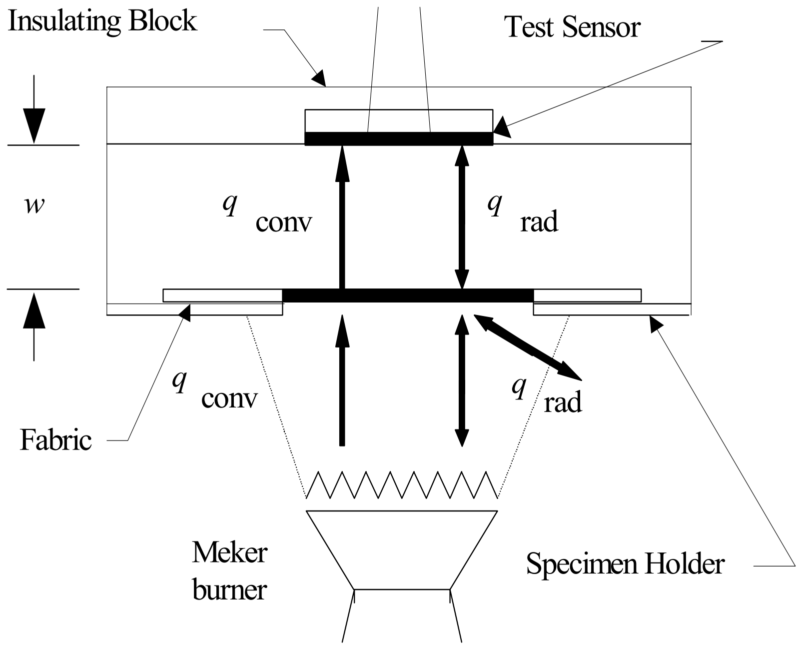

Figure 1.3 Schematic of the Bench Top Apparatus Used for Testing Thermal Protective Fabrics

The schematic shows that a Meker burner supplies the heat flux, which is located 50.8 mm (2 in.) directly below the center of the fabric. The Meker burner utilizes a propane source regulated to 55 kPa (8 psi) and used to simulate an industrial accident or the exposure of a fire fighter to a room engulfed in flames. In the apparatus used in these experiments, the exposure time of the fabric to the heat flux is controlled using a water-cooled shutter. The nominal heat flux provided by the burner is 80 kW/m^2 and is approximately 70% convective and 30% radiative [2].

The thermal protective value of the fabric is determined using a test sensor located on the backside of the fabric. This test sensor measures the amount of energy that is transferred through the fabric and this information can be used to predict the time to a second-degree burn by utilizing the Stoll Criterion (Section 1.4.1). The dimensions of the apparatus are shown in Figure 1.4.

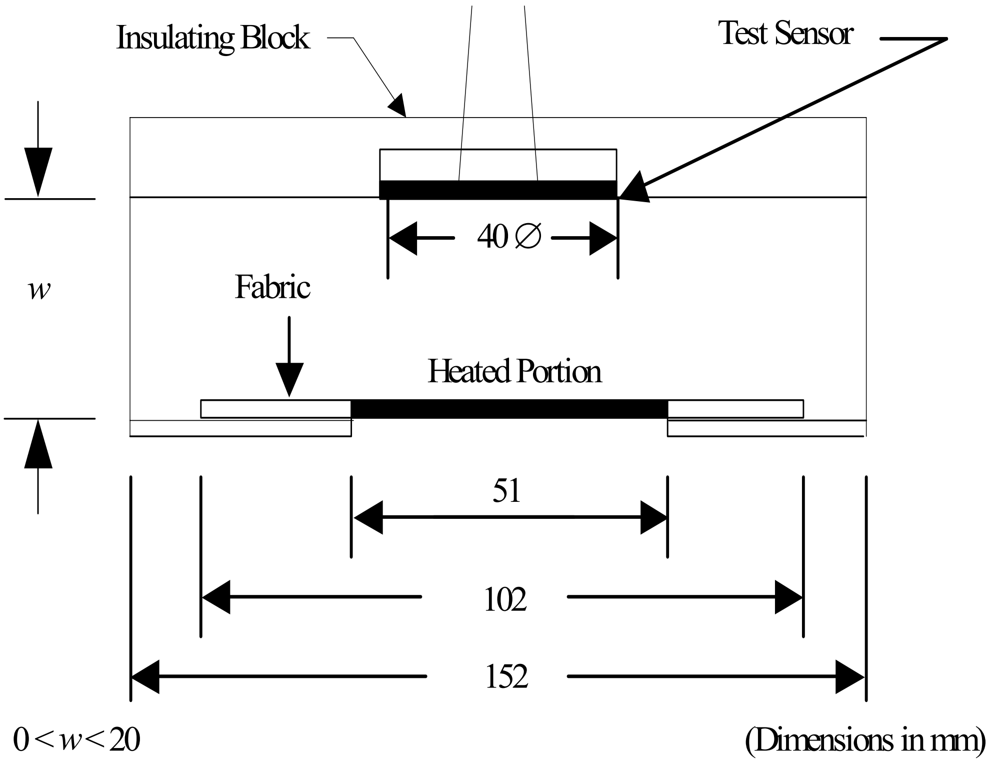

Figure 1.4 Dimensioned Drawing of the Bench Top Testing Apparatus

The specimen holder is 152 mm by 152 mm (6 in. by 6 in.). The test specimen (fabric) is 102 mm by 102 mm (4 in. by 4 in.), while the portion of the test specimen that is heated is 51 mm by 51 mm (2 in. by 2 in.). The copper disc test sensor, or calorimeter, is 40 mm (1.57 in.) in diameter and is mounted in a Kaowool^{TM} insulating block. The size of the air gap is controlled using a number of metal spacers, of different heights, that are placed between the specimen holder and the Kaowool^{TM} block.

1.2 Enclosure of Air

In real life situations, clothing may be in direct contact with skin (e.g., around the shoulders), and in other areas the clothing may hang loosely (e.g., the lower back in some situations). This phenomenon also appears in the differences between various test standards, and thus depending on the test standard, the test sensor is placed either in direct contact with the fabric or there is an air gap of 6.4 mm (1/4 in.) between the fabric and the sensor.

As seen in Figure 1.3, if an air gap is present, there is an enclosure of air created. It is well known that as long as the layer of air remains stagnant, the heat transfer across the enclosure will be limited to conduction and radiation. Thus, the insulating value of the air gap will increase as the width of the air gap increases. However, if either the temperature difference across the enclosure or the width of the air gap becomes sufficiently large, then natural convection cells will develop which will increase the heat transfer rate across the enclosure.

There have been many investigations that have attempted to postulate a 'critical' air gap for protective clothing systems (e.g., [9]), which will provide the maximum insulation before convection begins to occur. A summary of research aimed at determining this critical air gap width can be found in Torvi [2]. Unfortunately the critical values reported are for very specific enclosure orientations and heat flux magnitudes or in other cases, the specifics are not even provided.

The ideal enclosure used in the classic Rayleigh problem appears in Figure 1.5. The Rayleigh problem investigated the driving mechanisms for the transition from conduction to convection heat transfer. The size of the plates are considered to be much larger than the width of the air gap ($L >> w$). Also, the temperatures of the top and bottom plates, T_1 and T_2 ($T_2 > T_1$) respectively, are isothermal in time and space.

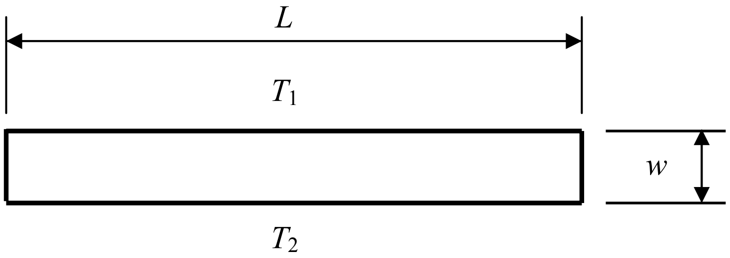

Figure 1.5 Two Dimensional Schematic of the Ideal Rayleigh Enclosure

The Rayleigh number is used to determine the ratio of the buoyant forces to the viscous forces present in an air gap and is defined by

$$Ra = \frac{g\beta(T_2 - T_1)w^3}{\alpha v} \tag{1.1}$$

where g = acceleration due to gravity (9.81 m/s^2)

β = volumetric expansion coefficient of the fluid (1/K)

α = thermal diffusivity of the fluid (m^2/s)

v = kinematic viscosity of the fluid (m^2/s)

w = width of air gap (m).

The accepted critical Rayleigh number for a horizontal enclosure for which natural convection will occur is 1708 [10]. For Rayleigh numbers smaller than 1708, the fluid motion will remain stagnant and thus conduction heat transfer will occur.

1.3 Previous Heat Transfer Model

Previously a model was developed by Torvi to simulate the heat transfer within the entire bench top testing apparatus [2]. The previous model was one-dimensional and used a number of finite elements to model the fabric, the air gap, and the test sensor. The work that went into the development of the model studied in great detail aspects such as the boundary conditions on the front (exposed) side of the fabric, the flame temperature distribution and emissivity of the Meker Burners' flame, and the thermo-chemical reactions that take place within various fabrics.

This model is able to predict the time to second-degree burn, using the Stoll criterion, quite well for the standard air gap of 6.4 mm (1/4 in.) during a bench top test. However, this model also attempted to predict the time to second-degree burns for other air gap sizes, ranging from 1 mm to 20 mm, but these predictions were not as accurate. For example, Figure 1.6 compares the predicted and measured times to exceed the Stoll criterion for tests of Nomex® IIIA fabric specimens for various air gap widths. Comparisons were also made for Kevlar®/PBI fabric and steel shim.

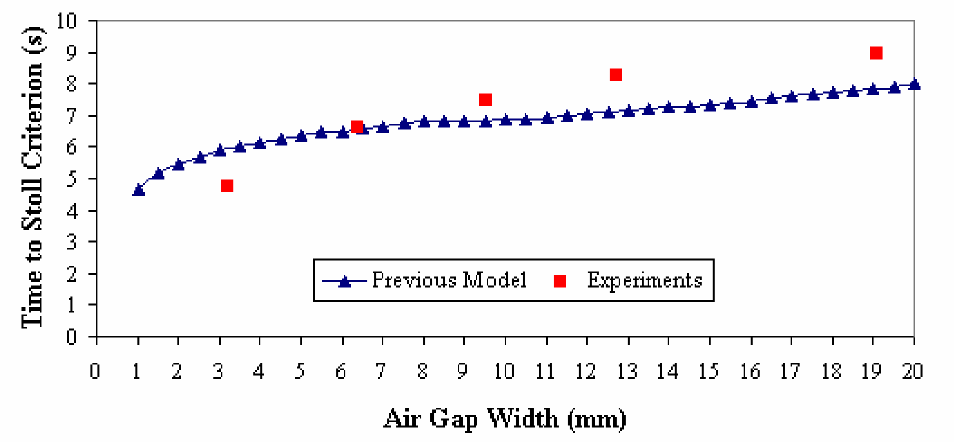

Figure 1.6 Comparison of Previous Model and Experiments for the Predicted Time to Second-Degree Burn (Nomex® IIIA) (Torvi [2])

It is important to note the fact that the previous model is one-dimensional in its treatment of the heat transfer between elements. This means that the entire front face of the fabric, and back face, are assumed to be at uniform temperatures at any given time step. The validity of this one-dimensional treatment will be investigated in this work both experimentally and numerically.

Predicted temperatures on the backside (non-exposed side) of the fabric were very close to those encountered experimentally. The following two figures show this comparison.

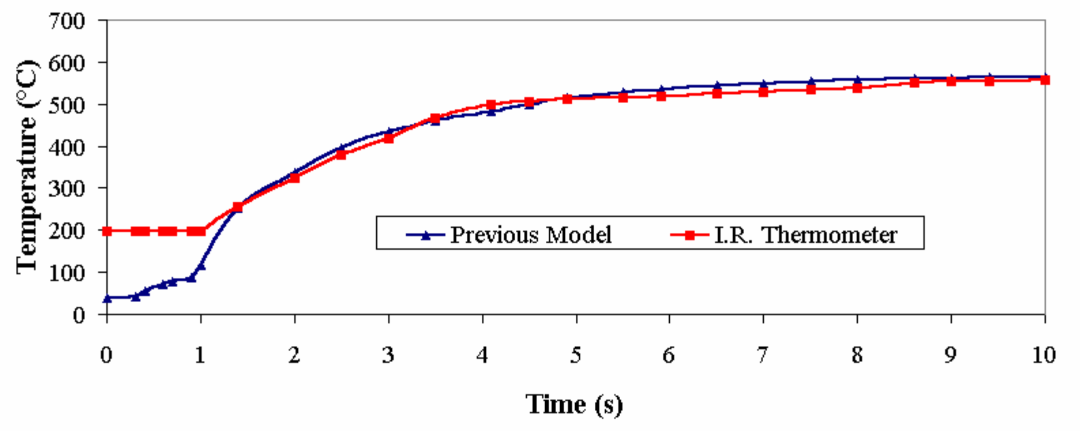

Figure 1.7 Temperatures on Backside of Fabric (Nomex® IIIA) (Torvi [2])

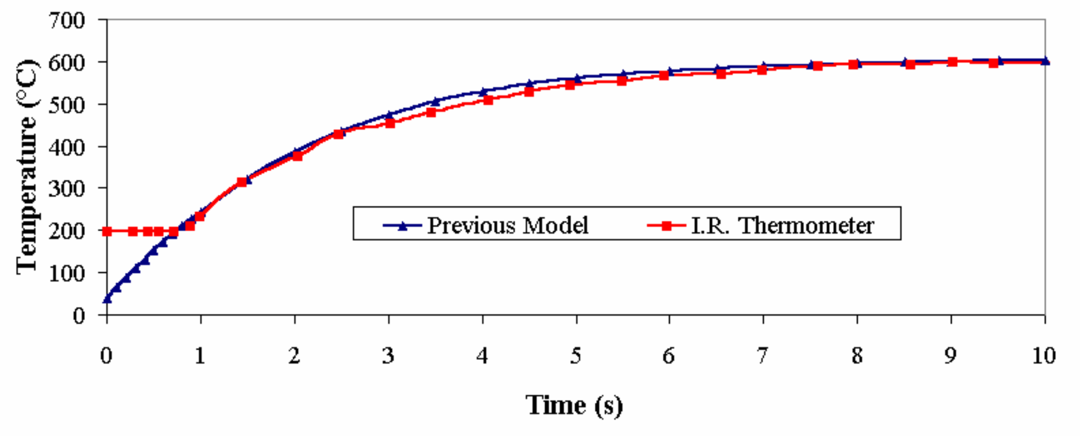

Figure 1.8 Temperatures on Backside of Painted Steel Shim (Torvi [2])

In both Figures 1.7 and 1.8, the infrared (I.R.) thermometer used was incapable of measuring below 200°C, which explains the initial plateau in both experimental temperature curves. Although not shown here, thermocouples were also used to measure the fabric and shim stock temperatures. The steel shim stock was investigated in order to establish the behavior of a non-porous boundary and also because of the relative ease of obtaining experimental data when compared to the fabrics, especially when using thermocouples to measure temperature. The shim stock allows thermocouples to be spot welded to its surface, whereas on the fabric specimens, the thermocouples have to be sewn in place. The steel shim stock thickness was chosen such that the heat capacity of the shim was similar to that of the fabrics.

In these two figures, when the temperatures exceed 200°C, approximately 1.5 seconds into the exposure, the difference between the absolute predicted temperatures and those obtained experimentally are less than 2.4% in both the Nomex® IIIA and steel shim cases. This indicates that the model was accurately capturing the heat transfer details across the fabric and steel shim stock. For this reason, it was thought that the 'weak-link' in the model, when predicting test results for larger air gap sizes, was the treatment of the heat transfer from the back of the fabrics to the copper calorimeter or in other words, across the air gap. Herein lies the motivation for this research project; improving the model of heat transfer within a horizontal air gap during bench top testing of thermal protective fabrics.

1.4 Related Work

Heat transfer in enclosures has been studied extensively. The convection cell patterns and air movement within these enclosures have also been widely investigated. Moreover, the heating of human skin as well as the pain threshold and the resulting injury has been investigated. The following sections briefly indicate some of the work that has been performed and how this work is pertinent to this study. This section is not intended to be a comprehensive literature review. This section is used to illustrate the uniqueness of the bench top enclosure and the conditions encountered during a standard bench top test. The following papers include a more comprehensive review of the earlier literature in the study of heat transfer within enclosures [11,12].

1.4.1 Second-Degree Burn Predictions

Various methods are used to convert the data from full scale and bench top tests into a second-degree burn time. The two most commonly used are the Stoll Second-Degree Burn Criterion and Henriques' Burn Integral.

The Stoll Criterion [13] is based on the total amount of energy that must be absorbed by the skin in order to produce a second-degree burn. This method is advantageous due to its simplicity. A copper calorimeter can be used as a test sensor by comparing the energy absorbed by the sensor to the Stoll criterion in order to determine burn times. There are disadvantages to the implementation of this method. The data set obtained by Stoll and Chianta [13] were experimentally determined using a constant magnitude of heat flux. They stipulate that this criterion is not necessarily valid for time varying heat fluxes, such as measured behind fabrics during bench top tests [2]. However, this criterion is widely used in test standards. The Stoll criterion temperature is calculated using

$$T_{\text{Stoll}} = 8.871465\left(t^{0.2905449}\right) + T_{\text{o}} \tag{1.2}$$

where T_{Stoll} = Stoll criterion temperature (˚C)

t = time into exposure (s)

T_{o} = original temperature of skin or test sensor (˚C)

The point where the temperature of the test sensor exceeds T_{Stoll} is the time at which a second-degree burn is predicted to occur. Basically, this method is a comparison of temperature rise versus time, or the amount of energy absorbed by the skin, to what was experimentally found to cause a certain degree of damage.

Henriques' burn integral on the other hand [14,15], is valid for any heat flux pattern. Henriques and Moritz found that skin damage could be estimated using a chemical rate process, and a first order Arrhenius rate equation could be used to determine the rate of tissue damage.

The equation

$$\Omega = \int_0^t P \exp\left(-\frac{\Delta E}{RT(t)}\right) dt, \tag{1.3}$$

where $P =$ pre-exponential factor (3.1 x 10^{98} 1/s)

$\Delta E / R =$ ratio of activation energy to the ideal gas constant (75 000 K)

$T =$ temperature of the basal layer of skin (K),

is integrated over the time that the temperature of the basal layer of the skin is greater than or equal to 44°C during heating. The basal layer is the bottom of the epidermis, the outer layer of skin, which lies on top of the dermis [16]. The value of Ω required to produce a second-degree burn is 1.0 and a value of 0.53 is required for a first-degree burn. Calculating this integral requires more sophisticated equipment such as a computer with specialized software. This increased complexity was not required in this project since the Stoll Criterion is an easier method by comparison and is also widely used in standard tests. For this reason, the Stoll Criterion will continue to be used as a method for comparing the performance of the heat transfer models to experiments.

1.4.2 Size of Air Gaps in Protective Clothing Systems

Kim, et al. investigated the size of air gaps entrapped in protective clothing systems [17]. There are no heat transfer or burn injury aspects of this work, as this investigation was primarily interested in the identification and quantification of the air gaps that are present over the entire body for a worker wearing various protective garment ensembles. Achieving these results was made possible by the use of a three-dimensional whole body digitizer. The digitizer was used to scan the entire surface of an unclothed mannequin to produce a three-dimensional contour. The mannequin was then outfitted with various single layer and multi-layer thermal protective garments and the scanning process was repeated. The two contours were compared and a differencing scheme was used to map the air gaps that were present over the entire surface of the mannequin's body. These findings were compared with the burn patterns of real life burn victims. The areas found to have the smallest or no air gaps present were the same areas to receive the burns of the highest severity in the accident victims.

The quantification of the air gaps present on a full scale mannequin is useful information to this and other groups that perform bench top testing. The air gap range investigated in this authors' research is 1 mm to 20 mm, which according to this three-dimensional digitization study, accounts for 60% – 70% of the air gaps present in real life situations depending on which type of garment ensemble is worn.

1.4.3 Partially Heated Enclosures

There have been a large number of experimental and numerical studies of heat transfer in partially heated enclosures, such as in the bench top test of interest. A few examples of these studies are given in this section.

J.G. Maveety and J.R. Leith investigated heat transfer in Rayleigh-Bernard Convection with air in moderate sized containers (<1 m sides) [18]. The apparatus used for these experiments consisted of an aluminum horizontal enclosure, heat flux gauges, and thermocouples. The top and bottom plates were kept isothermal via water channels. The temperature of the bottom plate was larger than the temperature of the top plate providing a heated bottom boundary. The temperature difference was measured using two 36-gauge copper-constantan thermocouples attached to each aluminum plate. The temperature difference was also measured using a differential thermocouple mounted in the horizontal center of the enclosure with thermocouple junctions attached to each plate. Also, the mean temperature of the air layer was kept close to the surrounding room temperature to prevent significant heat transfer occurring through the sidewalls.

As expected, the heat transfer rate across the air gap increased as the temperature difference increased. The maximum temperature difference encountered across the air layer during these tests was 20ºC and the plates were isothermal in time and space. However, these conditions are very different from those encountered during the bench top testing of thermal protective fabrics.

A.F. Emery and J.W. Lee numerically investigated the effects of property variations on natural convection in a square enclosure [19]. In this investigation, temperature and velocity fields were resolved and heat transfer rates calculated. Hot and cold vertical walls were used along with adiabatic top and bottom walls. Thus, this particular situation involves a vertical enclosure of air instead of a horizontal enclosure. However, it is important to note that the wall temperatures in this investigation were isothermal and steady during the simulations. Also, the temperatures involved in this study were much lower than those encountered during a standard bench top test.

P.H. Oosthuizen has performed several numerical simulations (e.g., [20]) of convection heat transfer within enclosures of various shapes, particularly a cube with horizontal top and bottom faces. In these simulations one wall will have either a section of elevated temperature or a heat flux element. The other walls will either be adiabatic or at a constant temperature which is lower than the 'heated' wall. The location of the heated wall and various combinations of the other wall boundary conditions can be altered.

One example of this work is an investigation of the effects of the size of a heated wall section on the critical Rayleigh number as well as the flow pattern that develop in the enclosure [20]. The Nusselt number was investigated over a range of Rayleigh numbers from 1000 – 400,000.

K.G.T. Hollands, G.D. Raithby, and L. Konicek, have performed numerical and experimental studies of convection heat transfer in horizontal layers of air and water (e.g., [21]). The focus of their research was to produce correlation equations for the Nusselt number as a function of Rayleigh number. These equations were found to be very accurate for conditions similar to these experiments. Once again, it is important to note that the temperature difference between top and bottom plates encountered during these tests were of the order of 10ºC.

R.J. Goldstein and R.J. Volino performed experiments on the development of natural convection above a suddenly heated horizontal surface [11]. This work was of interest to the author because it was one of the few investigations that did not treat the boundaries isothermally. The thermal properties were treated as constants but this assumption was valid due to the small changes in temperature. The temperature difference across the horizontal fluid layer never exceeded 5ºC in their experiments, which used a heat flux of 2.1 kW/m^2. An interferogram as well as a liquid crystal sheet were independently used to produce pictures of the flow patterns and isothermal lines present within the fluid. Both were used to deduce the presence of repeatable structures given the Rayleigh number and geometry of the enclosure.

The above numerical and experimental research investigated the heat transfer within various enclosures. Unfortunately, the specific situations involved temperatures and temperature differences that are extremely small compared to those encountered in the bench top testing of thermal protective fabrics. For this reason, many of the models were able to make such simplifications as ignoring the changes in material properties due to temperature variations or ignoring the radiation heat transfer altogether.

The numerical models, while extremely useful within their own range of applicability, would not be able to properly simulate the heat transfer within the enclosure of this study since the radiation heat transfer is the dominant mode of energy exchange in the bench top apparatus. Since many of these numerical models mentioned only calculating the flow fields or convection heat transfer rates, they cannot solely be employed in this situation. The relative magnitudes of the radiation and convection heat transfer as calculated by the previous model are shown in Figure 1.9 to illustrate this point.

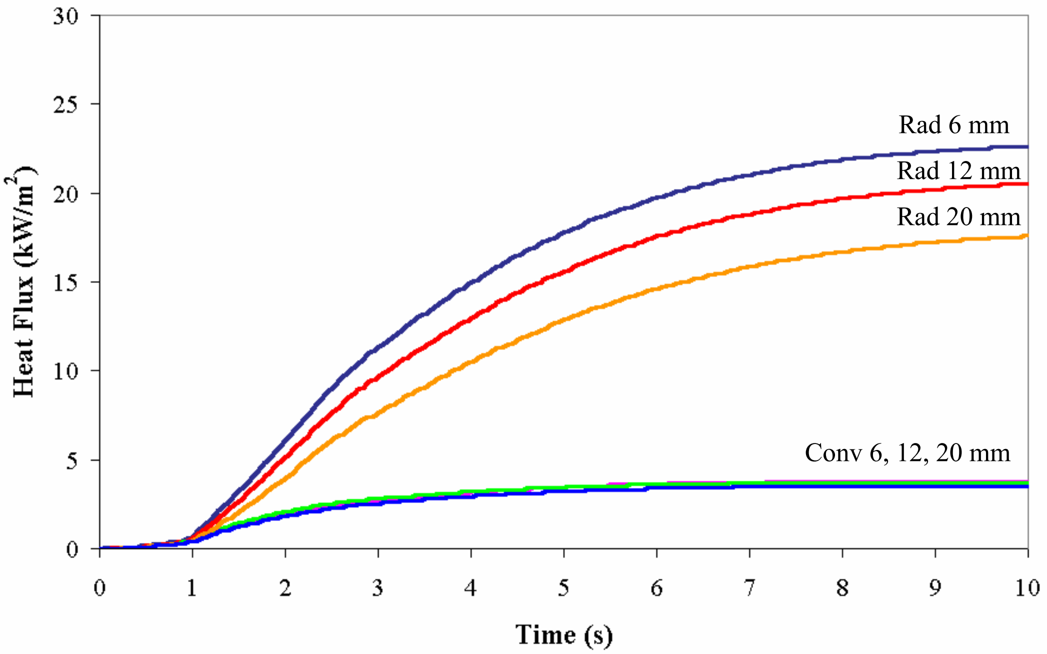

Figure 1.9 Relative Magnitude of Radiation and Convection to the Test Sensor as Predicted by the Previous Model [2] for Various Air Gap Widths

There are highly sophisticated commercial software packages available that can resolve both the radiation and convection heat transfer rates simultaneously, such as SMARTFIRE [22] and NIST's Fire Dynamic Simulator (FDS) [23]. These models however are generally considered to be for industrial applications, where a typical accuracy of within 10% is more than adequate for the users' needs. The purpose of this research was to improve the accuracy of an already accurate working model and thus the implementation of a commercial software package seemed counter-productive. Furthermore, the thermal boundary conditions that can be implemented in these packages are unsuitable for the bench top apparatus since they are limited to boundaries that are isothermal or have a prescribed constant heat flux.

1.5 Unique Aspects of the Bench Top Test Enclosure

There are many other numerical and experimental studies on the convective heat transfer within an enclosure, but none have investigated conditions that are encountered during a standard bench top test. The following subsections describe the uniqueness of the bench top test.

1.5.1 High Heat Fluxes, Temperature Differences, and Rayleigh Numbers

The 80 kW/m^2 heat flux used for these tests can increase the fabric temperatures to hundreds of degrees Celsius in a few seconds, providing a temperature difference as large as 600ºC as seen in Figure 1.7. These temperatures are much larger than those currently encountered in most experimental and numerical studies. The temperature of the apparatus also becomes significantly hotter than the surrounding laboratory conditions. Due to the large temperature differences, radiation heat transfer becomes a very significant mode of energy transport. Since most other investigations have not dealt with elevated temperatures, the magnitude of the radiation heat transfer is usually much lower than the magnitude of the conduction and convection heat transfer.

Another significance of the large temperature difference across the air layer in bench top tests is the presence of high Rayleigh numbers (see Equation 1.1). There are other investigations that consider much higher Rayleigh numbers, but this is due primarily to much larger enclosures, on the scale of meters. The Rayleigh numbers in these cases are large since the Rayleigh number is a function of the enclosure size cubed. This research considers air gaps ranging up to only 20 mm, but still encounters fairly high Rayleigh numbers. The effect of having large Rayleigh numbers in a relatively small enclosure, as is the case in the bench top apparatus, requires more investigation.

1.5.2 Non-Uniform Boundary Conditions

Another unique aspect of this particular problem is the fact that the use of a high heat flux generates boundary conditions on the bottom plate that are extremely non-uniform as will be seen in Chapter 3. During a typical exposure to 80 kW/m^2 for 10 seconds, the center of the bottom plate, which also coincides with the centerline of the Meker burners' flame, can rise to a temperature of approximately 650ºC. The outer regions of the bottom plate however, can remain as low as 50ºC. These substantial temperature differences across a square plate of only 150 mm, results in very significant temperature gradients in the boundary of any model to be constructed.

Furthermore, it was decided that due to these large temperature variations in the bottom boundary, that a more sophisticated radiation network would have to be developed as part of the new model in order to accurately account for the energy transfer from the fabric to the test sensor.

1.5.3 Highly Transient Behavior

Yet another unique aspect of this problem is that the bench top test provides for an extremely transient situation. As previously mentioned, the temperature of the bottom boundary can reach hundreds of degrees Celsius in only a few seconds. Modeling this situation is very different from current numerical investigations that are being performed for this type of enclosure. The reason of course is that many of the numerical models involving smaller horizontal enclosures, involve steady state boundary conditions. Therefore, any model capturing the physics of a bench top test would have to be carefully constructed with a sufficiently small temporal resolution.

1.6 Purpose of this Research

A model of the heat transfer in the air space between the fabric and test sensor was previously developed as part of a larger more comprehensive model of the overall fabric-air space-test sensor system [2]. In this previous model, heat transfer is assumed to be one-dimensional across the air space, radiation and convection are assumed to be uncoupled, and an effective thermal conductivity is used to represent the air gap. As mentioned in Section 1.3, the previous model predicted times to second-degree burns very accurately for the standard air gap of 6.4 mm (1/4 in.). However, the model did not predict the second-degree burn times as accurately for the other air gap sizes. This is thought to be mainly due to the simplicity of the representation of both convection and radiation heat transfer in these larger air spaces. Other possible reasons have been postulated such as moisture vapor transfer to the test sensor, the influence of combustion products on heat transfer within the enclosure, and a dynamic behavior of the air gap size during tests. However, the research in this thesis focuses on only one of these aspects: the treatment of radiation and convection heat transfer within the air gap and the corresponding influence on predicted results.

Therefore, the model developed in this research was intended to produce more accurate predictions for the heat transfer in the larger air spaces while maintaining accuracy in predicting the heat transfer in smaller air spaces. One significant change to the model was the development of a more sophisticated radiation network that would treat the heat transfer two-dimensionally in order to properly capture the energy transport phenomena. Another significant difference of the new model was the more localized treatment of the convection heat transfer, which was made possible through careful observations of the flow visualization images. The details of these changes will become clear in Chapter 4. In order to validate the new model, it was decided to compare the numerical and experimental results for the painted steel shim stock samples and for a thermal protective fabric, Kevlar®/PBI.

1.7 Outline of this Thesis

In this chapter, the apparatus used in the bench top testing of thermal protective fabrics was introduced and many of the details were discussed. In addition to this, the supplementary apparatus used while investigating the boundary conditions of this test is detailed in Chapter 2. Experimental data collected will be presented and the corresponding impact on the development of the new model will be discussed in Chapter 3. The various working details of the numerical model will be presented in Chapter 4 and the numerical results generated by the model will be compared to those obtained experimentally in Chapter 5. Finally, in Chapter 6, some conclusions will be presented based on observations made of the model as well as some recommendations for future work.

1.8 Chapter Summary

In this chapter, the bench top test for the performance evaluation of thermal protective fabrics was presented. Also, a previous heat transfer model used to predict the heat transfer within the entire bench top apparatus was discussed. The performance of this model was shown to be excellent when using a standard air gap of 6.4 mm (1/4 in.). However, as was also demonstrated in this chapter, the previous model was not as accurate at other air gap sizes. Therefore, the need for a new model was introduced as well as improvements that can be made over the previous model.

CHAPTER 2 APPARATUS AND PROCEDURE

In this chapter, the bench top apparatus for the evaluation of thermal protective fabrics is described. The procedure for using this apparatus and the method used to test thermal protective fabrics is presented. Also, the additional equipment used to take temperature measurements and to perform flow visualization are introduced and discussed. The results of all of the experiments performed using the apparatus described in this chapter are presented in Chapter 3.

2.1 Bench Top Testing Apparatus

In Chapter 1, the overall bench top testing apparatus was presented. However, in this section, further details of the individual portions of the apparatus will be provided.

2.1.1 Specimen Holder

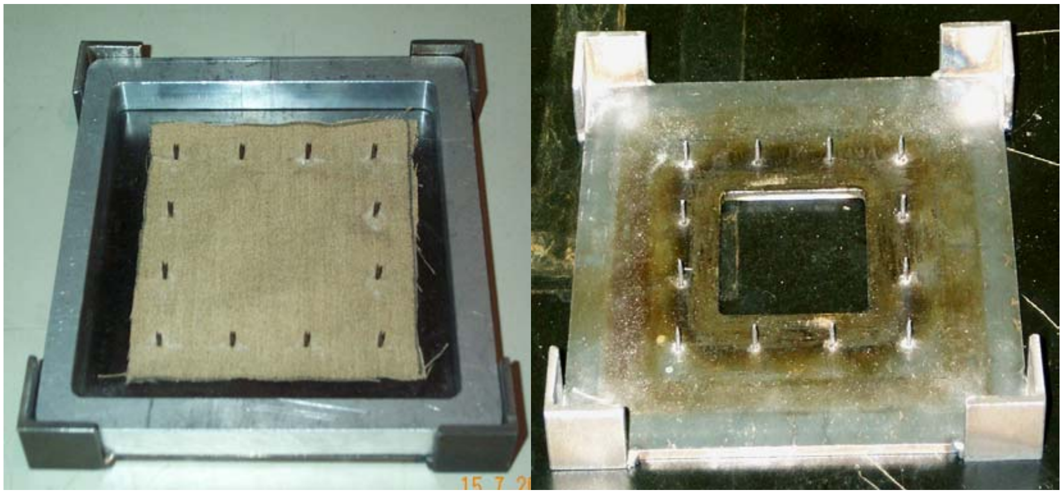

Figure 2.1 Specimen Holder with/without Fabric Sample and Aluminum Spacer

The specimen holder, as shown in Figure 2.1, is a 9.5 mm (3/8 in.) thick steel plate with a 51 mm (2 in.) square hole in the middle. This hole is the area through which the fabric specimens are exposed to the flame of the Meker burner. The specimen holder is mounted such that it is 51 mm (2 in.) above the Meker burner. Pins are used to hold the fabric specimens in place during the exposure to the flame in accordance with CGSB 155.1 [8]. The pins act to partially test the fabric's structural integrity along with its thermal protective properties. A number of different aluminum spacers can be placed onto the perimeter of the specimen holder. The test sensor and an insulating Kaowool^{TM} board are placed on top of these spacers (see Figure 2.1) and this is the means by which the air gap is created and altered. The specimen holder is heated during each test to approximately 80ºC and must be cooled off to room temperature before each test.

2.1.2 Fabric Specimens and Steel Shim Stock

All test samples were cut into 102 mm (4 in.) squares. The fabric specimens tested in this research are Kevlar®/PBI and were cut from the same fabric sample as the specimens tested by Torvi [2]. The fabric sample has a nominal mass per unit area of 200 g/m^2 (6 oz/yd^2), a thickness of 620 μm, and the weave pattern of the fabric is 2/1 twills, which is typical of the materials used in protective coveralls. The fabrics were conditioned by placing them for 24 hours prior to any testing in a chamber controlled to 20˚C ± 2˚C and 65% ± 5% relative humidity. The use and testing of Kevlar®/PBI in this research is not an endorsement of this product. Kevlar®/PBI was chosen because it was readily available and a direct comparison could be made to the previous research.

Obtaining surface temperatures of a fabric sample using thermocouples can be difficult. The thermocouples, if held to the surface of the fabric, can unintentionally measure the temperature of a finite depth into the fabric. This is possible since the fabric surface is porous and penetration may occur. Also, the fabric surface is not considered flat since the size of the thermocouple wires used were on the same order of magnitude as the yarns present in the fabric samples. For this reason, steel shim stock was also tested.

In the preliminary tests, the fabric specimen was replaced by a 76 μm (.003 in.) thick piece of steel shim stock. Shim stock was used so that a simpler case, a solid bottom boundary, could be studied before moving to the case of a fabric, which is a porous bottom boundary. Also the use of shim stock made it much easier to obtain temperature measurement data since thermocouples could be spot welded to its surface. The particular thickness of the shim stock was chosen so that the specimens would have approximately the same volumetric heat capacity as protective fabrics commonly used. The shim stock samples were lightly painted with TREMCLAD® black high heat enamel (TREMCO LTD., Toronto, ON), in order to more closely approximate the emissivity of the fabrics. This will be discussed in the next chapter. As will be mentioned in Section 2.2.2, this paint also becomes very important to the flow visualization experiments since when heated, it introduces a smoke to the enclosure.

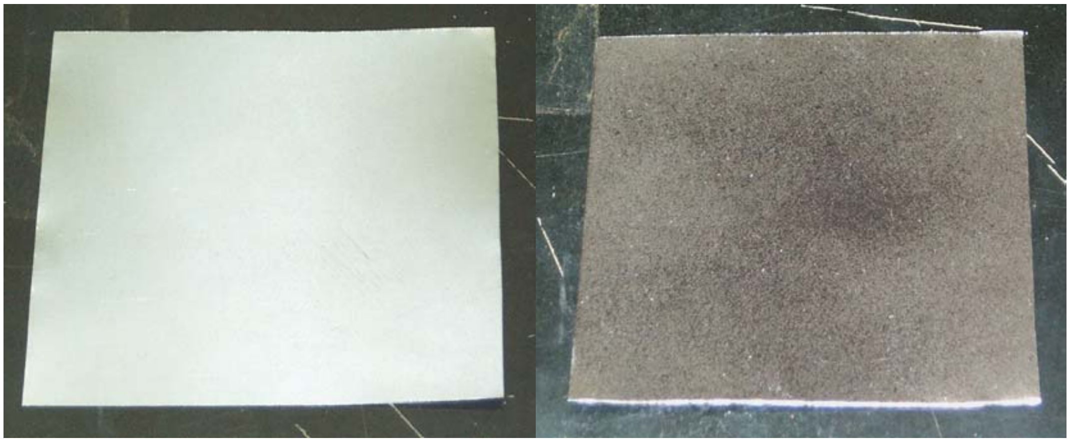

Figure 2.2 Steel Shim Stock (As Received and Lightly Painted)

2.1.3 Test Sensor

Figure 2.3 Copper Calorimeter in Kaowool^{TM} Insulating Board and Alone

The test sensor used to measure the heat flux through the fabric is shown in Figure 2.3. A copper calorimeter is used in accordance with the ISO 9151 test standard [1]. This standard specifies that the mass of the copper disc be 18.0 g ± 0.05 g and that one copper-constantan (Type "T") thermocouple be soft soldered to the back surface of the disc. Silver solder was necessary due to the high temperatures reached (e.g., 200˚C) when the heat flux from the Meker Burner is calibrated by directly exposing the sensor to the flame.

The data obtained from the test sensor is useful in two ways. One use is to predict second-degree burn times for human skin that would be in the same location as the sensor. This was achieved by comparing the temperature history of the copper disc to the Stoll Criterion (Section 1.4.1). The other use for the copper disc is to calibrate the heat flux produced by the Meker burner. The information from the copper disc test sensor and the various other thermocouples used in the following experiments were processed using an Agilent 34097A (AGILENT TECHNOLOGIES INC., Loveland, Colorado) data acquisition system and a desktop PC. Using this system, temperatures measurements were obtained with a resolution of approximately 0.125 s – 0.333 s, depending on the number of thermocouples used during a given test.

2.2 Experiments Performed

In order to properly model heat transfer in enclosures during bench top tests of thermal protective fabrics, the boundary conditions were determined using two major sets of experiments. Temperature measurements were made of the whole bottom boundary of the enclosure during a 10 s exposure to the burner. Also, flow visualization experiments were performed to investigate the convection heat transfer and the movement, if any, and resulting flow pattern of the entrapped air. Both of these experiments are described in the following sections.

2.2.1 Temperature Measurements

The temperature variations on the bottom boundary of the bench top enclosure were investigated. This was done in order to determine the validity of the assumption that the heat transfer was one-dimensional within the air space, and to provide information that would be useful in developing an improved model of the heat transfer in the air space.

A Minolta® Cyclops 300bAF infrared thermometer (THERMO-KINETICS COMPANY LTD., Mississauga, ON) was used to measure the temperature at various positions on the unexposed surface of shim stock, and the specimen holder during a 10 s exposure to the Meker burner. This infrared thermometer was different from the one used in Torvi [2], since it was capable of measuring below 200˚C and thus covered the whole range of temperatures encountered. The interrogation area of this I.R. thermometer is dependent on the distance from the surface investigated. However, the interrogation area used in these experiments was measured to be approximately 1 mm by 3 mm, or the same order of magnitude as a thermocouple junction.

Also, 36-gauge chromel-alumel (Type "K") thermocouples were used to supplement and verify the results of the infrared thermometer. The location of the measurement points and the infrared thermometer for the first set of tests is shown in Figure 2.4. The points were chosen within one quadrant, assuming that the temperature distribution would be symmetric. This assumption will be investigated in a second set of tests, the results of which are presented in Chapter 3.

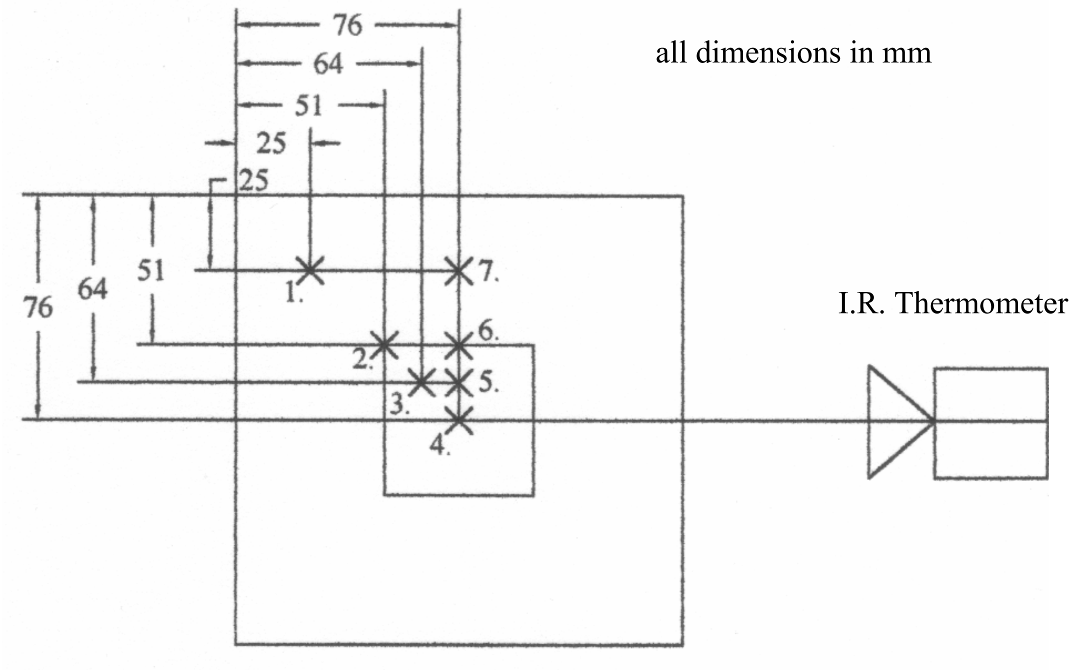

Figure 2.4 Points Selected for Temperature Measurements of Entire Specimen Holder Using Lightly Painted Steel Shim Stock

The infrared thermometer was located 45 degrees from horizontal and was aimed at the unexposed (back) side of the steel shim stock. The temperature measurements using the thermocouples were performed separately from those using the infrared thermometer since the infrared thermometer can only measure the temperature at one point at a time. The thermocouples were spot welded to the surface of the steel shim stock and specimen holder using 1 J of electrical energy, which was experimentally determined to provide a sufficient bond between the metals without damaging the fine thermocouple wires.

The second set of temperature measurement points are located between those points indicated in the first set and are only within the exposed area of the shim (51 mm or 2 in. square center). This was because the largest variations were anticipated in this region and also so that the symmetry of the data could be investigated.

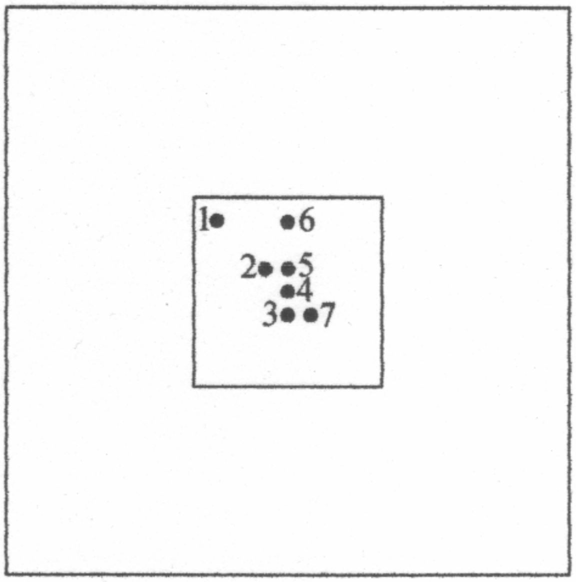

Figure 2.5 Points Selected for Temperature Measurements within Heated Region Using Lightly Painted Steel Shim Stock

The points measured during the second set of tests are shown as dots in Figure 2.5. Notice that the mid-point (Point 4) is measured again to ensure repeatability. Also, points 2 and 7 and points 3 and 5 are equidistant from and on opposite sides of center in order to check the symmetry of the behavior.

Temperature measurements were performed on the Kevlar®/PBI fabric samples at the locations shown in Figure 2.6. Since the thermocouples could no longer be spot welded onto the fabrics' surface, they had to be sewn in place using Nomex® or Kevlar®/PBI threads. A photograph of what this set up looked like appears in Figure 2.7. The specimen holder and fabric are viewed from the side and the threads shown are red Nomex®.

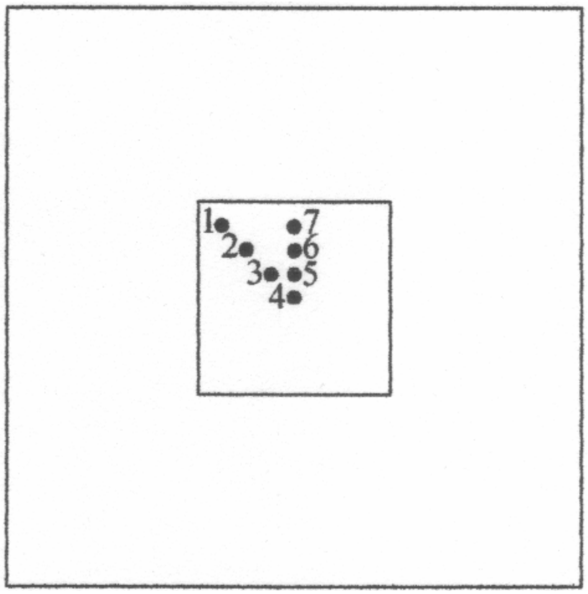

Figure 2.6 Points Selected for Temperature Measurements within Heated Region Using Kevlar®/PBI Specimens

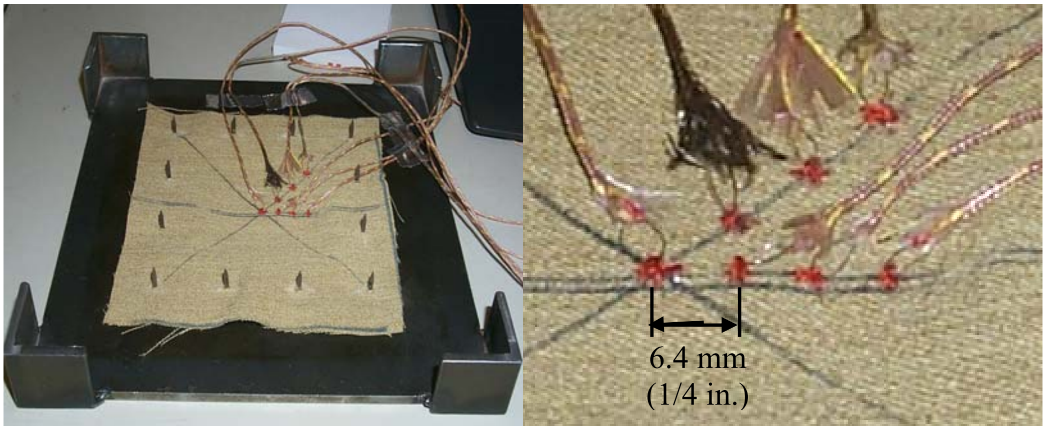

Figure 2.7 Photograph of Temperature Measurement Apparatus (Kevlar®/PBI)

The previous set of data points were concentrated within the heated portion of the fabric since this is where the largest temperature variations occurred. However, another set of temperature measurements were taken of the outer regions of the heated fabric. This set of points is shown in Figure 2.8.

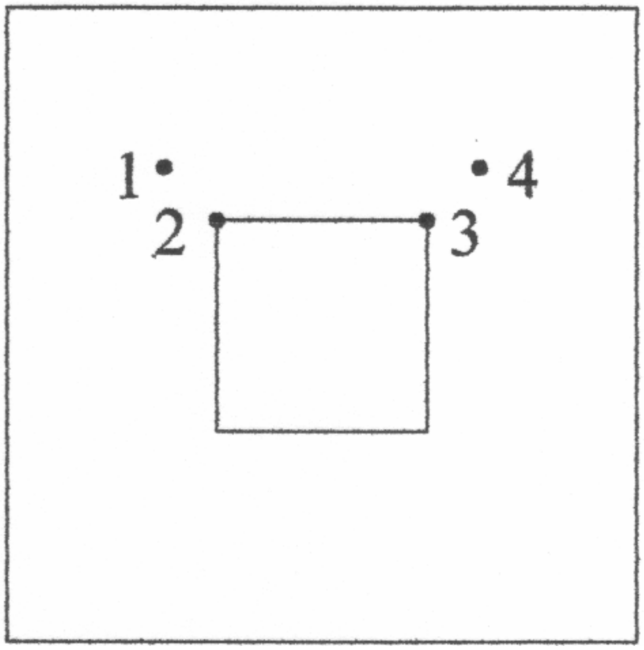

Figure 2.8 Points Selected for Temperature Measurements of Entire Specimen Holder Using Kevlar®/PBI Specimens

2.2.2 Flow Visualization

A flow visualization experiment was performed to assist in the development of the convection heat transfer portion of the model. In order to visualize the motion of any convection cells that may develop during the bench top testing of thermal protective fabrics, the apparatus needed to be altered and additional equipment needed to be employed. The method outlined here is similar to the flow visualization study performed in Torvi [2].

First of all, it was important that the flow was visible to an observer outside of the enclosure. Therefore, the Kaowool^{TM} insulating board and copper disc test sensor, which make up the top plane of the enclosure, were replaced with a 152 mm by 152 mm (4 mm thick) glass plate as shown in Figure 2.9. Secondly, seed particles are usually introduced during flow visualization to mark the flow. However, smoke is produced during the burning of the fabric. Also, the paint on the steel shim stock begins to smoke almost immediately after being exposed to the flame. This smoke provides excellent seed particles for flow visualization. Therefore, no external smoke sources were used in the flow visualization experiments performed for this research.

A light sheet is usually employed to visualize particular portions of the flow. For this purpose, a 500 W halogen flood lamp was modified to emit light in a plane of about 3 mm in thickness. As shown in Figure 2.10, this light sheet was positioned directly above the enclosure to illuminate a cross section of the flow through the center of the enclosure. Sidewalls of 2 mm thick transparent acrylic were used to provide a clear view of the flow through the sides of the enclosure. The air gaps present within the enclosure were dictated by the height of the acrylic sidewalls used since the glass plate sits on top of these sidewalls. Air gaps of 9.5 mm (3/8 in.), 12.7 mm (1/2 in.), 15.9 mm (5/8 in.), and 19.0 mm (3/4 in.) were studied. Smaller air gap values were not investigated since the specimen holder utilizes pins that are 6.4 mm (1/4 in.) long in order to hold the samples in place.

A digital video camcorder and a 35 mm camera were used to record the results of the flow visualization experiments. In one set of experiments, both cameras were placed at the same elevation as the enclosure and viewed the flow from the front of the apparatus through the clear sidewall. In the second set of experiments, the cameras were above the enclosure and viewed the flow at an angle of approximately 30 degrees. The video camera was set to automatic exposure and the 35 mm camera used 800 ISO film, an f-stop of 4, and a shutter time of 1/50 s.

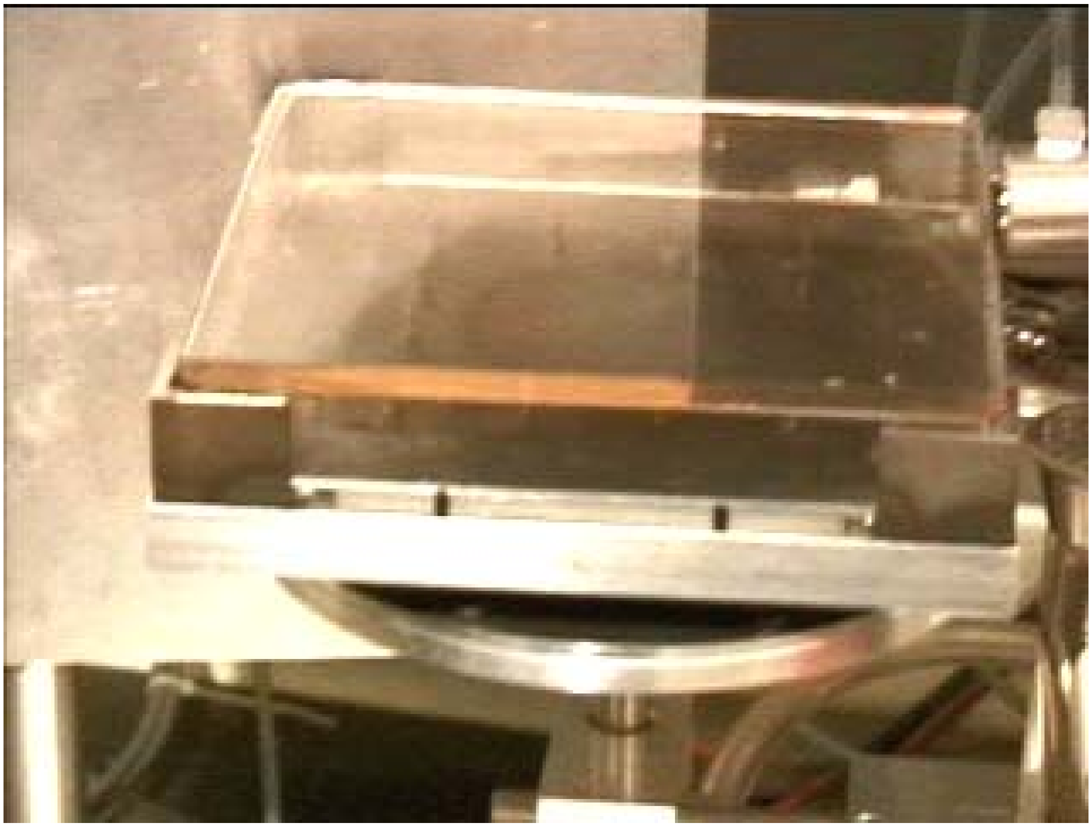

Figure 2.9 Photograph of the Enclosure (From Front at 30 Degree Angle)

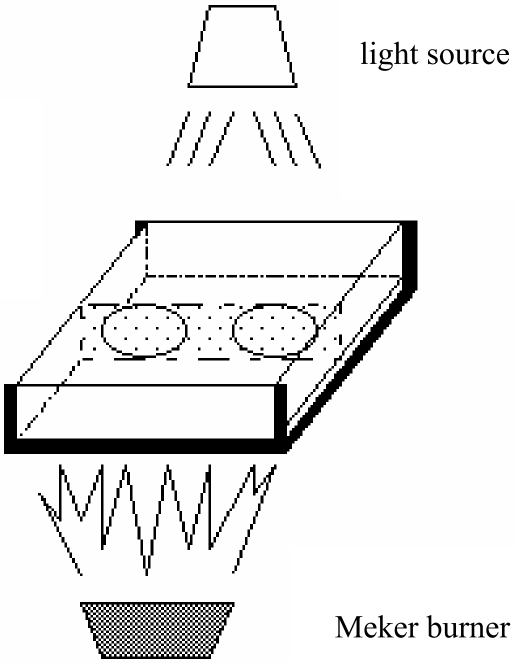

Figure 2.10 Schematic of Flow Visualization of Bench Top Test Enclosure

2.2.3 Measurements of Times to Exceed Stoll Criterion

The main purpose of the bench top testing apparatus is to evaluate the thermal protective performance of various materials. Therefore, the time required to exceed the Stoll criterion was experimentally determined for a range of air gap sizes using both the lightly painted steel shim stock and the Kevlar®/PBI fabric. The air gaps tested were 3.2 mm (1/8 in.), 6.4 mm (1/4 in.), 9.5 mm (3/8 in.), 12.7 mm (1/2 in.), 15.9 mm (5/8 in.), and 19.0 mm (3/4 in.). Occasionally, a thermocouple would be placed at the midpoint of the shim or fabric to obtain temperature histories for comparison with other results.

2.3 Procedure

All experiments were performed in a room that provided adequate ventilation by means of a fume hood directly above the entire apparatus. The source air to power the pneumatically-actuated water-cooled shutter and the cooling water sources were also turned on. The computer programs that controlled the experiments were initialized and the Agilent HP data acquisition system was powered and set. All items such as fabric, shim, and specimen holder were checked to ensure that they were at room temperature. Additionally, all fabric samples were conditioned in a chamber to approximately 20ºC and 65% relative humidity and all shim stock samples were lightly painted as shown in Figure 2.2.

The heat flux was calibrated by placing the test sensor and Kaowool^{TM} board in the specimen holder and exposing the copper disc directly to the heat source. The propane flow rate was adjusted until the appropriate nominal heat flux of 80 kW/m^2 ± 2 kW/m^2 was obtained in three consecutive tests. This procedure for preparing the apparatus is identical for all of the individual experiments. The specific details of each of the experiments are described in the following three sections.

2.3.1 Procedure - Temperature Measurements

The thermocouples were prepared by exposing approximately 10 mm of the wires and then crossing the wires perpendicular to each other such that an "X" was produced. The junction of this "X" was spot welded together to provide a completed thermocouple circuit. A painted sample of steel shim stock or a sample of Kevlar®/PBI was installed into the specimen holder. Depending on which material was used, shim or fabric, the mounting of the thermocouple was either spot welded to the unexposed surface or sewn to the unexposed surface. A steel spacer was used to provide the desired air gap and the Kaowool™ board/test sensor assembly was placed on top of the spacer to complete the enclosure. If the infrared thermometer was being used instead of the thermocouples to obtain the data, then this last step was not performed. The Meker burner was ignited and placed directly under the center of the specimen holder and the computer was used to control the exposure time to 10 s. The program was allowed to run and save the data to a Microsoft® Excel file on the desktop PC. This process was repeated a number of times for each material so that an average result of five successful tests could be obtained.

2.3.2 Procedure - Flow Visualization

A painted sample of steel shim stock or a sample of Kevlar®/PBI was installed into the specimen holder. An acrylic sidewall with the height of the desired air gap and the glass plate were then placed on the specimen holder. The halogen lamp was turned on and adjusted so that the plane of light was incident along the centerline of the enclosure. The video camera was then positioned at the same elevation as the enclosure to have a viewpoint parallel to the horizontal plates and then focused on the light sheet. The Meker burner was ignited and moved to the side of the enclosure until it was time to apply the heat source. All of the lights in the room were turned off to provide the highest level of contrast between the illuminated cross-section and the surroundings. The video camera was set on its record function during the video series of tests. Next, the Meker burner flame was placed directly under the center of the specimen holder and the computer controlled shutter was used to control the exposure time to 10 s. The camcorder was allowed to record for approximately 5 seconds after the end of the exposure and then the record function was stopped. If the still camera was used, photographs were taken at approximately 1 s, 3 s, and 10 s into the exposure. The flame was then extinguished and the halogen lamp was shut off. The entire process was repeated using the other sidewall heights.

2.3.3 Procedure - Times to Exceed Stoll Criterion

A painted sample of steel shim stock or a sample of Kevlar®/PBI was installed into the specimen holder. A steel spacer was used to provide the desired air gap and the Kaowool™ board/test sensor assembly was placed on top of the spacer to complete the enclosure. The Meker burner was then ignited and placed directly under the center of the specimen. The computer was used to control the water-cooled shutter in order to regulate the exposure time to 10 s. The program was allowed to run and save the data to a Microsoft® Excel file on the desktop PC. This process was repeated a number of times for each material and for each air gap size for statistical purposes and so that an average result of five successful tests could be obtained.

2.4 Chapter Summary

In Chapter 2, the bench top apparatus for the evaluation of thermal protective fabrics was described. The procedure for using this apparatus and the method used to test thermal fabrics was presented. Also, the additional equipment used to take temperature measurements and perform flow visualization were introduced and discussed. The experiments performed in order to investigate the boundary conditions of the bench top test enclosure were outlined and the results obtained during these experiments appear in Chapter 3.

CHAPTER 3 EXPERIMENTAL RESULTS

The results of the experiments outlined in Chapter 2 are presented in this chapter along with a discussion of the information that can be extracted. The results include temperature measurements of the bottom boundary when heating steel shim stock and Kevlar®/PBI samples. Also included are results obtained during the flow visualization experiments as well as times to second-degree burns predicted by the Stoll Criterion using experimental data.

3.1 Results - Temperature Measurements

As previously mentioned, temperature measurements were made using thermocouples and then repeated using an infrared thermometer. A test was conducted so that the temperature histories generated by both methods could be compared. Both instruments were used to measure the temperature at the midpoint of a prepared specimen of steel shim stock during a 10 s exposure to 80 kW/m^2. This test was performed five times for each instrument, and the average temperature histories recorded are shown in Figure 3.1.

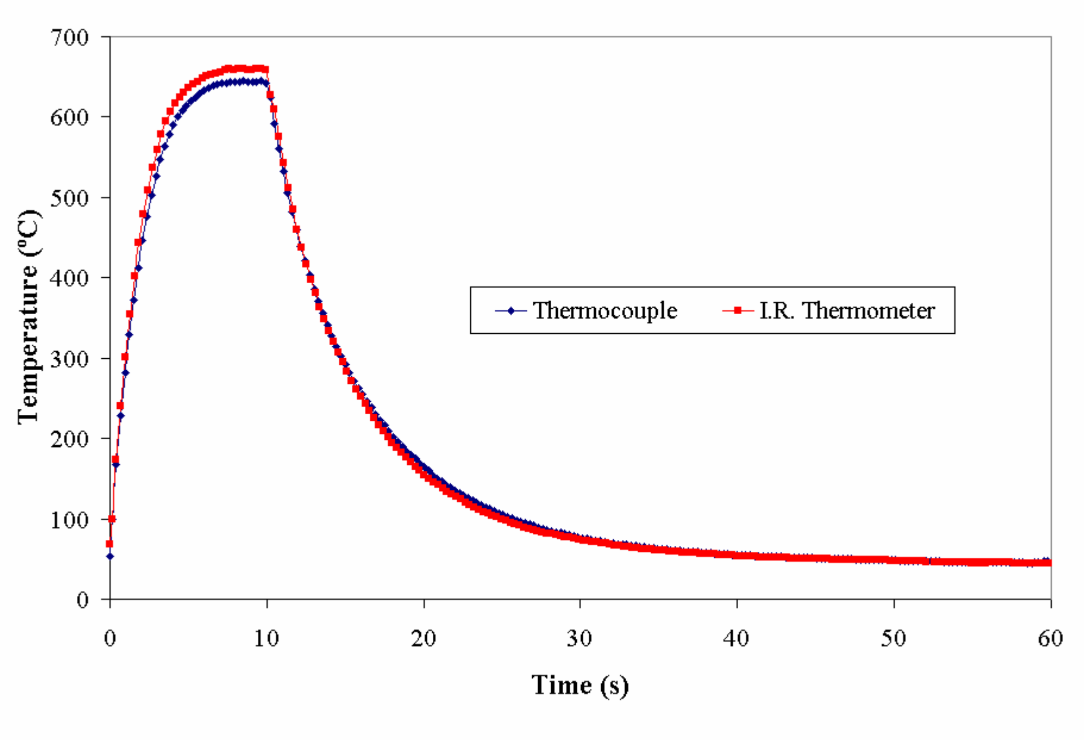

Figure 3.1 Comparison of Average Midpoint Temperatures Obtained Using Thermocouples and an Infrared Thermometer (Steel Shim Stock)

The temperatures measured by the infrared thermometer and the thermocouple are very similar as the heating and cooling curves are almost identical. This indicates that the thermal capacity of the thermocouple junction is sufficiently small in order to properly capture the response of the shim/fabric samples during these bench top tests. Also, during less transient regions, 7 – 10 s and 40 – 60 s, the difference in absolute temperatures is never more that 4.5%, which indicates that the emissivity setting of the I.R. thermometer ($\varepsilon = 0.95$) sufficiently approximated the emissivity of the actual shim surface. In the following results of temperature measurement experiments, data presented was obtained using thermocouples, unless otherwise stated.

3.1.1 Temperature Measurements Over Entire Specimen Holder (Shim)

The temperature histories at every point were compared individually first to ensure that no experimental anomalies had been introduced to the data. Examples of these anomalies would be spikes or sudden unexplained drops in the temperature curve. This behavior was sometimes encountered when using such fine gauge thermocouples since the wires were easily broken before or during an experiment. After these occurrences had been removed from the data set, an average of all of the trials for a single test point was calculated. An example of this procedure is shown in Figure 3.2 for the midpoint of the exposed area (Point 4). Notice that the temperature measurements are repeatable, with very little difference between trials.

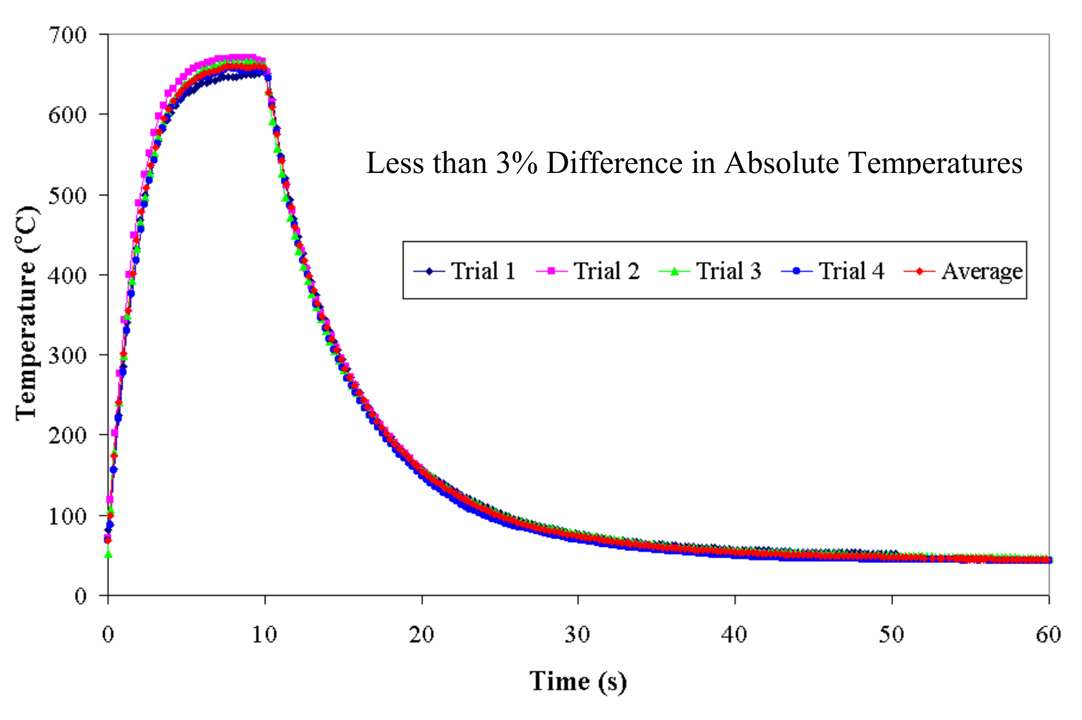

Figure 3.2 Comparison of the Temperature Histories of a Number of Trials for the Midpoint (Point 4) (Steel Shim Stock)

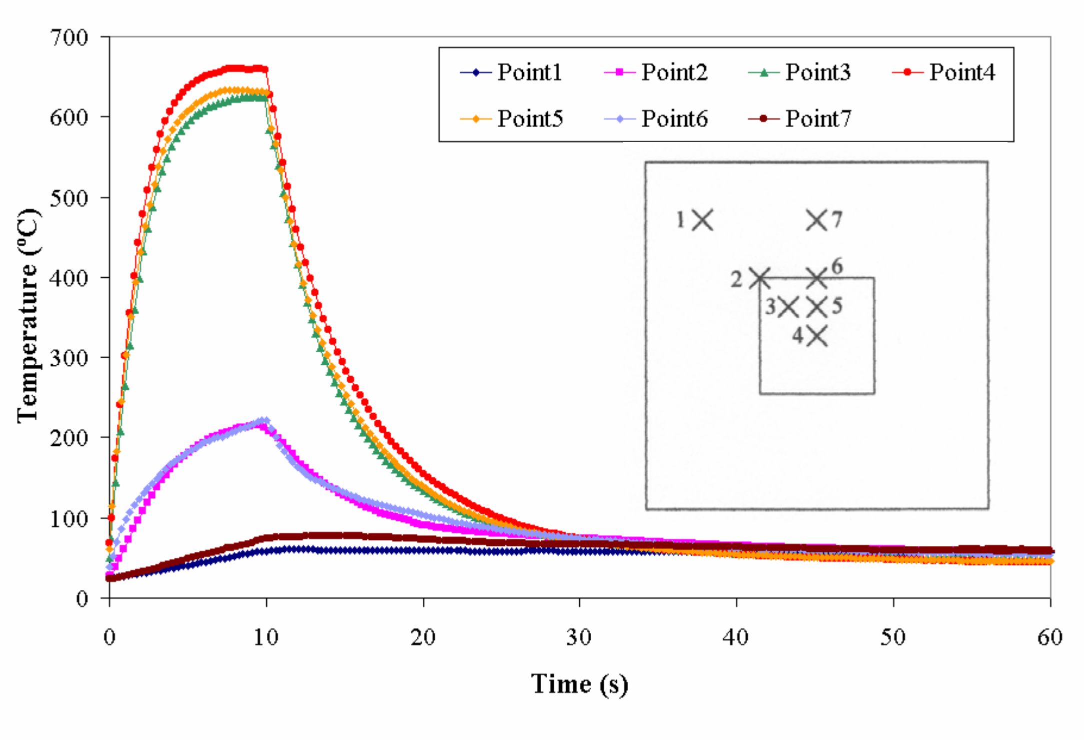

Figure 3.3 Comparison of Average Temperature Measurements Over Entire Specimen Holder (Steel Shim Stock)

After an average temperature curve was calculated for each location, temperatures at the seven points could be compared as shown in Figure 3.3. Not only are there very large temperature variations with respect to time, but also there are also very large spatial variations in the temperature of the bottom of the enclosure. The center of the exposed area, Point 4, rises to approximately 660˚C before the end of the exposure, whereas Point 1, at the outer region of the specimen holder, only rises to approximately 60˚C. This behavior brings into question the validity of a one-dimensional heat transfer model and thus the new model developed must consider the enclosure with a greater sophistication. With only a short glance at Figure 3.3, because of the extreme variations in temperature both spatially and temporally, one can see why the heat transfer within this enclosure is very different from most of the other work in the literature.

3.1.2 Temperature Measurements Over Heated Region (Shim)

After the first set of temperature measurements had been completed, it was decided that another set of measurements should be made in order to increase the resolution of experimental information. Therefore, these points were chosen in between the previously measured points within the exposed area, where the largest spatial variations in temperature were found during the first set of tests. The location of these test points was shown in Figure 2.5 but is shown again for clarity along with the temperature histories in Figure 3.4.

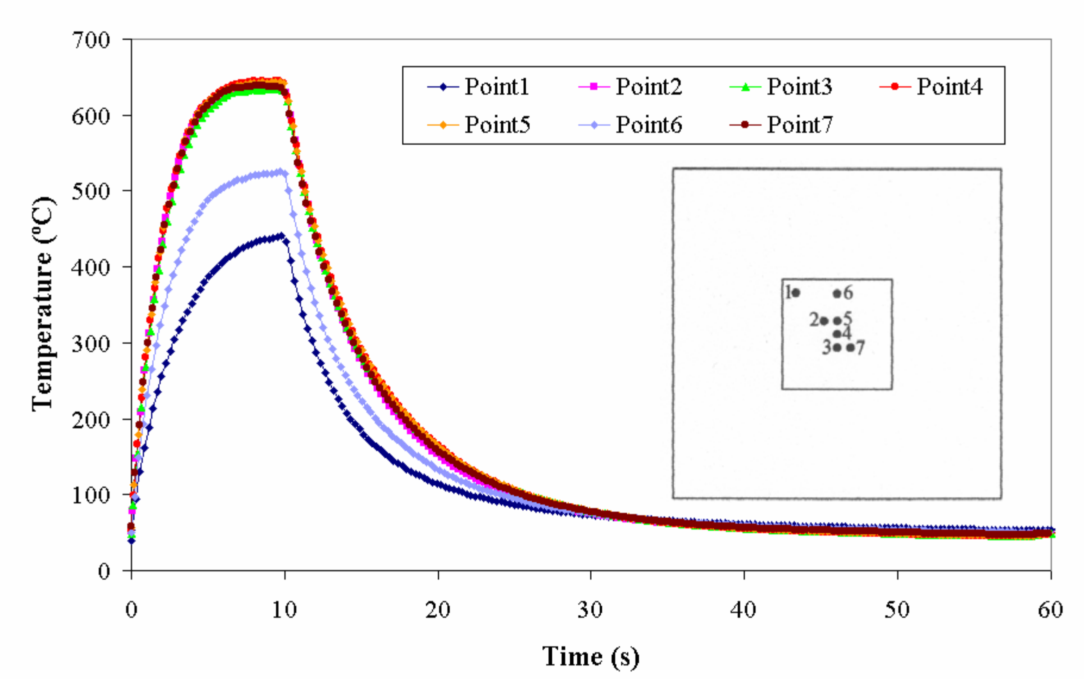

Figure 3.4 Comparison of Average Temperature Measurements Over Heated Region (Steel Shim Stock)

From Figure 3.4 it can be seen that the temperature histories of all of the data points within approximately 6.4 mm (1/4 in.) of the center of the heated region are almost identical. The temperature history of the midpoint (Point 4) is slightly higher than the temperature histories of the surrounding points. The information gathered during this set of experiments contributes to the overall research by increasing the resolution of the boundary conditions of the bottom boundary, with the exception of Points 3 and 7. These two points were placed such that the symmetrical behavior of the boundary conditions could be investigated.

There is evidence in Figure 3.5 that supports the assumption of a symmetrical bottom boundary. The difference in absolute temperatures is less that 1.0% over the entire temperature history for Points 3 and 7.

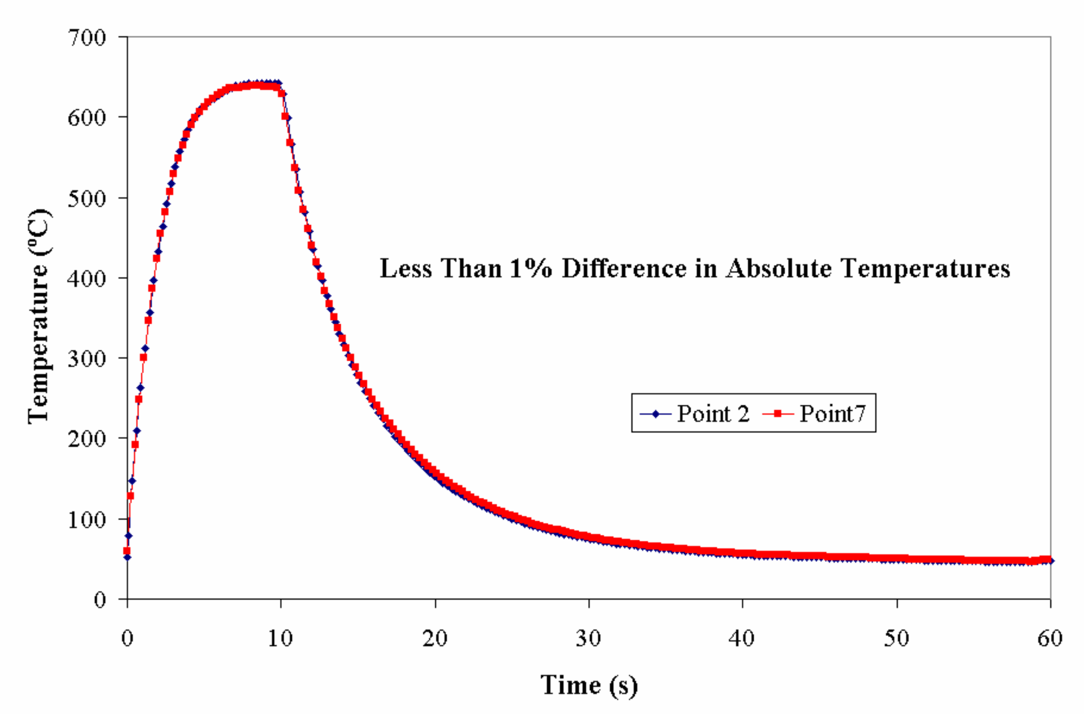

Figure 3.5 Investigation of the Symmetrical Behavior on the Specimen Holder

The symmetry of the bottom boundary was also investigated by measuring all seven data points within an entirely different quadrant. No noticeable differences between this data and other tests were encountered. Therefore, measurements could be taken within one quadrant and this information was expected to apply over the entire bottom boundary.

This concludes the temperature measurements performed on the lightly painted shim stock specimens. A summary of these findings appears in Figure 3.6. The maximum temperatures recorded for each point, which occurs immediately before the end of the exposure to the flame (10 s), are shown along two contours of the bottom boundary. These contours show the spatial variations in temperature along a diagonal and along a centerline.

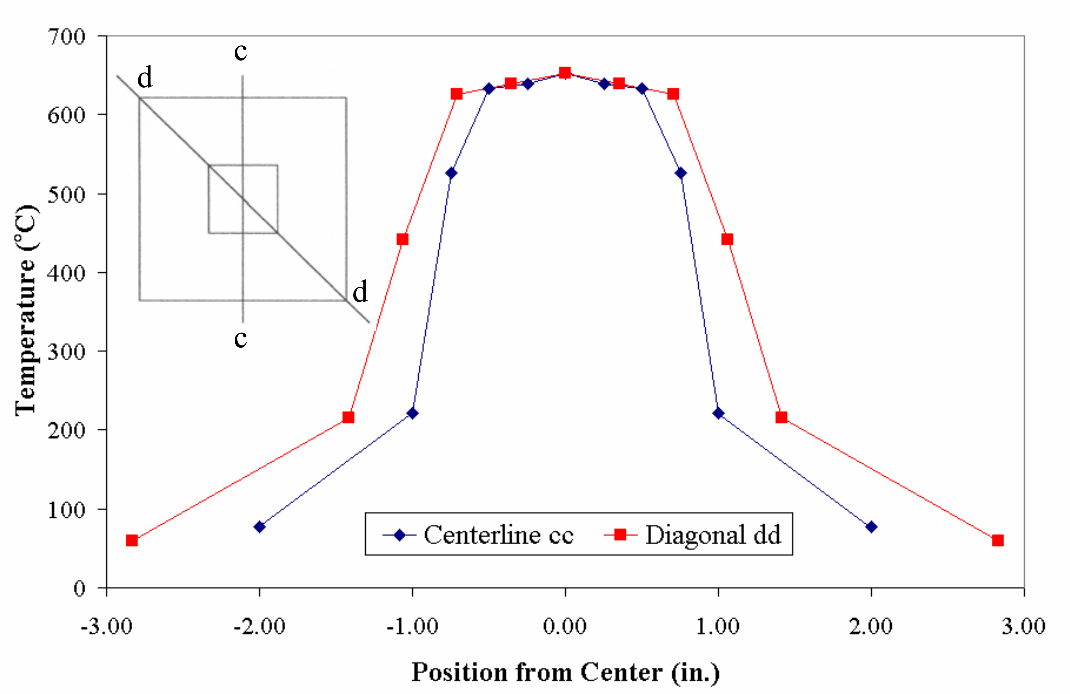

Figure 3.6 Maximum Temperature Along Two Contours of Entire Specimen Holder (Steel Shim Stock)

The rate of change of temperature with respect to distance can be seen in Figure 3.6 by observing the slope of the curves. The largest variation in temperature occurs near the edge of the opening in the specimen holder, which is located 25.4 mm (1 in.) from center in the case of the centerline and approximately 35.8 mm (1.4 in.) in the case of the diagonal. Another diagram that shows the distribution in maximum temperatures is shown in Figure 3.7. This figure illustrates the location of maximum temperatures during a bench top test utilizing a plan view of the specimen holder.

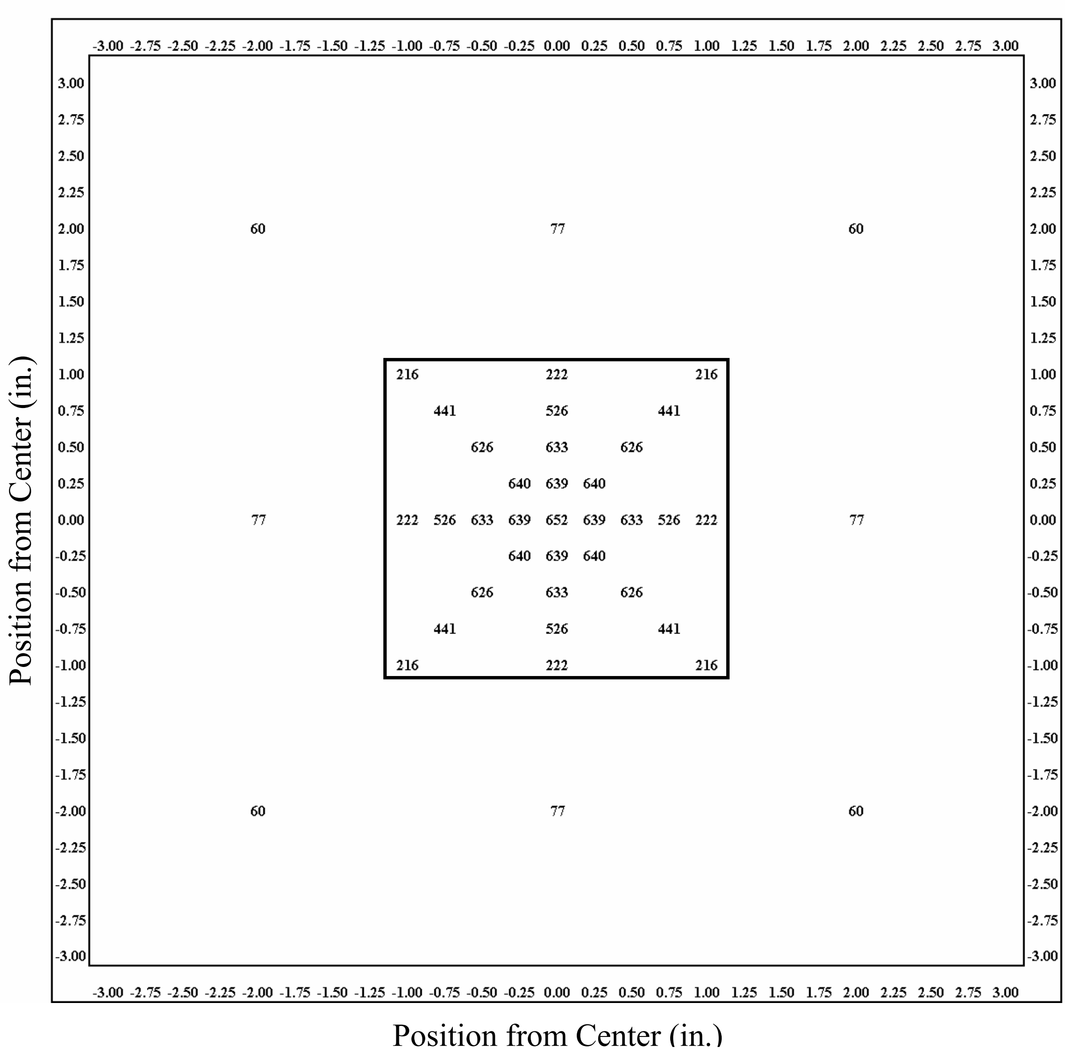

Figure 3.7 Plan View of Maximum Temperature Distribution on Bottom Boundary (Steel Shim Stock) (Temperatures in Degrees Celsius)

This figure clearly indicates the spatial variations encountered in the boundary conditions of this problem. Very large temperature differences occur within very short distances. As a matter of fact, as this figure is viewed on the page, the size of this plan view of the specimen holder is 90% of the true dimensions. This gives the reader an excellent indication of the difficulty in properly capturing the physics of this problem by treating the heat transfer one-dimensionally.

3.1.3 Temperature Measurements Over Heated Region (Kevlar®/PBI)

The third set of temperature measurements was performed on the unexposed side (backside) of the Kevlar®/PBI fabric samples. However, it was more difficult to execute these experiments since the thermocouples could no longer be spot welded to the surface of the material tested. Now the thermocouples had to be sewn in place using a thread that was capable of resisting degradation under high temperatures; the thread had to ensure the junction of the thermocouple remained in contact with the fabric surface during the entire exposure. At first, Nomex® thread was used to hold the thermocouples in place. The results are shown in Figure 3.8.

In some cases, the Nomex® threads broke and let the thermocouples rise off of the surface of the fabric. Therefore, the temperature of the surface of the fabric was not being measured, but instead, the temperature of the air a couple of millimeters above the surface of the fabric. This was verified through observations made during several tests. The locations subject to the highest temperatures showed the largest errors (e.g., Point 4) as the threads holding the thermocouple in place degraded more quickly.

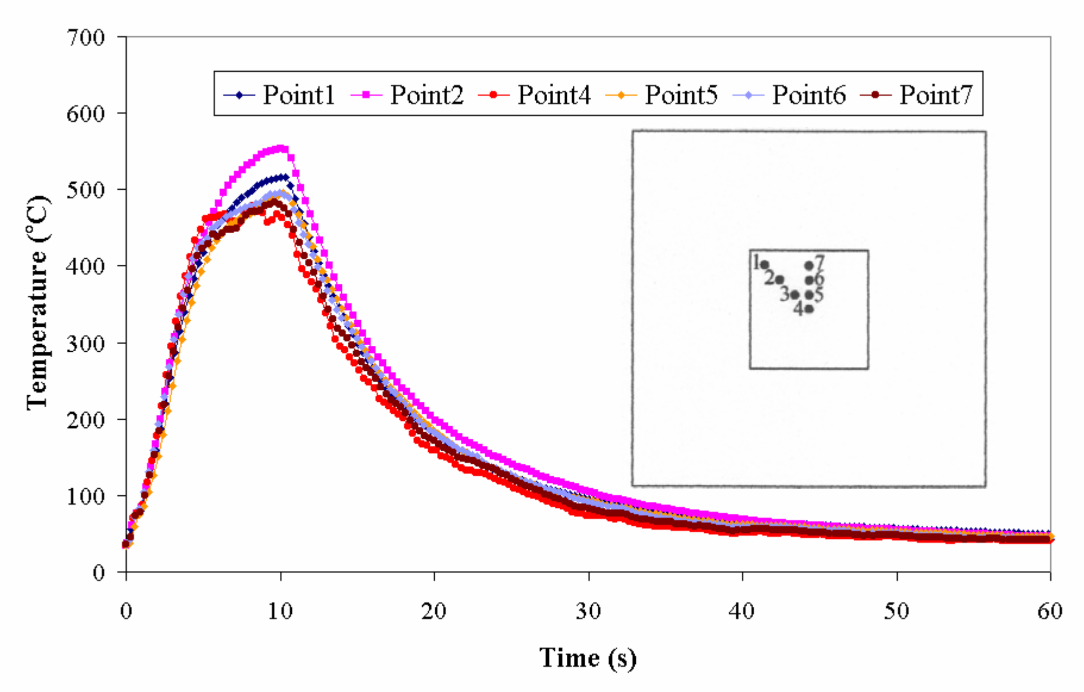

Figure 3.8 Temperature Measurements Over Heated Region Using Kevlar®/PBI Fabric Samples and Nomex® Threads to Hold Thermocouple Wires

To remedy this problem, a number of other high temperature threads were tested. The material that was found to perform the best for this purpose was the yarn from Kevlar®/PBI fabric samples. The length of the yarns (102 mm or 4 in.) made the sewing process difficult but not impossible and the temperature experiments were continued. All further temperature measurements were made using the Kevlar®/PBI yarns to hold the thermocouples in place.

The temperature histories of the center point (Point 4) are shown for a number of trails in Figure 3.9.

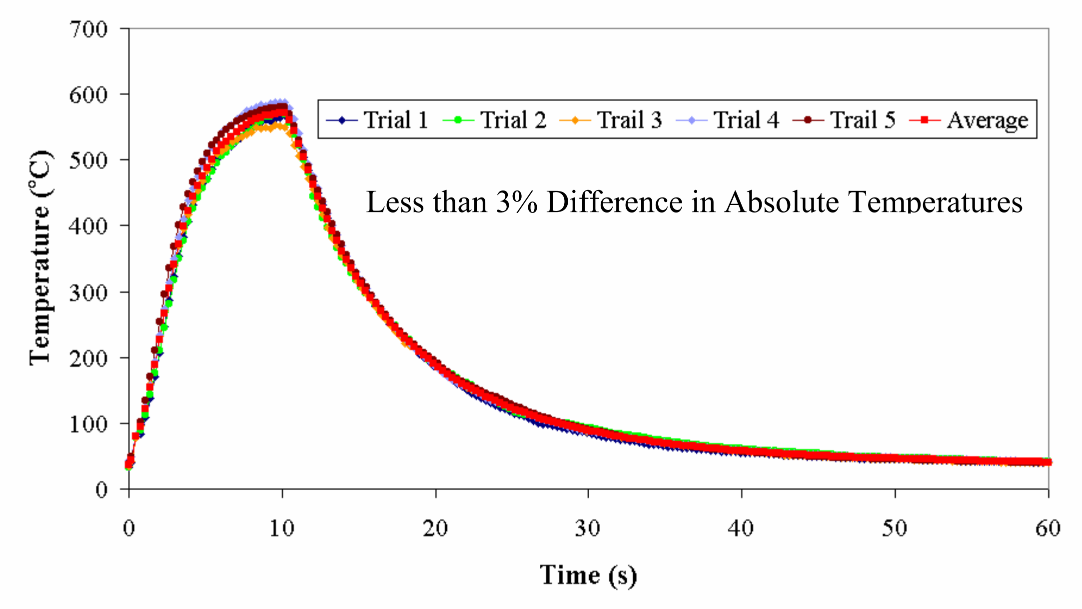

Figure 3.9 Comparison of the Temperature Histories of a Number of Trials for the Midpoint of Kevlar®/PBI Fabric Using Kevlar®/PBI Yarns

Immediately, the similarities and differences between testing the fabric and the steel shim stock become apparent. Both materials are seen to produce similar heating curves with no spikes or plateaus. Also, the results of testing both materials seem to be reproducible with very little variations between trials. The maximum deviation in absolute temperature is less than 3%, which equates to less than 20˚C at the end of the exposure. However, when comparing the average response of the shim stock to the average response of the Kevlar®/PBI, as is shown in Figure 3.10, the differences are profound.

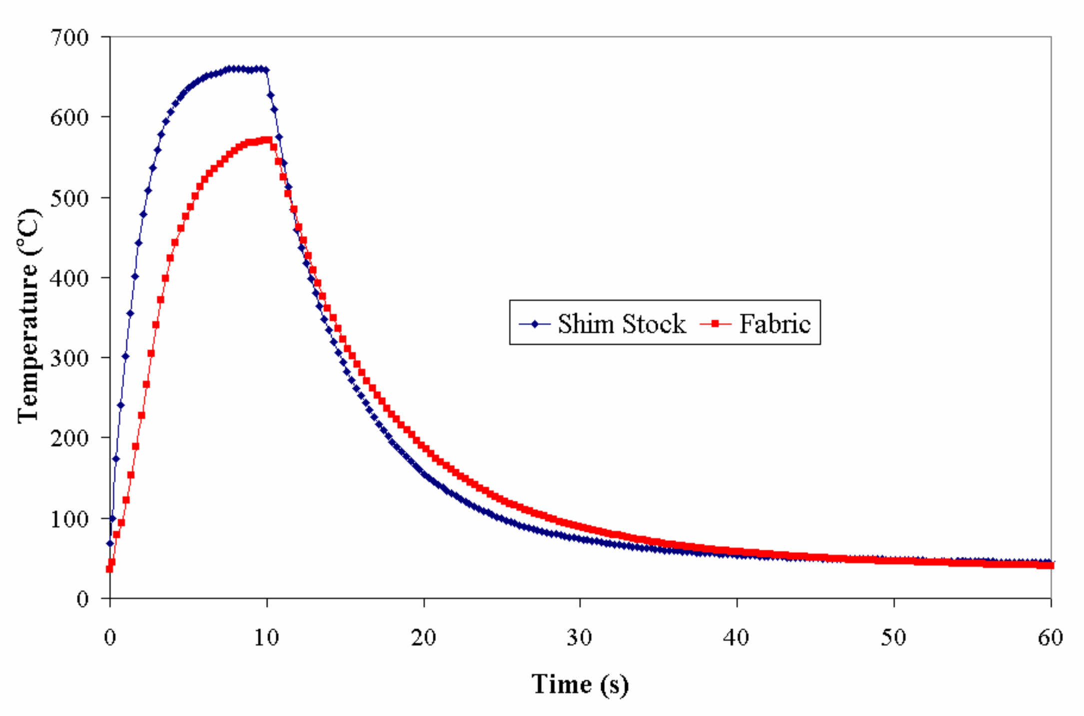

Figure 3.10 Comparison of the Measured Response of Steel Shim Stock and Kevlar®/PBI Fabric Samples for the Midpoint of the Heated Region

The heating portion of the fabric shows a slope of smaller magnitude, which can be attributed to the presence of moisture and the endothermic thermo-chemical reactions that take place in the fabric due to heating. Moreover, the maximum temperatures reached by the fabric are much lower than those reached when testing the shim stock. The shim stock reached a maximum of 660˚C ± 10˚C, whereas the maximum temperature reached by the fabric was only 571˚C ± 18˚C.

The complete results of the temperature measurements along the heated region of the Kevlar®/PBI fabric samples are shown in Figure 3.11 along with a reminder of which locations were investigated.

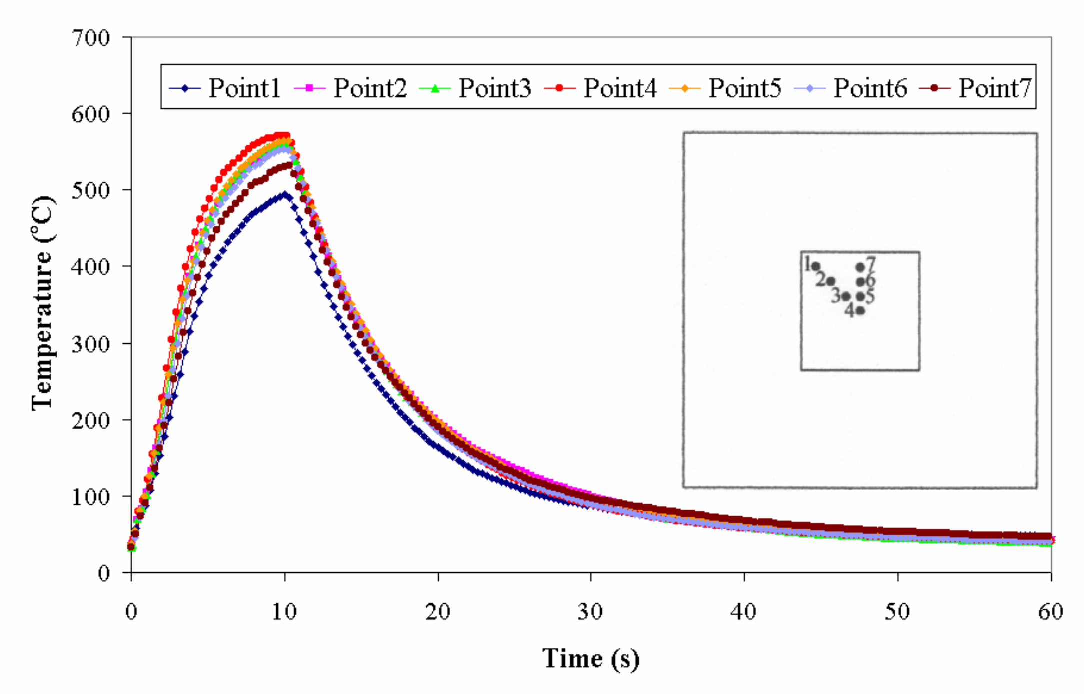

Figure 3.11 Comparison of Average Temperature Measurements Over the Heated Region (Kevlar®/PBI Fabric)

The temperature variations across the back surface of the fabric are smaller than the temperature variations across the steel shim stock. This becomes obvious when the temperature histories of four identical locations are compared in Figure 3.12. The higher thermal conductivity of the steel shim has two influences on the temperature distribution within the exposed area. The first influence is that there is less variation in the central portion of the exposed area than in the fabric case. However, the shims' higher thermal conductivity and better contact with the specimen holder, also produces more heat transfer to the specimen holder, which is a relatively large heat sink. Therefore, the steel shim stock temperatures at the outer region of the exposed area have a larger temperature difference from the inner data points when compared to the temperature differences in the fabric case.

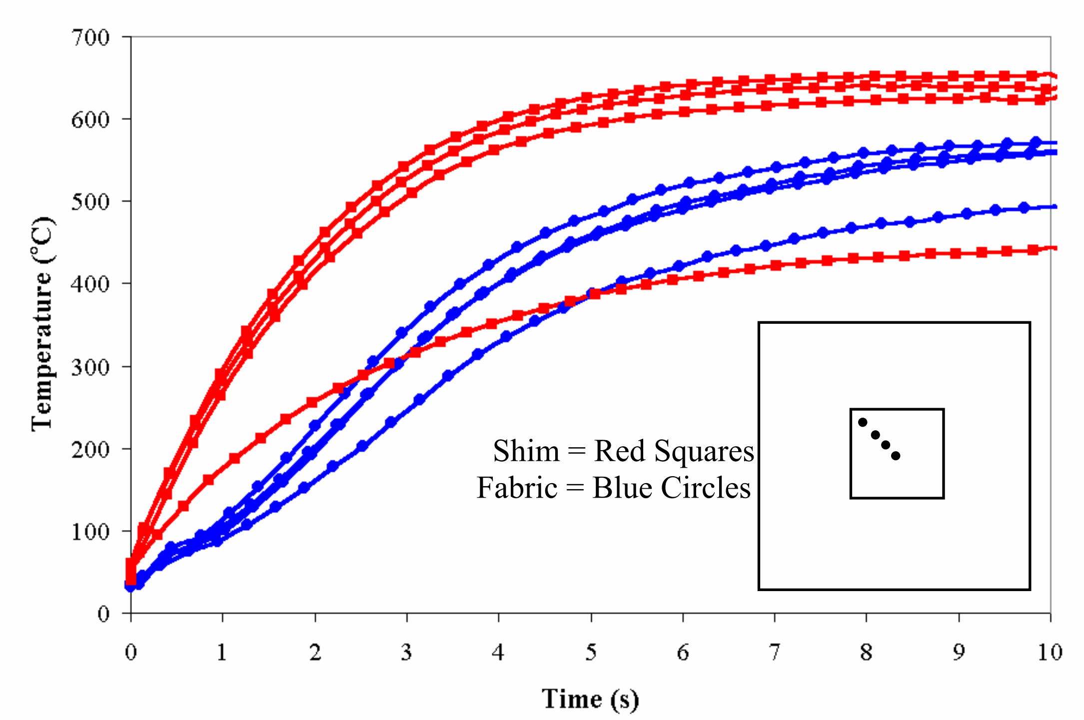

Figure 3.12 Comparison of the Measured Response of Steel Shim and Kevlar®/PBI Specimens Within the Heated Region

3.1.4 Temperature Measurements Over Non-Heated Region (Kevlar®/PBI)

The temperature histories of locations outside of the exposed area were measured in this set of tests. This information was used to increase the overall knowledge of the boundary conditions in the bench top testing of thermal protective fabrics. Therefore, the maximum temperatures found over the same contours as shown earlier in Figure 3.6, are reinvestigated for the fabric case. Remember that these contours are a diagonal and a centerline across the specimen holder.

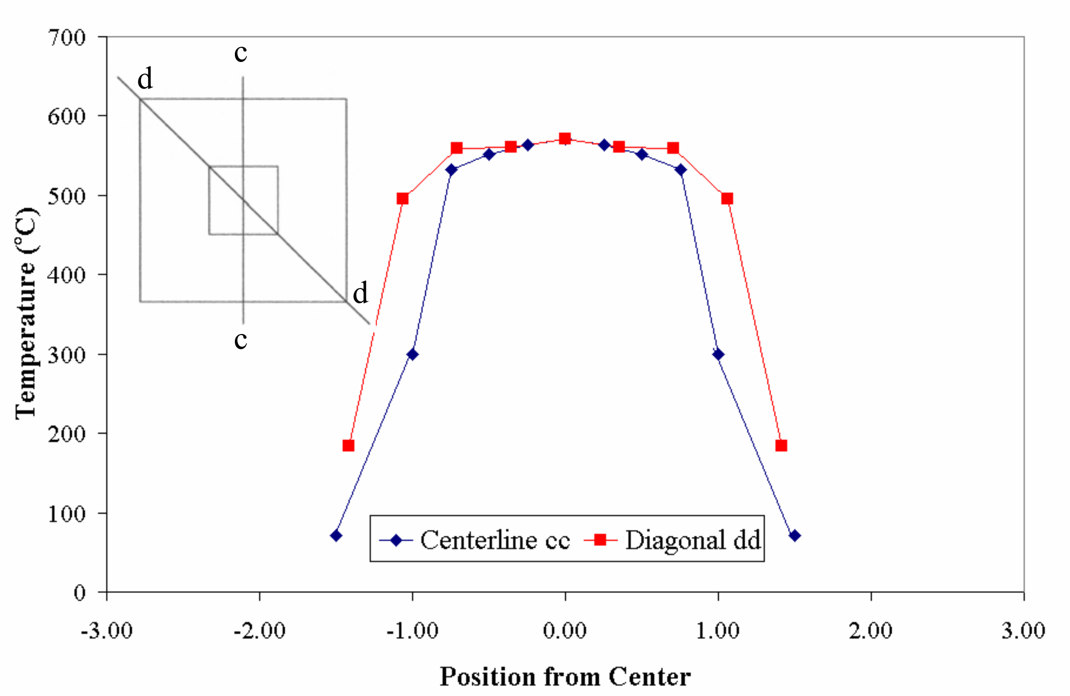

Figure 3.13 Maximum Temperature Along Two Contours of Entire Specimen Holder (Kevlar®/PBI Fabric)

The maximum fabric temperature profiles generated along these contours look similar to those generated using the steel shim stock data. However, the fabric profiles shown in Figure 3.13 appear to be sharper and have more of a top-hat shape than the profiles shown in Figure 3.6 for the steel shim. The maximum temperatures throughout the entire heated region of the fabric are less than 50°C different in magnitude excluding the points along the edge. The behavior of the Kevlar®/PBI demonstrated here is very different from the behavior seen in the steel shim stock. The one-dimensional treatment may still be proven to have its merits.

As before, a plan view of the specimen holder and fabric is shown in Figure 3.14 where the maximum temperature distribution is illustrated.

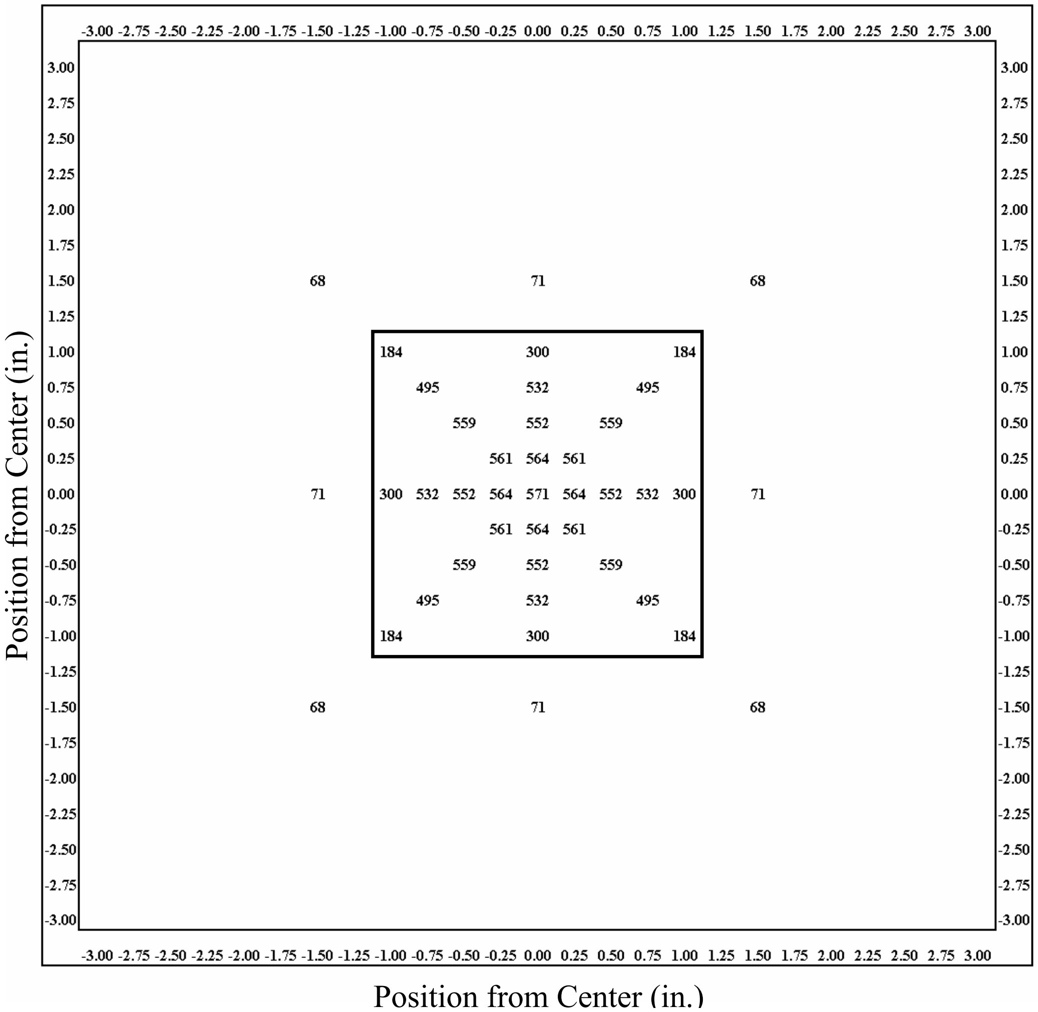

Figure 3.14 Plan View of Maximum Temperature Distribution on Bottom Boundary (Kevlar®/PBI Fabric) (Temperatures in Degrees Celsius)

The spatial variations in the fabric differ greatly from those in the steel shim stock. As previously mentioned, the higher thermal conductivity of the steel and better contact with the specimen holder are reasons for this behavior. Since the specimen holder has a much larger heat capacity than the steel shim specimen, more heat is transferred from the shim to the specimen holder and thus relatively lower temperatures occur near the outer region of the exposure area.

3.1.5 Additional Observations

When the temperature measurement experiments were being performed, some other interesting observations were made. When the steel shim stock or fabric samples were being heated, the boundary conditions on the bottom boundary of the enclosure were dependent on the bench top testing apparatus, in that the shape of the exposed area cutout of the specimen holder is square. Therefore, even though the flame from the Meker burner provides a heat flux that is axi-symmetric or circular, the area of exposure on the specimen itself is not axi-symmetric. Hence, isotherms on the fabric specimens are shaped more like squares than circles, as seen in Figure 3.15.

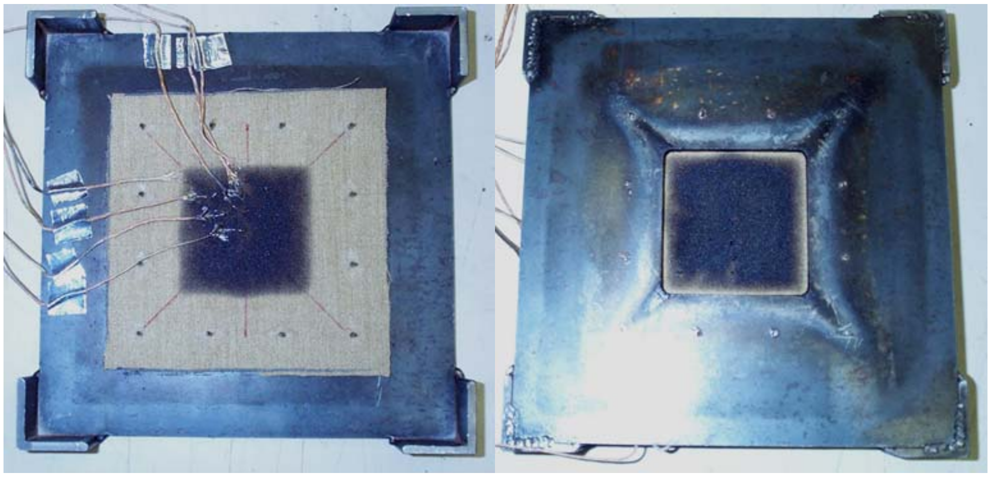

Figure 3.15 Kevlar®/PBI Specimen After Exposure (Back and Front)

The same pattern was noticed during the steel shim stock testing. The visual observations were made even easier on the steel samples because the smoke liberated was not as excessive as in the fabric case. Also, the rainbow of colors that steel goes through as it is heated provided a good indication of isotherms within the bottom boundary. These isotherms can be clearly seen in Figure 3.16.

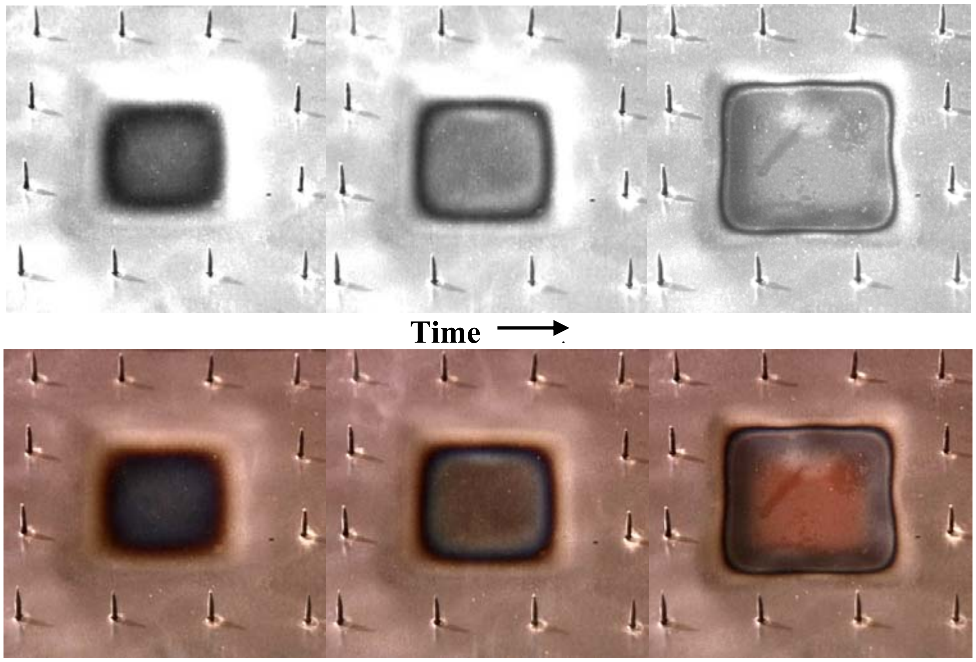

Figure 3.16 Photographs of the Steel Shim Stock During Heating After (From Left to Right) 1 s, 3 s, and 10 s of Exposure

From the photographs, the thermal boundary conditions of the bottom of the enclosure clearly have a square shape. Regions with a similar temperature will have a similar color due to material properties. Therefore the colored bands in the photographs indicate different isotherms. The black and white photographs are included to more clearly show the isotherms as shades of gray.

The colored photographs provide additional visual information. When a material is heated to above approximately 550˚C, its surface will begin to glow red [24]. The photograph on the bottom right shows clearly an area that is glowing red. This result is consistent with the temperature measurements shown previously for the steel shim stock samples (e.g., Figure 3.2).

3.2 Results - Flow Visualization

The following photographs were taken during the flow visualization experiments. These experiments were performed using a procedure very similar to the work of Torvi [2].

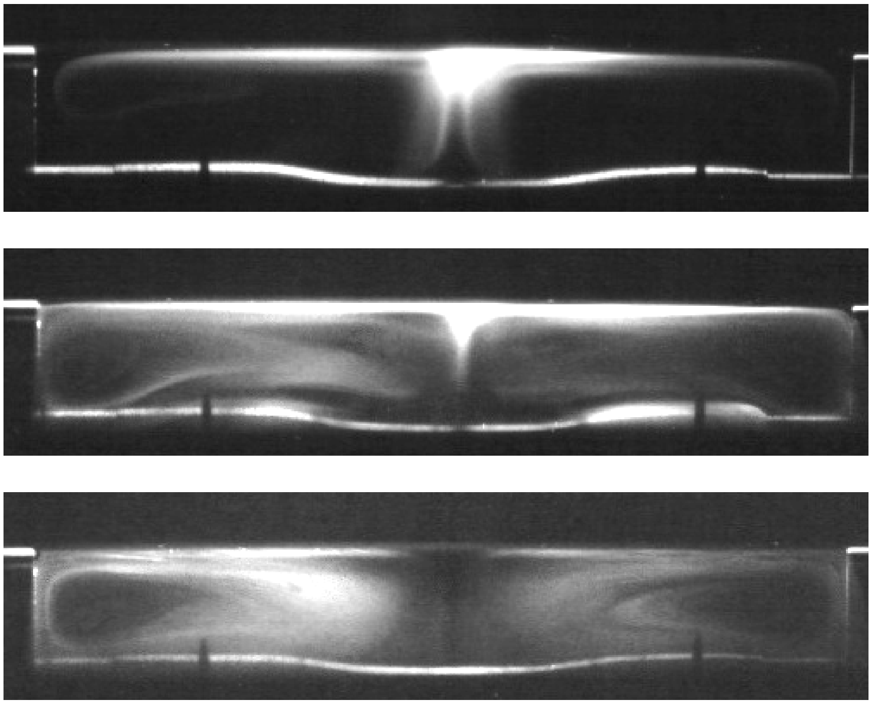

Figure 3.17 Flow Visualization of 19 mm (3/4 in.) Air Gap After (From Top to Bottom) 1 s, 3 s, and 10 s of Exposure

The fluid motion is easily visible in these photographs obtained during the flow visualization experiments. The largest air gap, 19 mm (3/4 in.), is shown in Figure 3.17. Clearly the air is not stagnant within the enclosure during this test. The transition from conduction to convection has occurred and a large convection cell is evident.

The following is an explanation for the development of the convection cells. At the center of the enclosure, where the heat is applied, the air becomes buoyant and rises until contact is made with the top glass plate. As the rising air encounters the top plate it is forced to move out along the length of the top plate towards the sidewalls. While traveling near the top plate, the air loses momentum due to friction and loses heat energy to the cooler surroundings. This loss of momentum and temperature (buoyancy) causes the air to fall back down towards the bottom plate where the air becomes heated and the cycle continues. In the picture, the light sheet illuminates a plane along the centerline. However, in three dimensions, the structure is a toroid or doughnut shape.

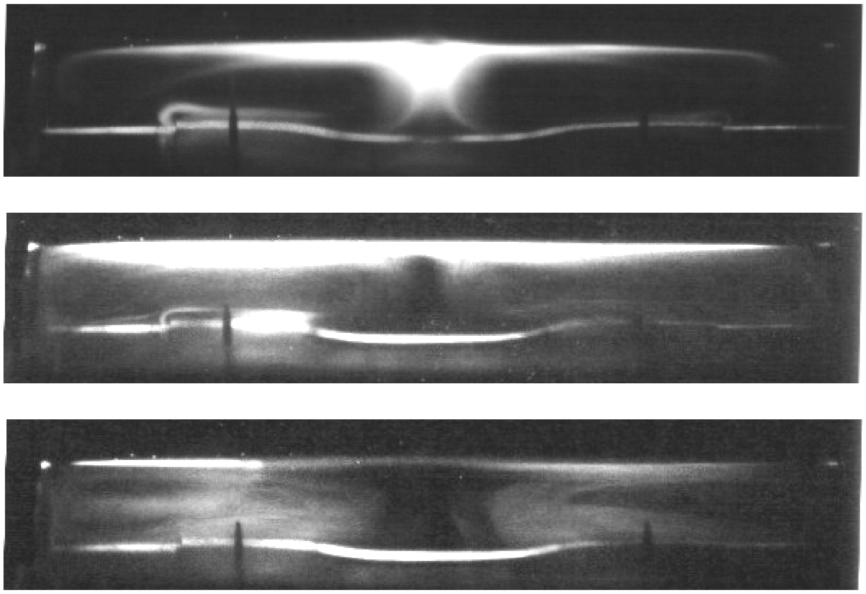

Figure 3.18 Flow Visualization of 15.9 mm (5/8 in.) Air Gap After (From Top to Bottom) 1 s, 3 s, and 10 s of Exposure

The fluid motion in the 15.9 mm (5/8 in.) air gap is very similar to the fluid motion in the 19 mm (3/4 in.) air gap. Photographs of the convection cell are shown in Figure 3.18. Again there is a very large convection cell that extends throughout the enclosure. The three-dimensional action is once again a toroid or doughnut shape.

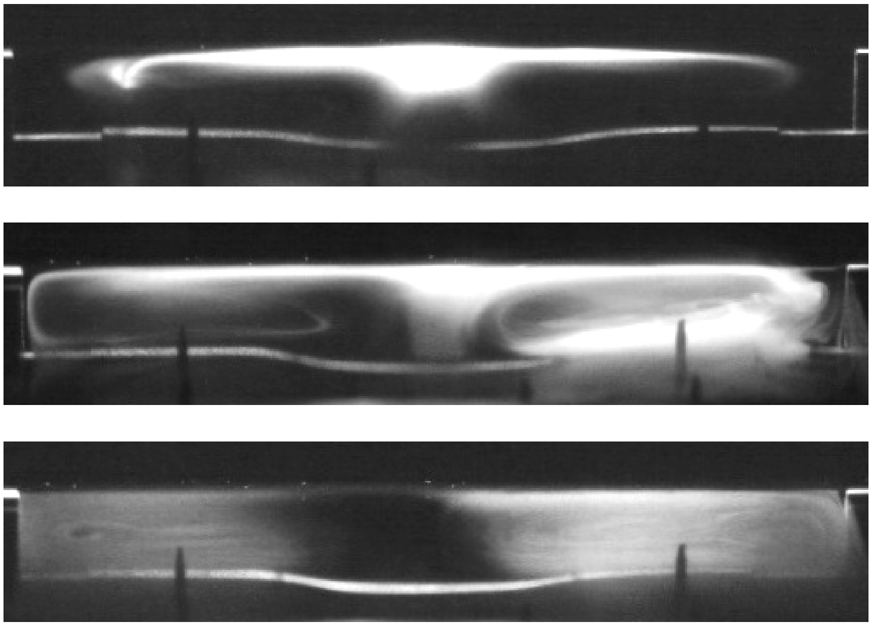

Figure 3.19 Flow Visualization of 12.7 mm (1/2 in.) Air Gap After (From Top to Bottom) 1 s, 3 s, and 10 s of Exposure

Photographs of the flow visualization experiment using an air gap size of 12.7 mm (1/2 in.) are shown in Figure 3.19. The convection cell in this case continues to extend throughout the entire enclosure. However, as evident in the video, the motion is not as strong and has lower speeds than was present in the larger air gap spaces. This is due to a relative increase in the viscous shear forces, associated with a smaller air gap, compared to the buoyancy forces. In other words, the air is more restricted and closer to the walls more often than in the larger air gap spaces and the relative amount of open space decreases with air gap size reduction.

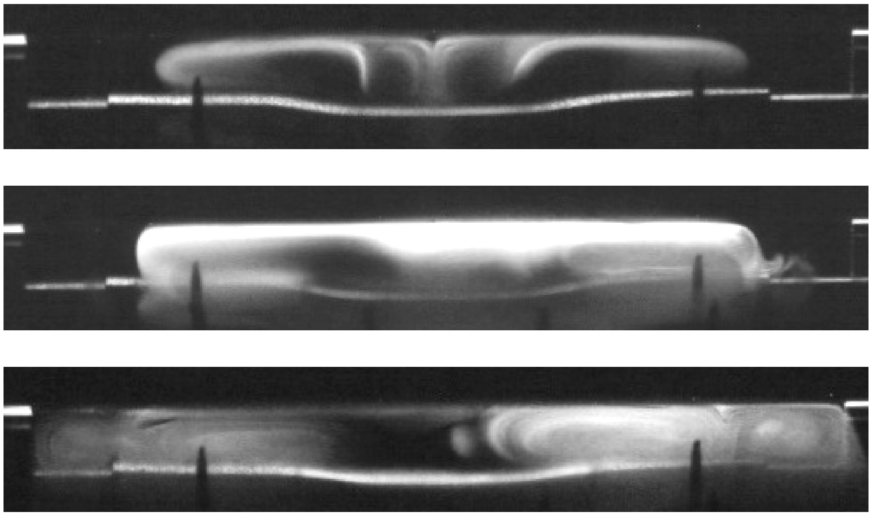

Figure 3.20 Flow Visualization of 9.5 mm (3/8 in.) Air Gap After (From Top to Bottom) 1 s, 3 s, and 10 s of Exposure

Flow visualization photographs of the smallest gap spacing tested are shown in Figure 3.20. In this case, a decrease in the strength of the convection cells was observed. There is a strong cell present, but it is relatively small compared to the larger air gap spaces. This cell occurs in the very center of the enclosure, where the heat flux is applied, and is visible in the top photograph. Away from the center the motion decreases rapidly. The air barely moves only a small distance away from the heat source and is almost completely stagnant in the region near the sidewalls. This is the first evidence we see that conduction heat transfer occurs in smaller air gaps.

This phenomenon also alerts us to the most important difference between this case and the idealized Rayleigh case discussed in Section 1.2. In the ideal case, the temperature of a plate is uniform. In this experiment however, the heating is localized and the temperature variations are large.

3.3 Rayleigh Number Histories

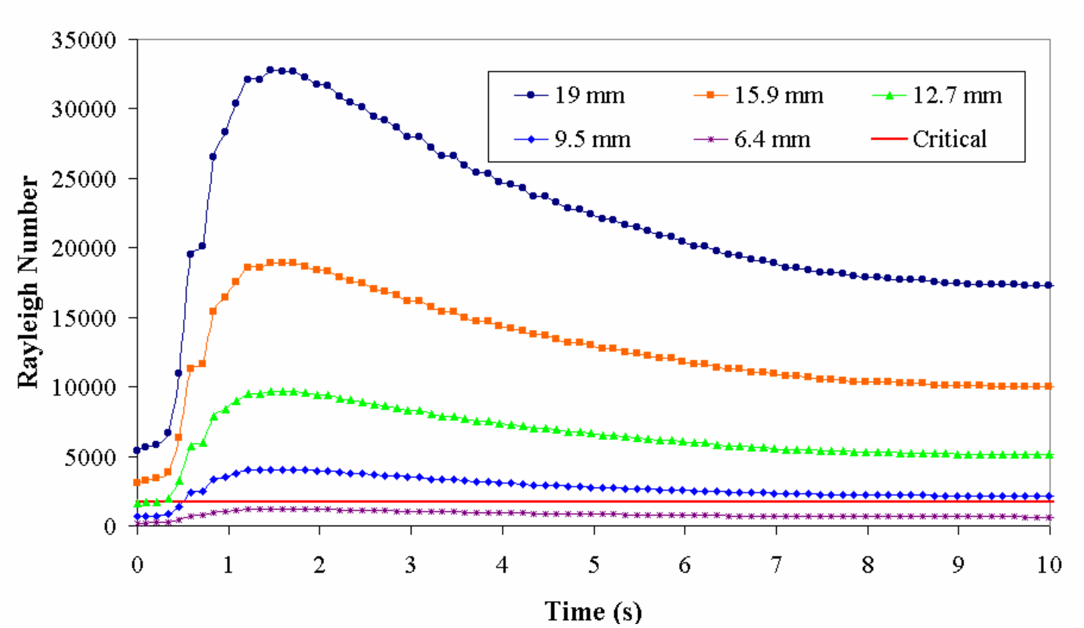

Figure 3.21 Rayleigh Number Histories for Various Air Gap Sizes

The Rayleigh number ties both sets of experiments together in a dimensionless form. As discussed in Section 1.2, the Rayleigh number is a relative measure of the buoyant forces to the viscous forces in a fluid. If this dimensionless ratio is less than 1708, which is the critical Rayleigh number for a horizontal enclosure, then convection cells are expected to develop.

The Rayleigh number histories for the air gap sizes investigated are shown in Figure 3.21. The midpoint temperature of the steel shim stock was used to calculate the Rayleigh number. Therefore, this is more of a localized Rayleigh number history, for the center of the heated portion of the enclosure.

In the air gaps of 9.5 mm (3/8 in.) and larger, the Rayleigh number was greater than the critical number necessary to produce convection cells. This is consistent with the observations made during these flow visualization experiments since convection cells were witnessed. However, for the air gap of 6.4 mm (1/4 in.) and smaller, the Rayleigh number is smaller than the critical number. Therefore, the buoyant forces are too small to overcome the viscous forces in the enclosure and no air movement should occur. Although flow visualization was not performed for the air gaps of 6.4 mm (1/4 in.) and smaller in this study, this behavior is consistent with observations made in previous flow visualization experiments performed by Torvi [2].

3.4 Supplementary Study on the Influence of the Heat Flux Magnitude

In addition to the flow visualization and temperature measurements conducted to aid in the development of the new numerical model, additional experiments were performed using a heat flux of 60 kW/m^2 in order to ascertain the influence of the heat flux supplied by the Meker burner [25].

The heat flux from the Meker burner was reduced from the test standard 80 kW/m^2 to 60 kW/m^2 and similar temperature measurements and flow visualization experiments were performed. The midpoint temperature histories that were observed using the two heat fluxes are compared in Figure 3.22.

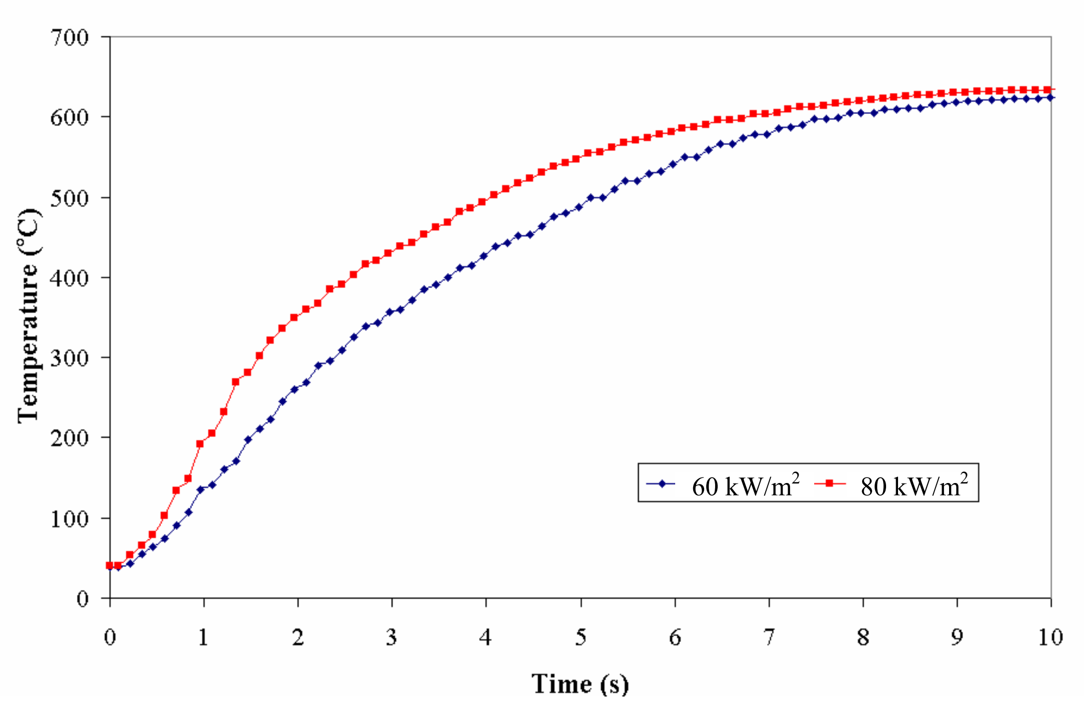

Figure 3.22 Midpoint Temperature History for Different Heat Fluxes

The temperature history comparison indicates that the steady state temperature of the center of the heated region was similar using both heat fluxes, however, the temperature rose much more quickly in the 80 kW/m^2 case. Since the temperature of the flame is the same in both cases, it seems logical that the steady state temperatures would be the same.

Sketches of the flow visualization experiments at approximately 5 s after the end of the 10 s exposures are shown in Figure 3.23. There was very little difference between the patterns that developed when changing the heat flux from 80 kW/m^2 to 60 kW/m^2. Since the temperature difference between the top and bottom plates of the enclosure was similar for both heat fluxes, the Rayleigh numbers should also be very similar. However, in the smallest air gap of 9.5 mm (3/8 in.), there was a noticeable difference in the flow patterns caused by the two heat fluxes after the exposure ended. In the 60 kW/m^2 case, larger cells extending throughout the enclosure did not form. This is because the Rayleigh numbers were only slightly larger than the critical value required to produce convection cells. Therefore, even though the temperature histories are similar, the difference is large enough to produce a noticeable effect in the case of the smallest air gap.

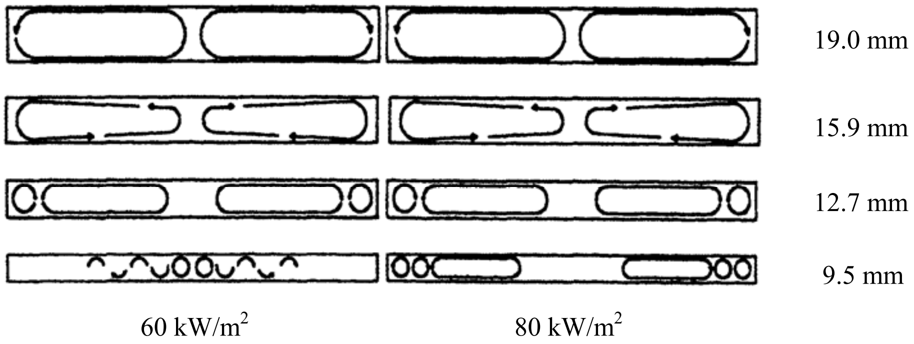

Figure 3.23 Comparison of the Steady Flow Patterns for Two Heat Fluxes (15 s)

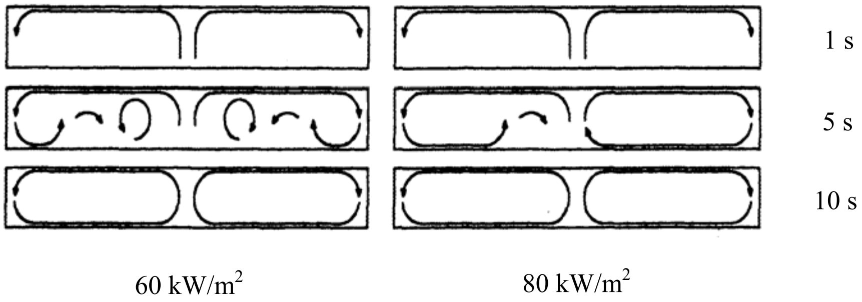

Figure 3.24 Comparison of the Flow Pattern Development for Two Heat Fluxes Using a 19.0 mm (3/4 in.) Air Gap

In addition to the sketches of the flow patterns in each of the air gaps after the end of the exposure, Fig. 3.24 shows the development of the flow patterns throughout the exposure for the 19.0 mm (3/4 in.) air space. As previously seen, the steady state flow patterns were very similar for both heat fluxes. However, the convection cells were almost fully developed at 5 s when using the 80 kW/m^2 heat flux, but were still developing at 5 s when using the 60 kW/m^2 heat flux. Therefore, the magnitude of the heat flux affected the transient period in the development of the convection cells but not the steady state flow patterns.

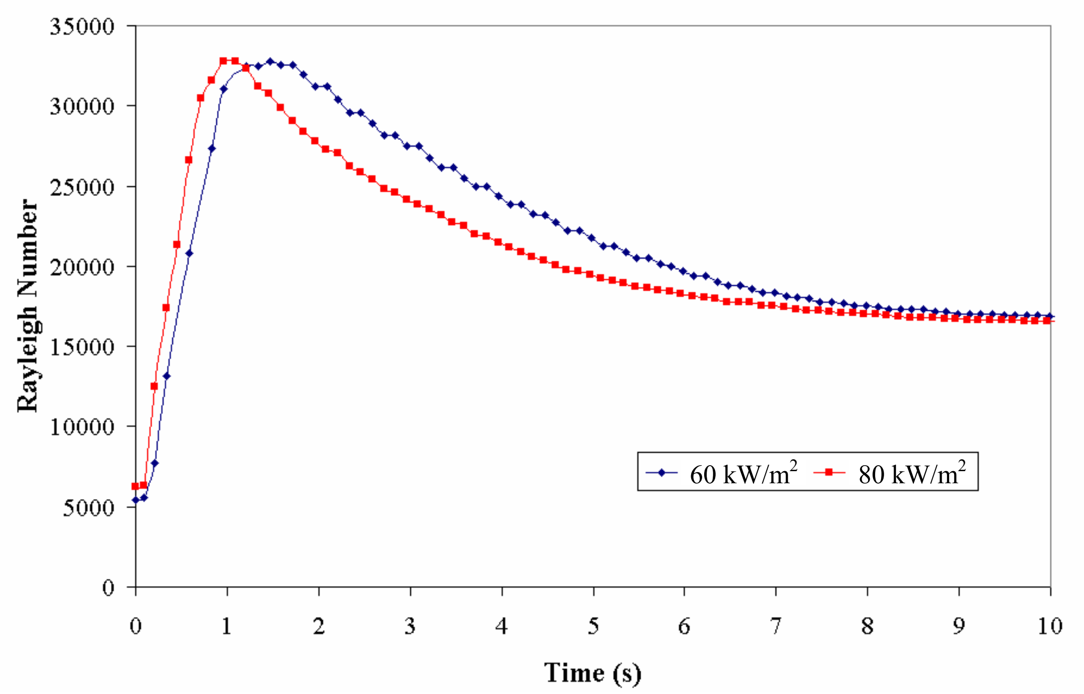

Figure 3.25 Rayleigh Number Histories for Two Heat Fluxes

The temperature histories in Figure 3.22 were used to produce the Rayleigh number histories shown in Figure 3.25 for a 19.0 mm (3/4 in.) air gap. The trends are similar during the end of the exposure but the transient periods are different. The Rayleigh numbers peak more quickly when using the larger heat flux as the Rayleigh number peaks at 0.7 s for 80 kW/m^2 and 1.6 s for 60 kW/m^2. This explains why the convection cells developed more quickly in the case of 80 kW/m^2, even though the maximum temperatures reached were similar.

A difference in transient behavior but similarity in steady state behavior was witnessed in both the temperature measurements and flow visualization results, which supports the use of the Rayleigh number to predict convective motion.

3.5 Results - Times to Exceed Stoll Criterion

A number of tests were conducted to obtain the time required to exceed the Stoll criterion for a number of air gap sizes. The results of these tests are shown in Figure 3.26 and Figure 3.27 for the lightly painted steel shim stock samples and for the Kevlar®/PBI fabric samples, respectively. The general results of these tests show that as the air gap increases, it takes longer for the Stoll criterion to be exceeded or for a second-degree burn to occur. However, there is a large amount of scatter observed for the shim stock tests at the smallest air gap size of 3.2 mm (1/8 in.). This is due to the thermal expansion of the steel. As the shim is heated it expands, as it expands it buckles in the heated region due to a restriction of movement by the mounting pins. If it buckles upwards, the shim makes direct contact with the test sensor and a very small time is predicted for a second-degree burn. If it buckles down, then the air gap increases by as much as 100% or 3.2 mm (1/8 in.). This air gap variation of 3.2 mm (1/8 in.) is also consistent for the larger air gaps tested.

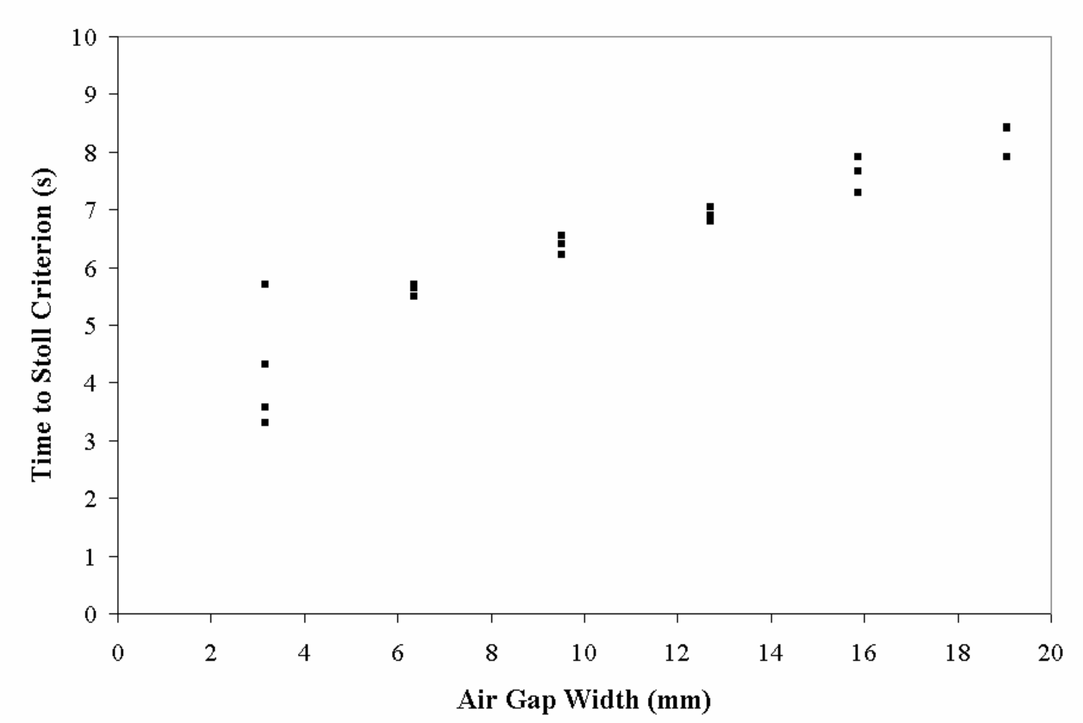

Figure 3.26 Times to Exceed Stoll Criterion (Steel Shim Stock)

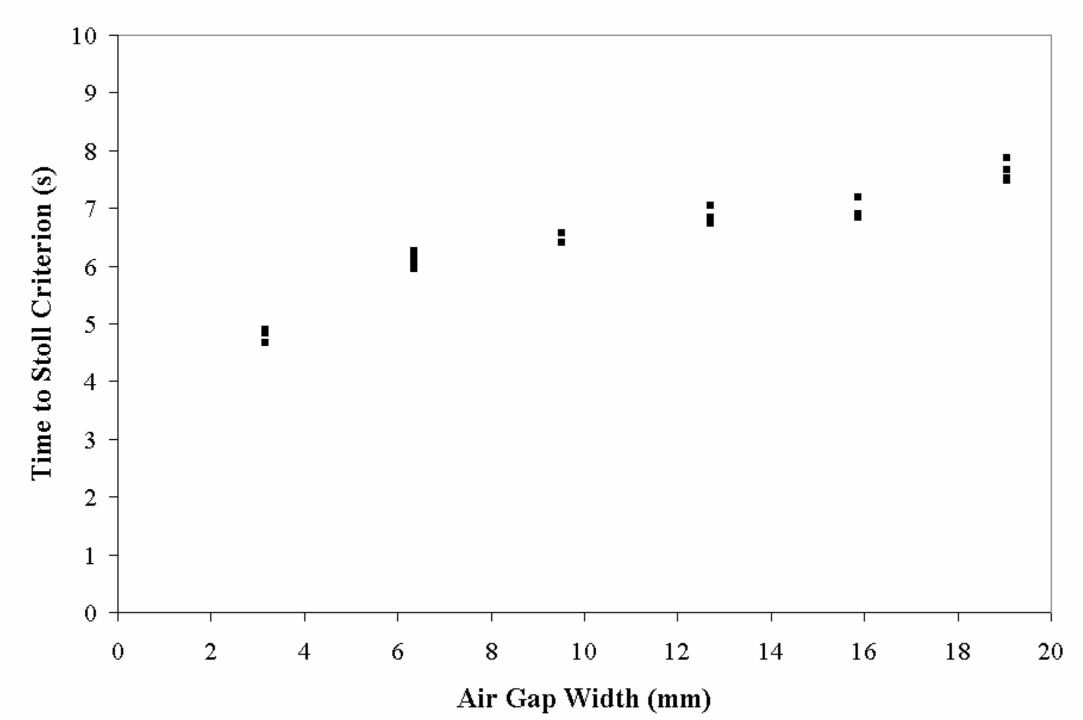

Figure 3.27 Times to Exceed Stoll Criterion (Kevlar®/PBI)

3.6 Chapter Summary

In this chapter, the results of all the experiments conducted in this study were presented and discussed. These results include temperature measurements of the bottom boundary when heating steel shim stock and Kevlar®/PBI specimens as well as flow patterns observed during the flow visualization experiments. Furthermore, times to second-degree burns predicted by the Stoll Criterion were presented that were calculated using experimental data. The implications of the results from these experiments on the development of the new model will be presented in Chapter 4.

CHAPTER 4 NUMERICAL MODEL

In this chapter, the numerical model is presented and discussed. The boundary conditions implemented in the new model, as a result of the experiments performed, are introduced. Specific details are presented for the various aspects of the model such as view factor calculations and the treatment of the different modes of heat transfer within the enclosure. An overview of the model is shown, including a flow chart of the major sections. Finally, model output variables are discussed.

Figure 1.4 is shown again here as Figure 4.1 in order to illustrate the portion of the bench top apparatus that is to be numerically modeled. This work concentrated on the heat transfer from the heated specimens to the test sensor. In the new model, the temperature distribution along the bottom boundary is considered to be known and the temperature of the test sensor is calculated.

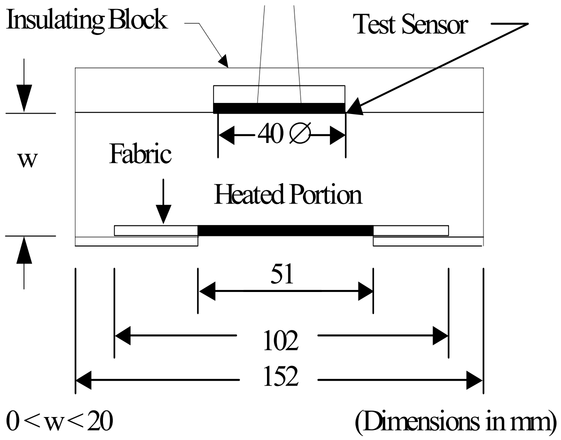

Figure 4.1 Dimensioned Drawing of the Bench Top Testing Apparatus

4.1 Influence of Experiments on the Development of New Model

In Chapter 3, the complexity of the boundary conditions found in the bench top testing of thermal protective fabrics was presented. Several experiments were performed to establish the temperature of the bottom boundary of the enclosure, both spatially and temporally. As seen in Figures 3.7 and 3.14, there are large spatial variations in the temperature across the bottom boundary. Figures 3.2 and 3.9 demonstrate the extent of the temporal variations of temperature that can occur in these tests.

4.1.1 Influence of Temperature Measurements

After establishing the complexity of the boundary conditions in this apparatus, it was decided to treat the heat transfer within the enclosure two-dimensionally instead of one-dimensionally as was previously done. This meant representing the bottom boundary of the enclosure with a number of elements instead of just one. The distribution, size and shape of these elements needed to be determined. By investigation of the photographic and video evidence, particularly the photographs in Figure 3.16, the shape and location of the elements were chosen. Concentric square elements were to be used to make up the bottom boundary or the specimen holder and shim/fabric. Figure 4.2 shows an isometric view of the bottom boundary of the enclosure and how these elements are arranged.

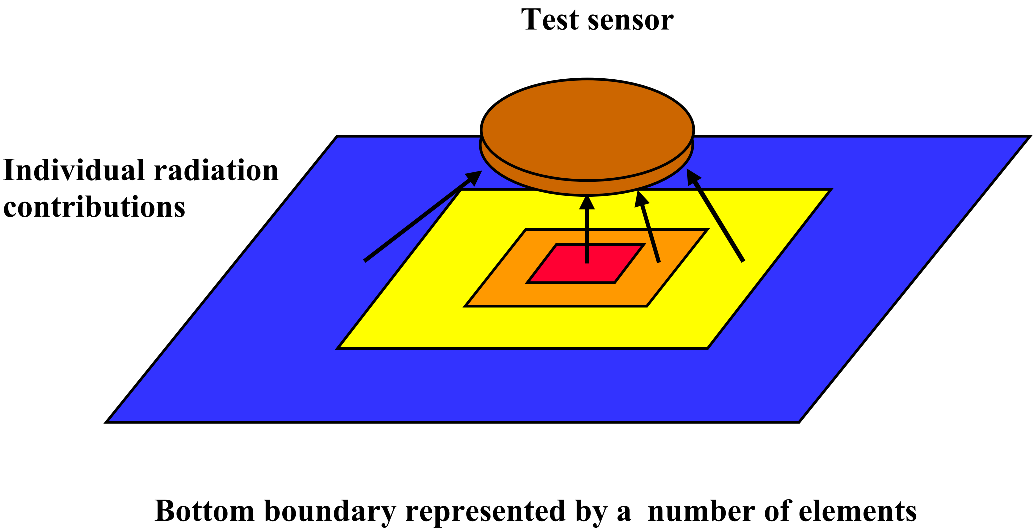

Figure 4.2 Isometric View of the Two-Dimensional Elements in the New Model

Four elements are shown in Figure 4.2, however the number of elements required to properly represent the spatial variation in temperature of the bottom boundary are yet to be presented. Four elements are used here to describe the basic premise of how the elements will be used in the model.

The idea is that each element in the model will have a temperature history curve assigned to the area that the element represents. This temperature history and area is based on the experimental results presented in Chapter 3. All heat transfer across the air gap is calculated using the temperature information that is assigned to these elements.

4.1.2 Influence of Flow Visualization

As witnessed during the flow visualization experiments, the fluid motion within the air gap was affected by the size of the gap itself. In the larger air spaces, 12.7 mm (1/2 in.) and up, the convection cells filled the entire enclosure. However, in the smaller air gaps, the convection became more of a localized phenomenon located directly over the heated portion of the specimen. This information was useful in the model development because it offered a more detailed way of calculating the convection heat transfer. In the previous model, an empirical correlation was used to calculate the Nusselt number. This correlation, shown in Equation 4.1, was based on experiments that measured the convection heat transfer between two large, isothermal, horizontal plates [21].

$$Nu = \frac{h_{\text{gap}} w}{k} = 1 + 1.44\left[1 - \frac{1708}{Ra}\right]^{\bullet} + \left[\left(\frac{Ra}{5830}\right)^{\frac{1}{3}} - 1\right]^{\bullet} \tag{4.1}$$

where Nu = Nusselt number (dimensionless)

h_{gap} = convection heat transfer coefficient ($\text{W/m}^2\cdot\text{K}$)

w = size of the air gap (m)

k = thermal conductivity of the fluid (W/m·K)

Ra = Rayleigh number (dimensionless)

In this equation, the notation $[\ ]^{\bullet}$ indicates that if the argument within the square brackets is negative, then the value should be taken as zero.

The equation for the Rayleigh number, Ra, was presented in Equation 1.1 and is repeated here.

$$Ra = \frac{g\beta(T_2 - T_1)w^3}{\alpha\nu} \tag{4.2}$$

where g = acceleration due to gravity (9.81 m/s^2)

β = volumetric expansion coefficient of the fluid (1/K)

α = thermal diffusivity of the fluid (m^2/s)

ν = kinematic viscosity of the fluid (m^2/s).

The main difference between the previous model and the new model in the treatment of the convection is the idea of a more localized treatment. The previous model had one temperature for the surface of the shim/fabric and one temperature for the surface of the copper disc test sensor. These two temperatures were used to calculate a temperature difference across the air gap and this temperature difference was used to calculate a Rayleigh number. This Rayleigh number was used in Equation 4.2 to calculate the Nusselt number and thus the convection heat transfer across the enclosure was obtained.

However, the new model benefits from the use of more boundary elements. Now, an area-weighted average of the elements can be used to determine a temperature difference across the enclosure. In the smaller air gaps the convection cells are more localized, thus, the central elements that represent only the heated portion of the specimen can be used to calculate a temperature difference across the enclosure. However, for the larger air gap sizes, where the convection cells are larger and more mixing occurs within the enclosure, more of the elements can be used in the calculation of a temperature difference. An explanation of how this method is implemented is shown in Section 4.4.

4.2 Overview of the Model Operation

The model is based on the assumption that a transient can be modeled using a quasi-steady state methodology as long as the time steps are small enough to capture the physics of the problem. In this model, the temperature map of the bottom boundary is input via a number of elements and then the heat transfer from this bottom boundary, across the finite air gap, to the copper calorimeter is calculated. The model was written as a Fortran77 code, which appears in its entirety in Appendix A for both the steel shim stock and the Kevlar®/PBI materials.

4.2.1 Element Temperatures

The element temperatures are specified from the experimental data as an input to the model. Figure 4.3 indicates how this was achieved using the experimental data. The experimental data was plotted as temperature in degrees Kelvin over the time of the exposure. Absolute temperatures were used here for convenience since they are necessary in the new model when calculating the radiation heat transfer rates. Once a temperature history curve was generated in

Microsoft® Excel, a sixth-order polynomial curve-fit trend line was added to the chart. A sixth-order curve fit was necessary in order to keep the errors involved to a minimum. The equation of the trend-line was extracted and compared with the experimental data in Figure 4.3.

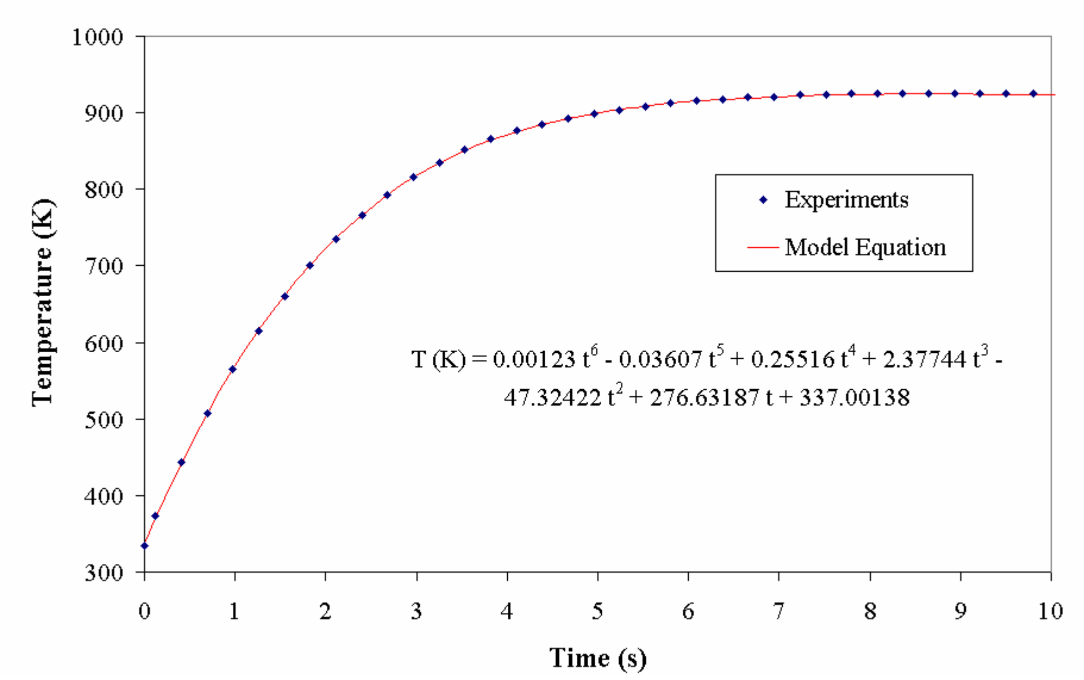

Figure 4.3 Element Temperature Equation for Point 4 Using Steel Shim Stock

As is clearly evident, the equation sufficiently approximates the experimentally determined temperature history. The error in absolute temperature between the two data sets is less than 0.1%. The equation used for the midpoint of the steel shim is

$$T(K) = 0.00123t^6 - 0.03607t^5 + 0.25516t^4 + 2.37744t^3 - 47.32422t^2 + 276.63187t + 337.00138 \quad (4.3)$$

where T = element temperature (K)

t = time into exposure (s).

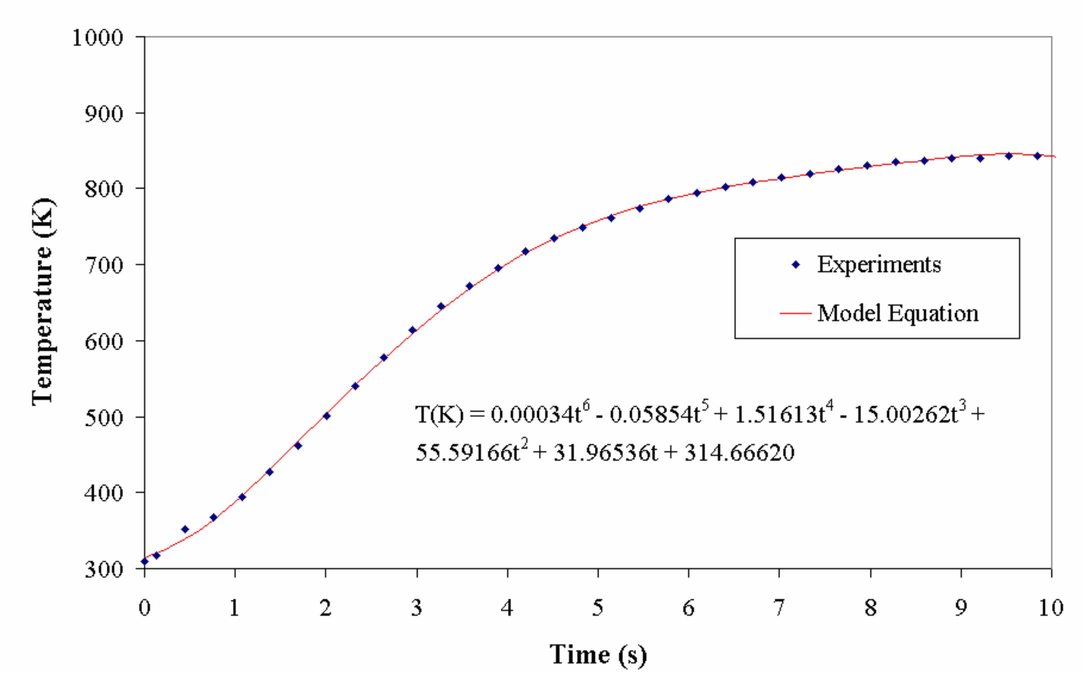

Figure 4.4 Element Temperature Equation for Point 4 Using Kevlar®/PBI

A similar figure showing the equation development for the midpoint of Kevlar®/PBI is shown above. The equation found using this process is provided in Equation 4.4.

$$T(K) = 0.00034t^6 - 0.05854t^5 + 1.51613t^4 - 15.00262t^3 + 55.59166t^2 + 31.96536t + 314.66620. \quad (4.4)$$

The error in absolute temperature between the two data sets is less than 1.0%. This process for determining temperature equations was repeated for all of the experimental data points for both the steel shim stock and the Kevlar®/PBI.

4.2.2 Elements Used in Steel Shim Model

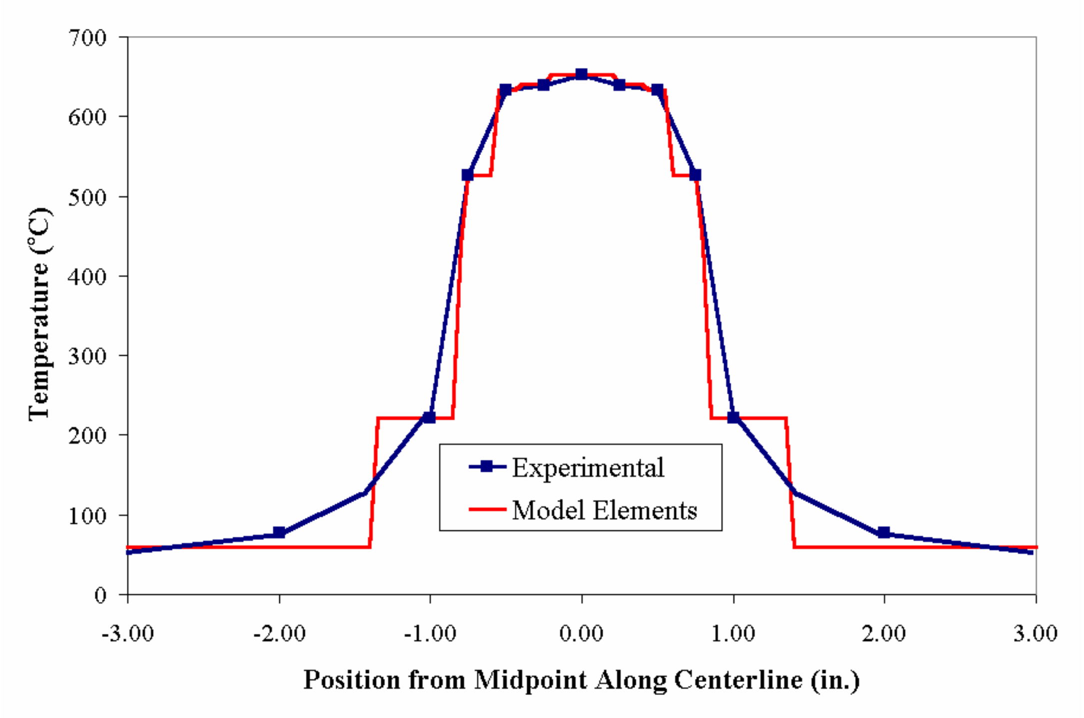

Figure 4.5 Element Sizes and Maximum Temperatures at t = 10 s for Steel Shim Model (Seven Elements Used)

After reviewing Figures 3.6 and 3.7, it was decided that seven elements would be used to represent the bottom boundary of the enclosure when using steel shim stock. The element size was chosen such that when comparing the maximum temperature maps of the bottom boundary for the experimental data and for the model elements, the difference was minimized. An example comparison is shown in Figure 4.5. In this figure, the areas under the curves are very similar, since the element profile was generated to match the experimental data as close as possible. Mathematically, if piecewise approximation were used to represent a function, more elements would provide a more accurate representation. However, without more refined experimental data, the use of more elements would be strictly speculation.

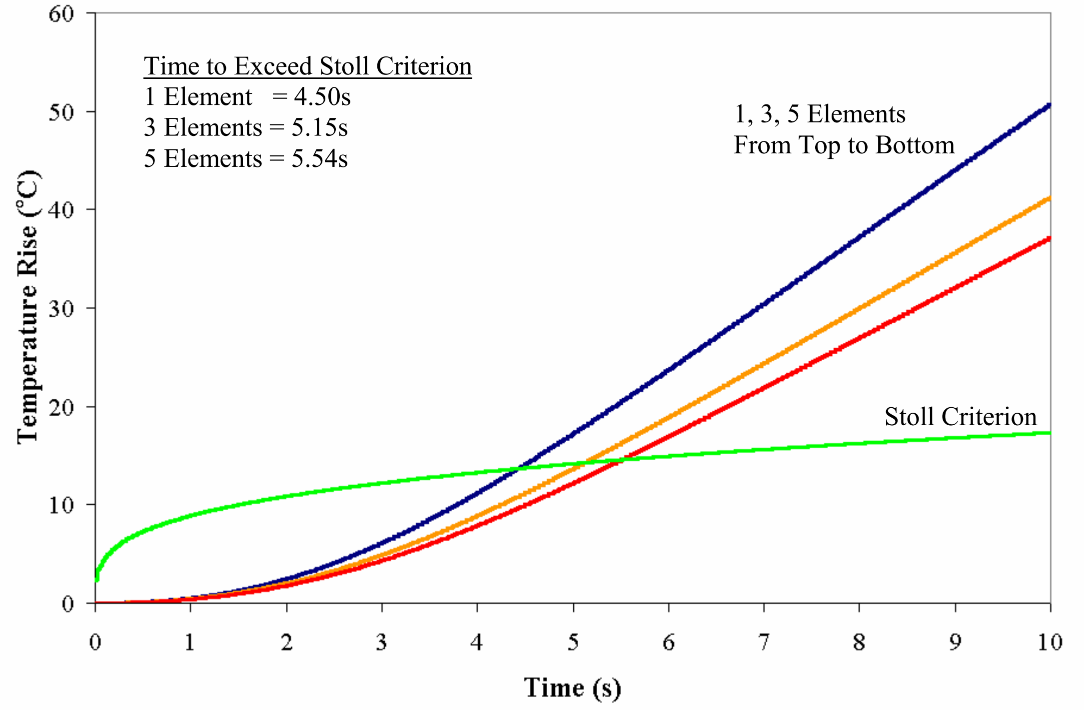

Figure 4.6 Comparison of Using One Element and Multiple Elements to Model the Heated Region of Steel Shim Stock

Figure 4.6 is included to demonstrate the effect of using five elements instead of just one element to model the heated region of the steel shim stock specimens. The temperature of the copper disc test sensor rises more quickly when using only one element because the temperature history used for this element was determined by measuring the center of the heated region (Point 4) or the hottest location. However, when five elements were used, relatively cooler locations were taken into account in the model. The difference in Stoll times as shown in this comparison is 23.1%, which indicates that the multi-dimensional treatment of the bottom boundary has a large influence on the predicted Stoll times from the model. Note that this modeling comparison was made using only the heated region of the specimens. Thus, the results do not coincide with the fully developed model.

4.2.3 Elements Used in Kevlar®/PBI Model

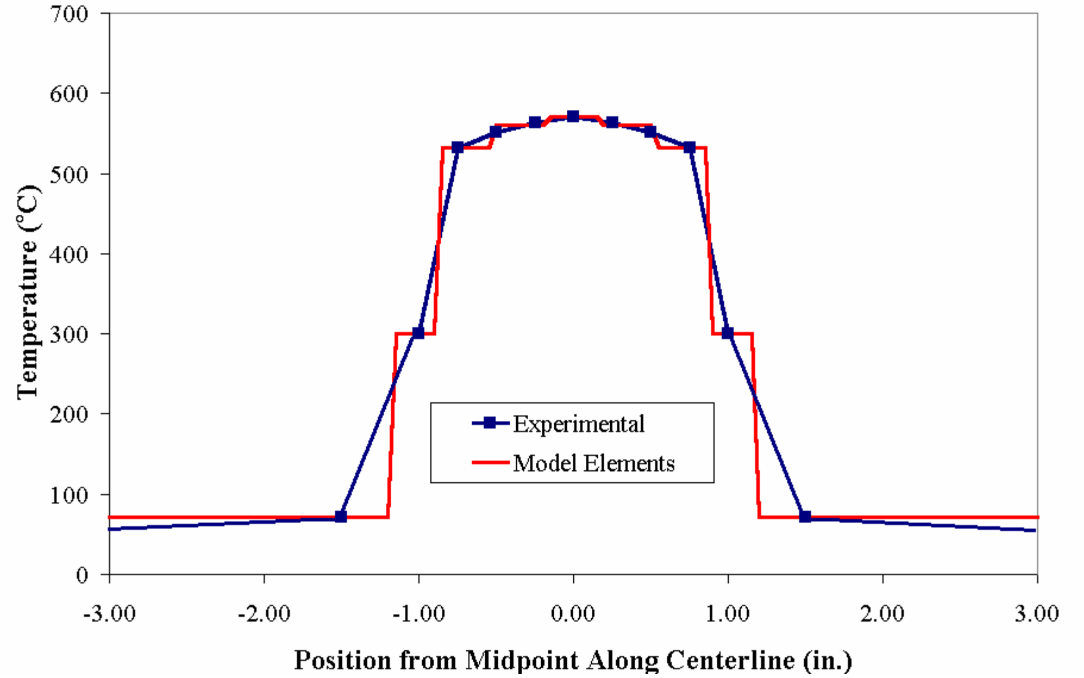

Figure 4.7 Element Sizes and Maximum Temperatures at t = 10 s for Kevlar®/PBI Model (Five Elements Used)

The procedure previously outlined for determining the number of, size, and temperature of the elements required in the model for shim stock is repeated here for the fabric, Kevlar®/PBI. Figures 3.13 and 3.14 were studied in order to approximate the proper element characteristics. However, the spatial variations in temperature of the fabric were smaller than in the steel shim stock case. Thus, only five elements were required to model the bottom boundary conditions of the bench top apparatus when using Kevlar®/PBI. The size and maximum temperatures of these five elements are shown in Figure 4.7, where they are compared with experimental data for the identical contour across the boundary.

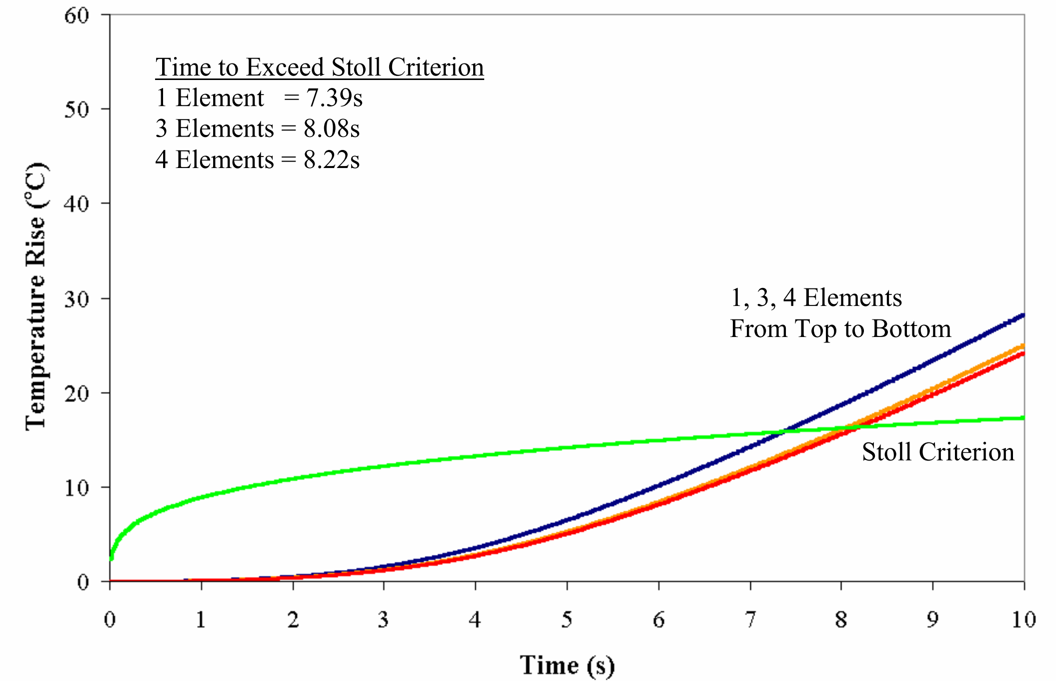

Figure 4.8 Comparison of Using One Element and Multiple Elements to Model the Heated Region of Kevlar®/PBI

As was done in Figure 4.6, Figure 4.8 is included to demonstrate the effect of using multiple elements instead of just one element to model the heated region of the Kevlar®/PBI specimens. Once again, the temperature of the copper disc test sensor rises more quickly when using only one element because the temperature history used for this element was determined by measuring the center of the heated region (Point 4) or the hottest location. However, when four elements were used, relatively cooler locations were taken into account in the model. The difference in Stoll times as shown in this comparison is only 11.2% compared to the difference of 23.1% in the steel shim stock case, which indicates that the multi-dimensional treatment of the bottom boundary has less of an influence on the predicted Stoll times when using Kevlar®/PBI because of the smaller temperature variations across the back surface of the fabric.

4.3 Treatment of Radiation

The radiation and convection heat transfer modes were treated independently in this model, as is commonly done. Chapman [26] states that when the convective fluid surrounding a surface is radiatively non-absorbing and non-emitting, one may treat the convection and radiation mechanisms as independent. Since the exact composition of the fluid is unknown, due to combustion products introduced by the burning of the fabrics, it is very difficult to determine the extent of the participation of this media. Therefore, for this work, the fluid was assumed non-participating.

The new model assumes a quasi-steady state treatment of the bench top test. Therefore, at a given time step, the radiation heat transfer from the bottom boundary to the test sensor must be calculated. However, as shown in Section 4.2, the bottom boundary is composed of a number of elements. Thus, the radiation heat transfer rate from these elements to the test sensor must be calculated. This was performed in the model using the following equation for the radiation heat transfer between two gray surfaces [27].

$$q_{12} = \frac{\sigma\left(T_1^4 - T_2^4\right)}{\dfrac{1-\varepsilon_1}{A_1\varepsilon_1} + \dfrac{1}{A_1F_{12}} + \dfrac{1-\varepsilon_2}{A_2\varepsilon_2}} . \tag{4.5}$$

where q_{12} = heat transfer rate to the test sensor (W)

σ = Stefan-Boltzmann constant (5.67 x 10^{-8} W/m^2·K^4)

T = absolute temperature of each surface (K)

A = area of each surface (m^2)

ε = emissivity of the surface (dimensionless)

F_{12} = radiation view factor from surface one to two

Here, surface 1 is an element of the bottom boundary and surface 2 is the copper disc test sensor.

The temperature of the test sensor from the previous time step and the current element temperature are used to calculate the radiation heat transfer at each time step. The element temperatures are calculated using the equations developed earlier (e.g., Equation 4.3) and the current time of the model.

The view factors between surfaces do not change over the course of a test and therefore are calculated before the main loop of the program begins at time equal to zero in the model. The view factor for each element had to be calculated by integrating the following equation over the surface of a square of the desired element size.

$$F_{(d1)2} = \frac{1}{2}\left(1 - \frac{1 + C^2 - B^2}{\sqrt{C^4 + 2C^2\left(1 - B^2\right) + \left(1 - B^2\right)^2}}\right) \tag{4.6}$$

where B = the ratio between the radius of the finite circular area and the distance between the two surfaces, and

C = the ratio between the distance from a point in the differential area to the central normal to the circular area, and the distance between the two surfaces (see Figure 31-3 in Jakob [28]).

The equation shown is for the view factor between two plane parallel surfaces, one of differential area and the other of finite area having a circular shape [28]. This equation had to be numerically integrated over the surface of each element in order to obtain the view factor necessary for the radiation heat transfer calculations. This was performed in a sub-routine of the program using Gaussian quadrature formulation and 16 Gauss points. The use of this many Gauss points may seem excessive, however, this number of points was found to produce the highest accuracy when solving known test cases and did not significantly increase the computation time of the model.

4.4 Treatment of Convection

Section 4.1.2 explained the theory used in this model to treat the convection heat transfer as more of a local phenomenon than the previous model. However, there are some important calculations within the model used to determine the convection heat transfer from the bottom boundary of the bench top enclosure to the copper disc test sensor, that are presented in this section. These topics are: the calculations used to account for variable fluid properties of the air in the enclosure as a function of temperature, and the smoothing of the transitions from one localized convection cell area to another within the model to eliminate discontinuities.

There are various material properties of the enclosed air that are used in Equations 1.1 and 4.1 to calculate the Rayleigh number and Nusselt number respectively. These properties, which are a function of temperature, are the kinematic viscosity, thermal diffusivity, and thermal conductivity. Due to the nature of the bench top test, there are large temperature variations present over the duration of an exposure (e.g., Figure 3.10). If the changes in the material properties are not accounted for, the introduced errors are very significant [2]. For example, Figure 4.9 shows the thermal diffusivity of air as a function of absolute temperature and the equation used in the model to account for these variations. The error between the equation and the tabulated data is less than 2.5%.

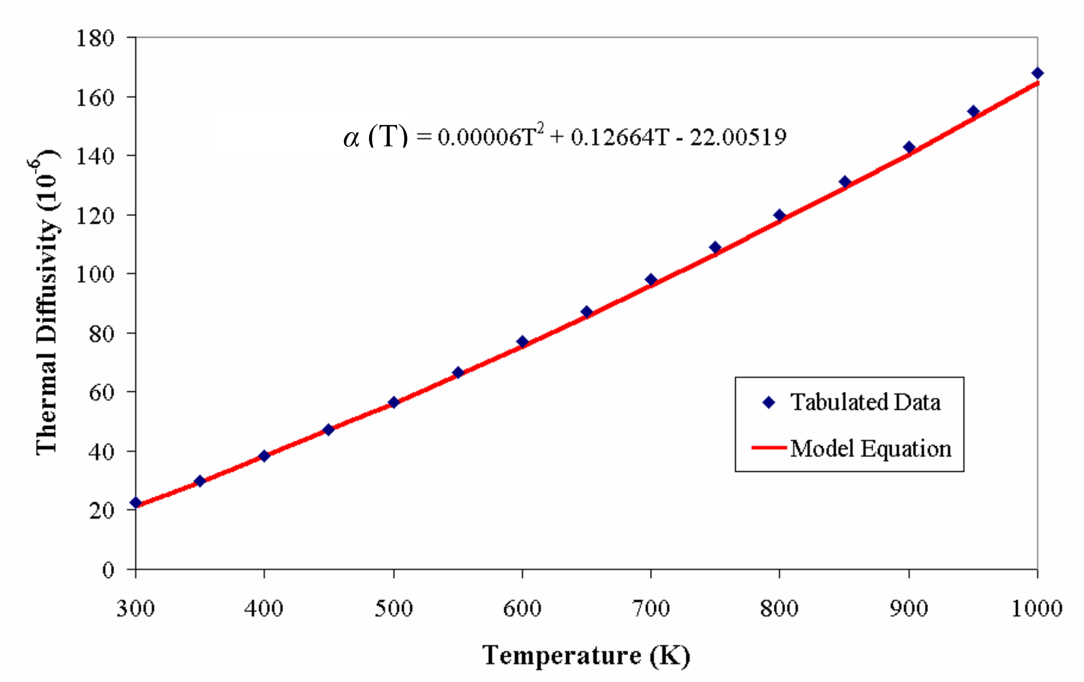

Figure 4.9 Variation of Thermal Diffusivity of Air with Temperature

The equations used in the model for the various material properties of air and copper are:

$$\alpha = 0.00006T^2 + 0.1266T - 22.005, \tag{4.7}$$

$$k = -0.0000266T^2 + 0.019437T + 1.41926, \tag{4.8}$$

$$v = 0.00007T^2 + 0.0607T - 9.0061, \tag{4.9}$$

$$c = 1.35(10)^{-7}T^3 - 0.000287T^2 + 0.27997T + 322.83, \tag{4.10}$$

where α = thermal diffusivity of air (m^2/s)

k = thermal conductivity of air (W/m·K)

v = kinematic viscosity of air (m^2/s)

c = specific heat of copper (J/kg·°C)

The area over which the convection cells occur in these bench top enclosures was shown in Chapter 3 to vary with the use of different air gap sizes. This phenomenon has been incorporated into the new model with the idea of calculating a localized convection area as a function of the air gap size. This idea is expressed in Figure 4.10.

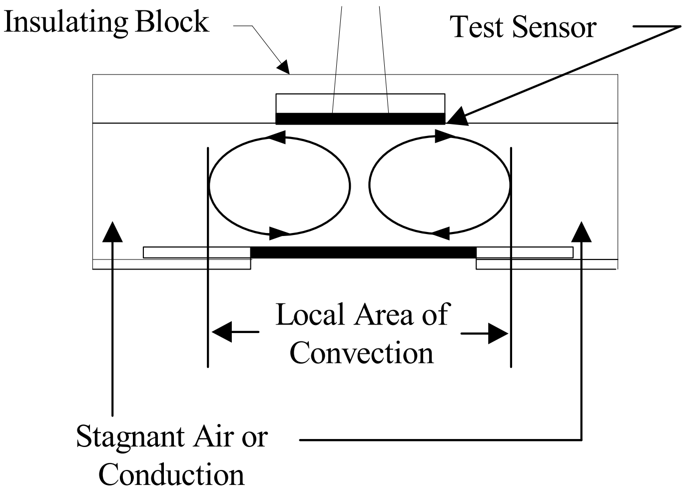

Figure 4.10 Schematic of the Localized Convection Treatment

Now the convection correlation, Equation 4.1, is calculated using temperatures that are weighted averages over the area of convection determined experimentally. The air gap widths of 9.5 mm (3/8 in.), 12.7 mm (1/2 in.), 15.9 mm (5/8 in.), and 19.0 mm (3/4 in.) have convection areas of 40.6 mm by 40.6 mm (1.6 in by 1.6 in.), XX mm by XX mm (YY in. by YY in.), XX mm by XX mm (YY in. by YY in.), and 152 mm by 152 mm (6 in. by 6 in.) respectively.

If there is an area where conduction heat transfer occurs, as in the outer portion of the enclosure shown in Figure 4.10 where the air is stagnant, then this area is of no consequence to the model since only the heat transfer to the test sensor is calculated.

Since there are only discrete points tested, i.e. the four air gap sizes investigated during the flow visualization study, the effects on the model would result in discontinuities in the predicted results. Therefore, a linear interpolation was incorporated into the model, which utilizes the information gathered at the discrete flow visualization air gap sizes, to predict the area over which the convection cells should occur for air gap sizes in between those investigated.

4.5 Test Sensor

The previous two sections dealt with the radiation and convection heat transfer to the copper disc test sensor, however, there is heat transfer that occurs from the sensor to the surroundings. The absolute temperature of the test sensor does not become much hotter than those of the surroundings, especially when compared with the bottom boundary of the enclosure that literally becomes red-hot. For example, during a typical test, the test sensor will not become hotter than 340 K (~ 67˚C). Therefore, the heat loss from the test sensor can be modeled using the form of a first-order difference in temperatures (T_1 - T_2) instead of a fourth-order difference in absolute temperatures (T_1^4 - T_2^4). Based on previous research [2] a cooling coefficient of 25 W/m^2·K was determined. Therefore, the same cooling coefficient has been implemented in this model and the heat loss from the test sensor is calculated as

$$Q_{losses} = 25A_{disc}\left(T_{disc} - T_{amb}\right). \tag{4.11}$$

The test sensor is treated in a quasi-steady state fashion identical to the rest of the model. Figure 4.11 shows a schematic of the heat transfer to and from the copper disc test sensor.

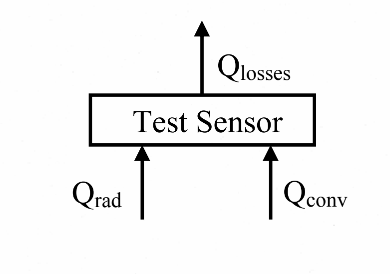

Figure 4.11 Schematic of the Heat Transfer to the Test Sensor

After the radiation, convection, and heat loss rates have been calculated in the model, a net heat flux to the copper disc test sensor is calculated at each time step using the equation

$$Q_{net} = \sum Q_{rad}(j) + Q_{conv} - Q_{losses} \qquad (4.12)$$

where

Q_{net} = net heat rate to test sensor (W)

$$Q_{rad}(j) = \frac{\sigma\left(T_{fab(j)}^4 - T_{disc}^4\right)}{\dfrac{1-\varepsilon_{fab(j)}}{A_{fab(j)}\varepsilon_{fab(j)}} + \dfrac{1}{A_{fab(j)}F_{12}} + \dfrac{1-\varepsilon_{disc}}{A_{disc}\varepsilon_{disc}}} \qquad (4.5)$$

$$Q_{conv} = h_{gap}A_{disc}\left(T_{fab} - T_{disc}\right) \qquad (4.13)$$

$$Nu = \frac{h_{gap}w}{k} = 1 + 1.44\left[1 - \frac{1708}{Ra}\right]^{\bullet} + \left[\left(\frac{Ra}{5830}\right)^{\frac{1}{3}} - 1\right]^{\bullet} \qquad (4.1)$$

$$Q_{losses} = 25A_{disc}\left(T_{disc} - T_{amb}\right) \qquad (4.11)$$

Note that Eqn. 4.13 becomes conduction heat transfer if the Nusselt number is unity.

A lumped capacitance method is used to determine the appropriate temperature rise of the test sensor over the duration of the time step used. This first-order explicit calculation is shown in Equation 4.13 and takes the form

$$T_{(i+1)} = T_{(i)} + \frac{Q_{net}(i)\left(t_{(i+1)} - t_i\right)}{cm_{disc}} \tag{4.13}$$

where c is the specific heat and m is the mass of the copper disc test sensor. The Biot number was much smaller than 0.1 (less than 0.001), which is the accepted criterion for using the lumped capacitance method and thus validated this treatment.

4.6 The Computer Program (Fortran 77)

A flow chart of the logical arguments and steps through the program is shown in Figure 4.12. The following is a brief description of these operations.

The first operation performed in the model is the initialization of the various variables such as the area and emissivity of the elements, the size of the air gap, and the duration of the exposure. The next step in the model is the calculation of certain variables that will not change over the course of an exposure. An example of these variables is the view factor from an element to the copper disc test sensor. Now the main loop of the program begins and continues until the time of the model exposure exceeds the preset exposure time initialized at the beginning of the program (e.g., 10 s).

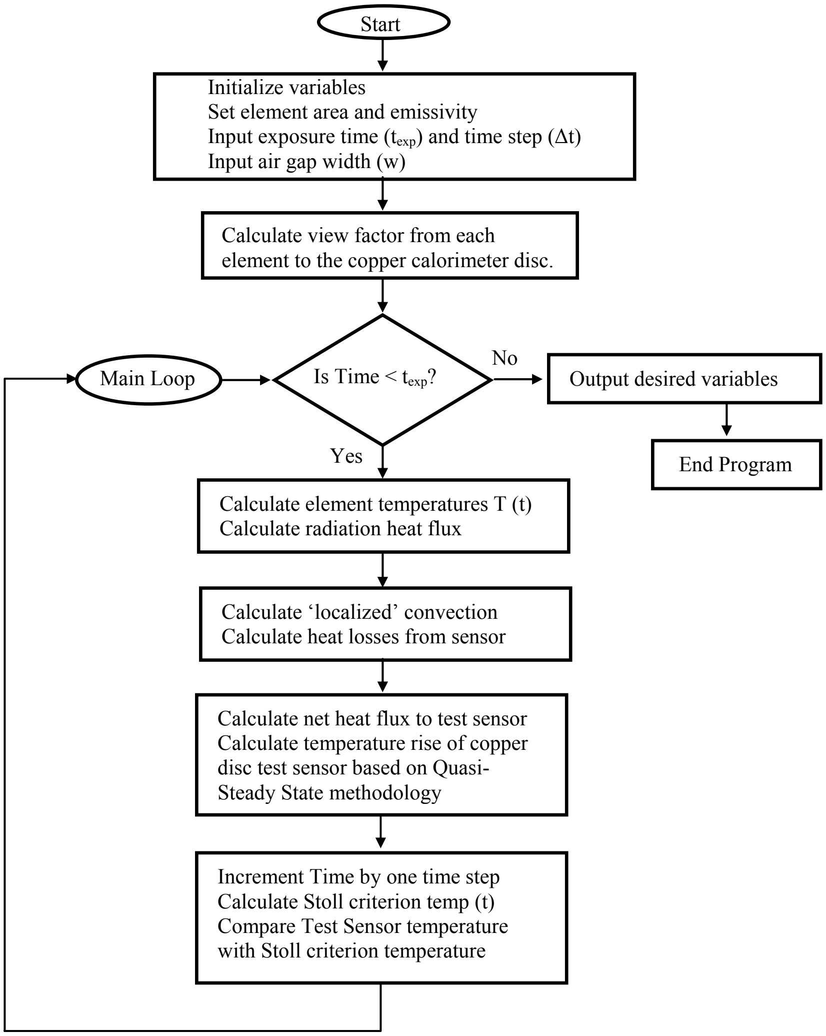

Figure 4.12 Flow Chart of the Computer Program

The validity of the quasi-steady state treatment was investigated by using a very simplified test case, in which the exact solution to the governing differential equations could be calculated. The simplified case implemented only one element and treated all variables except for the fabric/shim and test sensor temperatures as constants. In the model, the boundary conditions are calculated using the temperature of the previous time step for the test sensor. In the exact solution, an iterative process was implemented that calculated the boundary conditions using the temperature of the test sensor at the current time step. The maximum difference in the test sensor temperatures between the two methods was less than 0.0005%.

The element temperatures are calculated using equations that are a function of time and were generated using the experimental data. A description of the generation of these equations was shown in Section 4.2.1. The radiation heat transfer rate from the bottom boundary elements to the test sensor is calculated as well as the convection heat transfer rate. The heat loss rate from the test sensor to the ambient surroundings is calculated based on the current temperature of the test sensor in the program.

Now it is possible for a net heat transfer rate to the copper disc to be calculated. A corresponding temperature rise for the test sensor is computed using a quasi-steady state methodology over a time step of 0.01 s. This time step was chosen by comparing the relative transient scales observed in the experiments and ensuring that the physics could be captured. Figure 4.13 shows that the size of the time step chosen has practically no effect on the response of the copper disc test sensor and thus the predicted times to second-degree burns.

The Stoll criterion temperature is calculated using Equation 1.2 and the current temperature of the copper disc is compared to the Stoll criterion temperature. If the current temperature of the test sensor is greater than the Stoll criterion temperature, then the time to second-degree burn has been established. If a Stoll time has been found, the model no longer performs this comparison step. Finally, the time of the model is incremented forward by one time step and the main loop continues until the end of the exposure time.

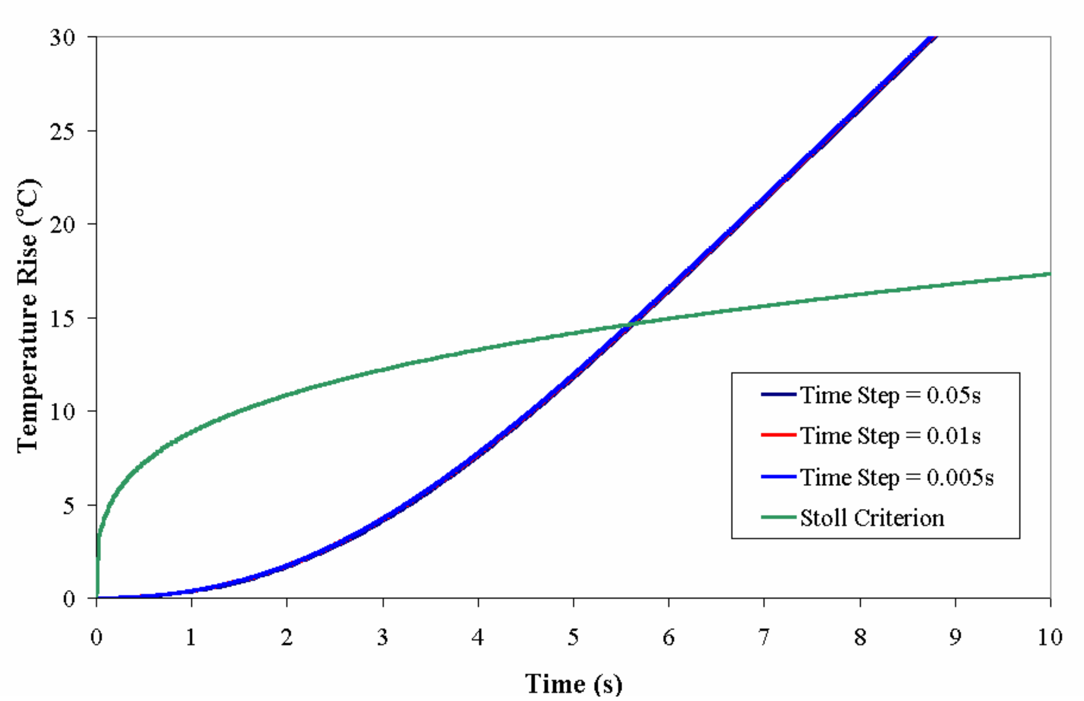

Figure 4.13 Effect of Changing Time Step in New Model

As seen in Figure 4.13, the choice of the time step of 0.01 s has a negligible effect on the calculated response of the copper disc test sensor and thus the predicted times to second-degree burns are practically identical. The absolute copper disc temperatures display a maximum difference of only 0.03% at 10 s.

4.7 Chapter Summary

In this chapter, the numerical model was presented and discussed. The influences of the experimental data on the boundary conditions in the new model and an overview of the new model were shown. The details for the various aspects of the model and the output variables were also presented.

CHAPTER 5 COMPARISON OF RESULTS

In this chapter, the numerical outputs of the new model will be compared with those predicted by the previous model, as well as the data collected experimentally.

5.1 Magnitude of Radiation and Convection Heat Fluxes

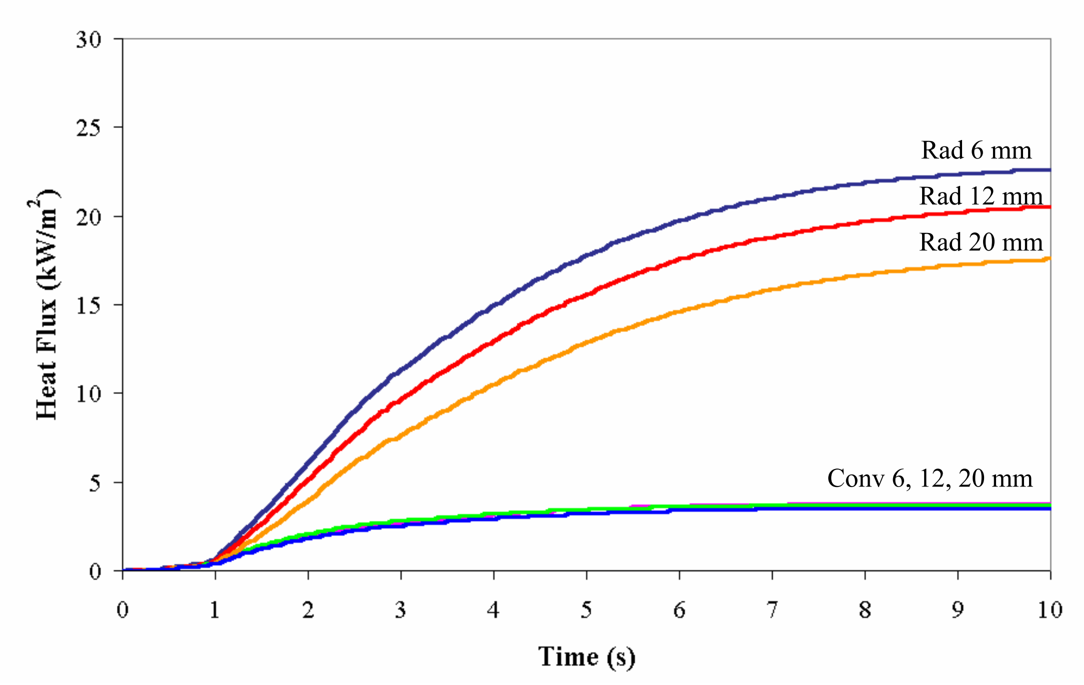

Figure 5.1 Comparison of Heat Fluxes in Previous Model [2] (Nomex® IIIA)

The heat fluxes shown in Figure 5.1 were calculated using the previous model for three air gap sizes of 6 mm, 12 mm, and 20 mm. There are some important trends that are evident from this figure. The relative magnitude of the radiation heat flux is much larger than the convection heat flux to the copper disc test sensor. Thus, at the elevated temperatures present in the bench top apparatus, radiation is the dominant mode of heat transfer across the enclosure. This information was known before the new model was undertaken, which is why proportionately more time was spent refining the radiation treatment in the model compared to the time spent modeling the convection.

Another interesting trend that can be deduced from this figure is that the magnitude of the radiation heat transfer has a much larger dependence on size of the air gap tested when compared to the convection heat transfer. For the three air gaps presented here, the radiation heat flux varies from 17.6 kW/m^2 to 22.6 kW/m^2, which is a difference of 28.4%. However, the convection heat transfer varies from 3.5 kW/m^2 to 3.8 kW/m^2, which is a difference of only 8.6%.

The reason that the radiation heat flux varies to the extent seen here is attributed solely to the decrease in view factor between the bottom heated boundary to the test sensor with an increase in air gap size since the other variables used in the radiation calculations remain constant as the air gap size is changed. For example, the view factor of the heated region to the test sensor increases from 0.30 to 0.45 when the air gap is decreased from 19.0 mm (3/4 in.) to 6.4 mm (1/4 in.).

The convection heat transfer on the other hand, has many variables that are a function of the air gap size. The Rayleigh number becomes increasingly large with an increased air gap size, which should increase the strength of the convection cells and thus the convection heat transfer. However, when calculating the convective heat transfer coefficient from the Nusselt number, there is an inverse relationship between the convection coefficient and the air gap. It is interesting that the previous model predicted that both of these factors would act to approximately balance each other, leading to the convection heat flux being relatively constant with air gap size.

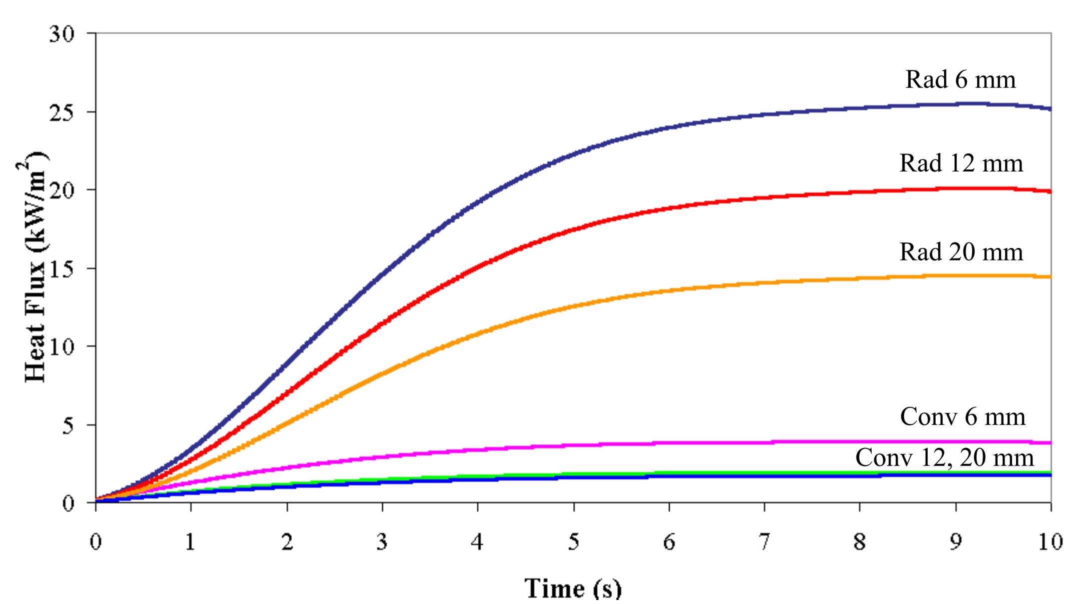

Figure 5.2 Comparison of Heat Fluxes in New Model (Shim)

The heat fluxes shown in Figure 5.2 were calculated using the new model and the air gap sizes of 6 mm, 12 mm, and 20 mm as before. Both models demonstrate the same difference in relative magnitudes between the radiation and convection heat flux to the copper disc test sensor. Also, a similar trend demonstrating the radiation heat flux dependence on the size of the air gap is witnessed for the new model. However, the observed independence of the magnitude of the convection heat flux with air gap size has been reduced.

Now there is a significant change in the magnitude of the convection heat flux as the air gap is changed. The maximum convection heat flux varies from 1.74 kW/m^2 to 3.87 kW/m^2 for a difference of 122%. This behavior is attributed to the localized treatment of the convection in the new model, which was a significant departure from the theory used in the previous model.

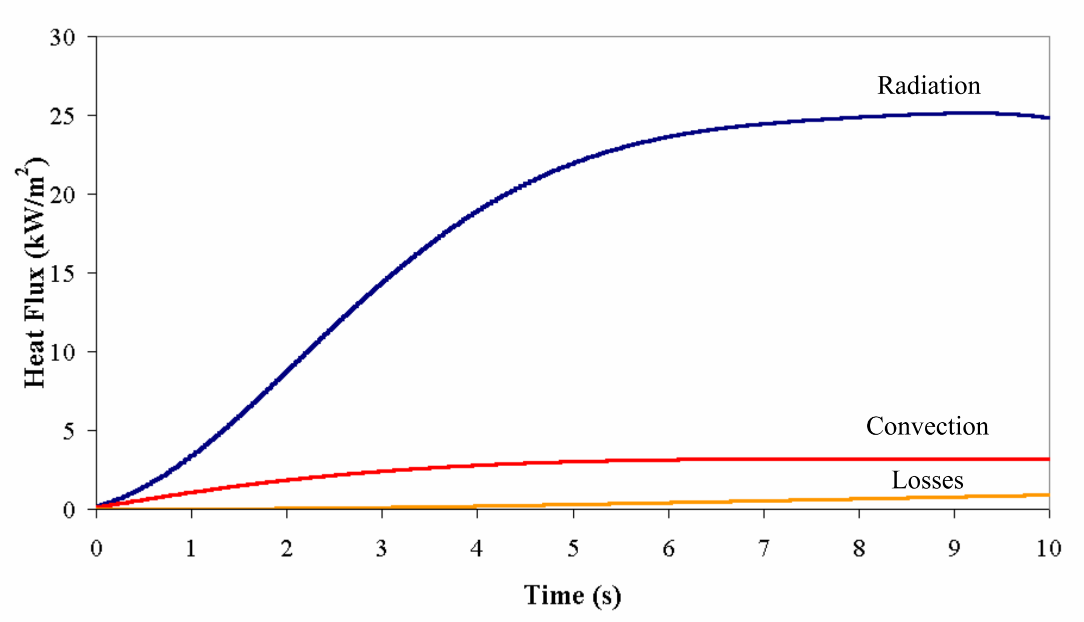

Figure 5.3 Comparison of Heat Fluxes in New Model (Shim, w = 6.4 mm)

Figure 5.3 shows a comparison of the relative magnitudes of the radiation and convection to the copper disc to the heat losses from the copper disc to the surroundings. It is seen here that the losses from the disc are very small in comparison to the heat transfer to the test sensor from the bottom boundary during the flame exposure. The maximum heat loss from the copper disc test sensor is 0.9 kW/m^2 whereas the maximum combined heat flux to the test sensor is 28.3 kW/m^2. Therefore the losses, although important to the overall modeling of the bench top apparatus, have a much smaller impact on the thermal response of the copper disc during the heating phase of the test procedure.

5.2 Test Sensor Temperatures and Times to Exceed Stoll Criterion

The purpose of this model is to calculate Stoll times, which are extracted from the temperature histories of the copper disc sensor when compared to the Stoll criterion. Figure 5.4 is an example of how this comparison is made.

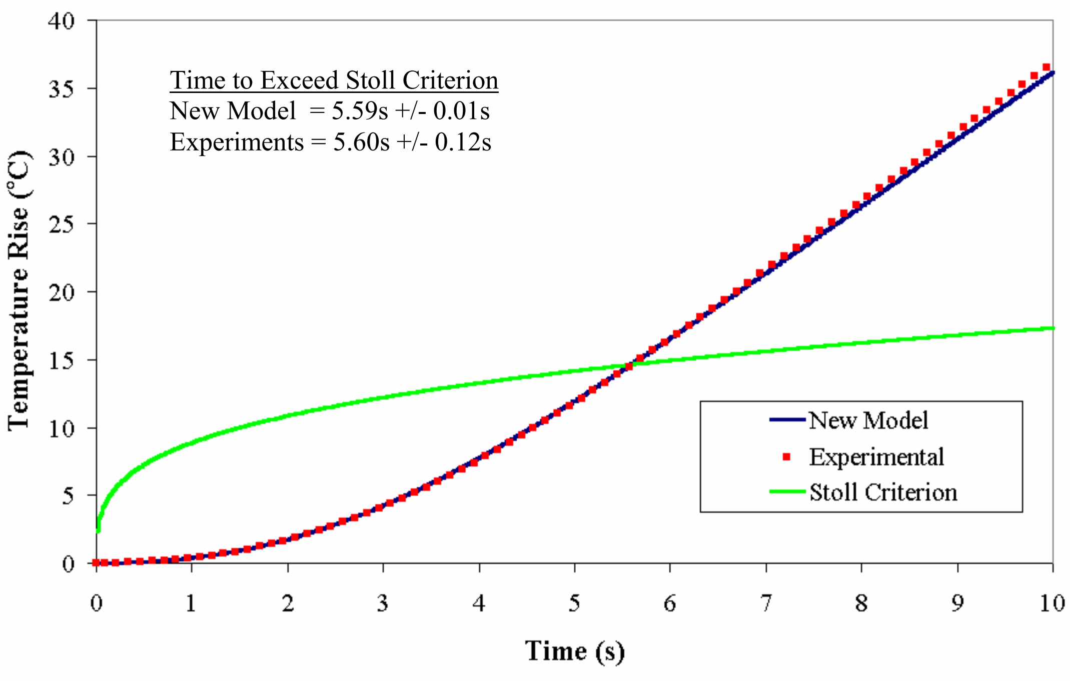

Figure 5.4 Test Sensor Response (Shim, w = 6.4 mm or 1/4 in.)

Experimental and predicted test sensor responses during a bench top test using an air gap of 6.4 mm (1/4 in.) are shown in Figure 5.4 along with the Stoll criterion. The data is presented here in terms of a temperature rise so that the average experimental response could be presented. Note that a second-degree burn is predicted to occur when the temperature rise of the test sensor is larger than the temperature rise of the Stoll criterion, or simply stated, when the two curves cross each other in the figure. From this figure it can be seen that the model does an excellent job of predicting the temperature rise of the copper disc test sensor as well as the associated time to second-degree burn. The experimental data almost reproduces the trend predicted by the model. Similar results are presented for the fabric (Kevlar®/PBI) model in Figure 5.5.

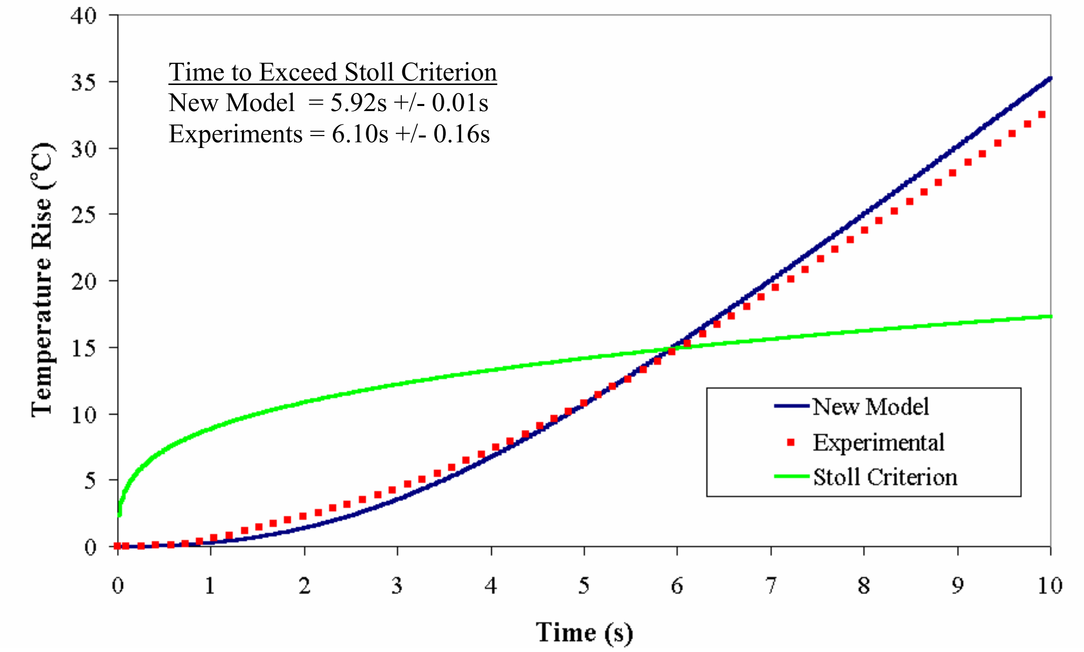

Figure 5.5 Test Sensor Response (Kevlar®/PBI, w = 6.4 mm or 1/4 in.)

The results of the fabric model are very similar to the results of the model using the steel shim stock. The predicted thermal response of the copper disc test sensor is closely matched by the experimental data. However, there are two regions where the trends diverge. In the first region, from 1 s to 4 s, the discrepancy may be due to the presence of moisture in the fabric specimens. The moisture is boiled off of the fabrics during heating and may condense on the copper disc sensor throughout the exposure. In the second region, after 7 s, the difference may be caused by the combustion products introduced into the enclosure during the heating of the fabric. The model assumes that the fluid is non-participating radiatively and has the properties of air for the convection modeling. Since the contributions of the combustion products are unknown, a more conclusive argument cannot be made here.

The following figures are the same comparisons as in Figures 5.4 and 5.5 except a larger air gap of 19.0 mm (3/4 in.) is used.

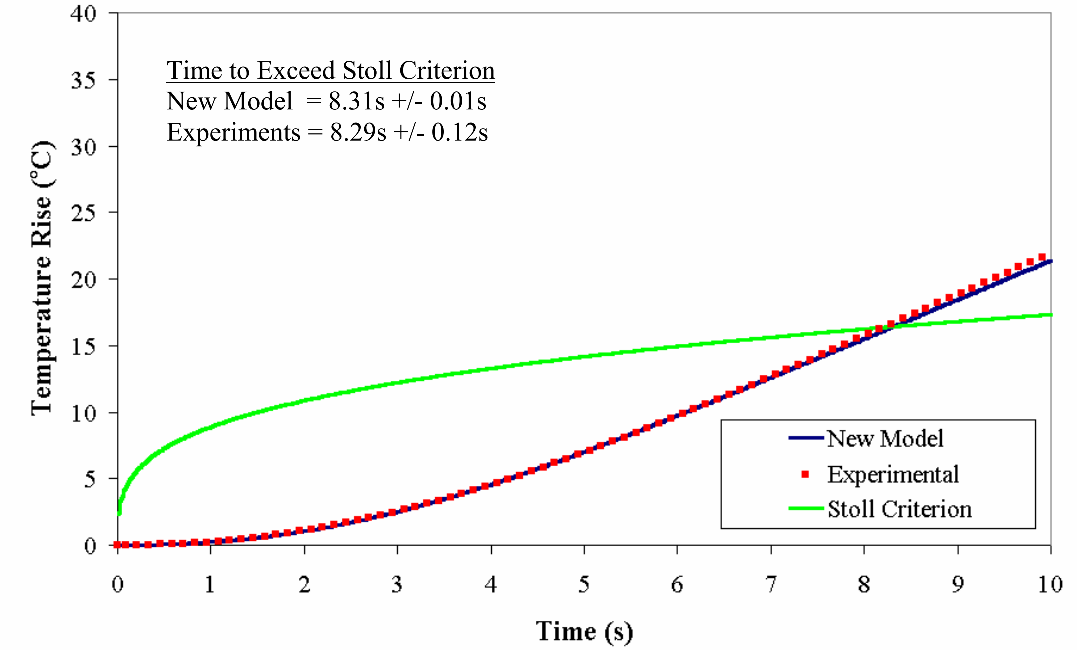

Figure 5.6 Test Sensor Response (Shim, w = 19.0 mm or 3/4 in.)

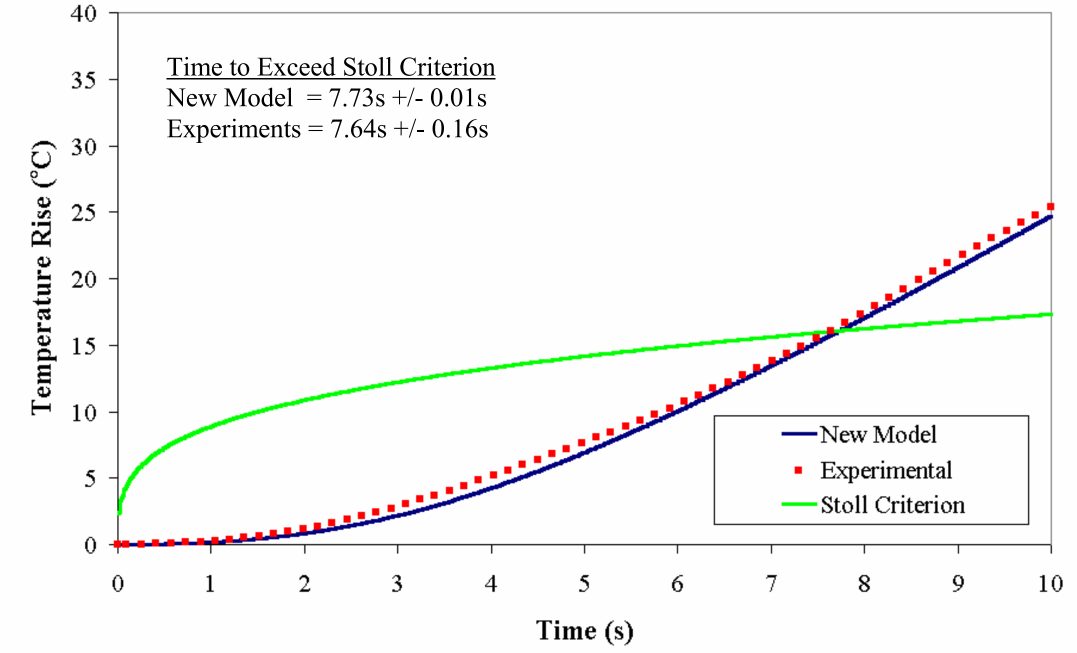

Figure 5.7 Test Sensor Response (Kevlar®/PBI, w = 19.0 mm or 3/4 in.)

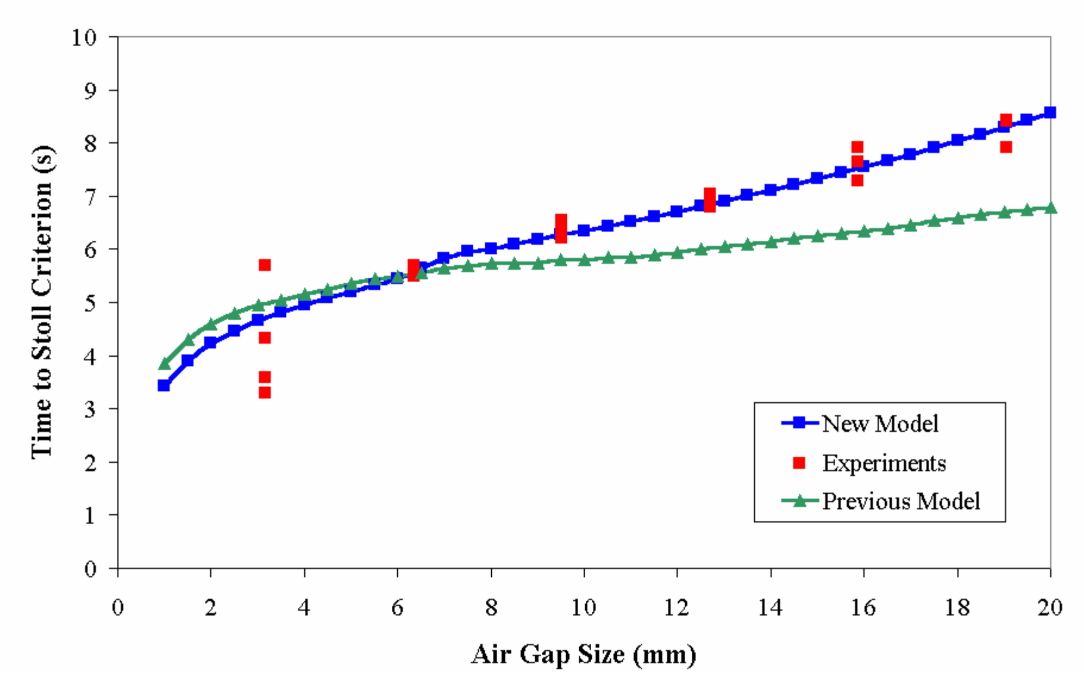

Figure 5.8 Stoll Time Comparison of Models and Experiments (Steel Shim)

As mentioned in Chapter 1, the previous model already was capable of making excellent Stoll time predictions for the standard air gap size of 6.4 mm (1/4 in.). The previous model however, over-predicted the heat transfer to the test sensor in the cases of the larger air gaps. The important contribution of this model is the increased the accuracy of these predictions at the other air gap sizes. The performance of both models is compared in Figure 5.8 along with the experimentally obtained second-degree burn times. The new model predicts the Stoll times at the larger and smaller air gap sizes more accurately than the previous model. The trend witnessed experimentally is more closely followed by the new model, which can be attributed to the two-dimensional treatment of the radiation heat transfer and the localized treatment of the convection heat transfer.

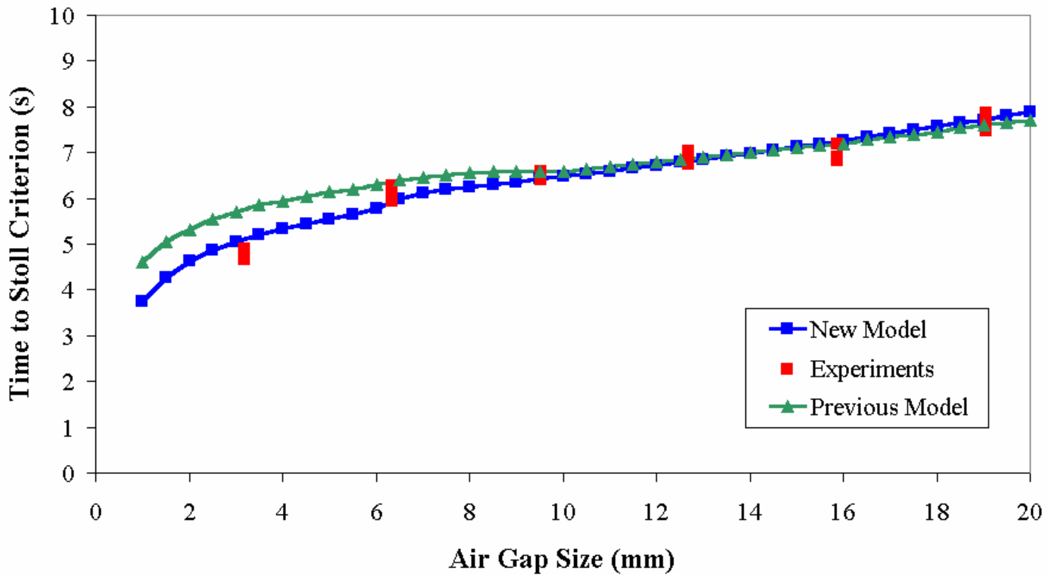

Figure 5.9 Stoll Time Comparison of Models and Experiments (Kevlar®/PBI)

The predicted results of the previous model were in fairly good agreement with the experimental data for the larger air gap sizes when testing Kevlar®/PBI. Therefore, a significant improvement in the performance of the new model is not evident in Figure 5.9. The new model does make more accurate predictions at the smallest air gap and slightly more accurate predictions for the remaining air gap sizes, but not to the extent witnessed in the shim stock model.

These last two figures do lead to an exciting revelation. If many of the figures outlining the results of the temperature measurements from Chapter 3 are recalled, in particular, Figure 3.11, the spatial variations of temperature in the steel shim stock were more pronounced than in the case of the Kevlar®/PBI. Since, the temperature variations were not as large, then a more sophisticated or refined treatment of these boundary conditions would have less of an influence on the predicted results of a model. This explains why there was such an increase in the accuracy of the predictions made by the shim model in comparison to those made by the fabric model. One may even conclude from these findings that since the temperatures across the heated fabric were very similar, that the one-dimensional treatment of the radiation and convection when using fabric may be very efficient.

The boundary conditions for the Kevlar®/PBI were established in this research using extensive experiments requiring many hours of apparatus construction and lab work. If a one-dimensional model performed almost as well as a model that treats the boundary conditions in a much more sophisticated fashion, then possibly the gains do not justify the means by which they are obtained.

The contributions of this work are not futile; on the contrary, the investigation of a more involved treatment of the boundary conditions has provided many insights. When the specimen tested has a high thermal conductivity or other material properties that may give rise to large variations in temperatures across the unexposed side, this model does a much better job of predicting second-degree burns than the previous model, as demonstrated in Figure 5.8. This work also demonstrated that with relatively small computation times and resources, the radiation and convection within these bench top enclosures can be resolved to a high degree of accuracy.

It is also important to note, that both the numerical models of the heat transfer in the bench top apparatus, are sensitive to the absolute temperatures of the fabric and shim specimens. An investigation into the sensitivity of these models showed that a 5% and a 10% change in the absolute temperatures on the backside of a specimen caused the predicted times to exceed the Stoll criterion to vary as much as 12% and 20% respectively. Another important characteristic to understand is that the air gap size does not remain constant over the duration of an exposure.

As mentioned previously, the air gap can increase or decrease as much as 3.2 mm (1/8 in.) in a random fashion. This change in air gap size can have a large effect on the experimental results as witnessed by the scatter in Figure 5.8. For example, at an air gap of 12.7 mm (1/2 in.), an increase of 3.2 mm (1/8 in.) in the air gap size will increase the predicted Stoll time by 9.3%, while a decrease of 3.2 mm (1/8 in.) will decrease the predicted Stoll time by 8.6%. However, at a smaller air gap of 6.4 mm (1/4 in.), an increase of 3.2 mm (1/8 in.) in the air gap size will increase the predicted Stoll time by 12.0%, while a decrease of 3.2 mm (1/8 in.) will decrease the predicted Stoll time by 16.1%.

5.3 Chapter Summary

In this chapter, the numerical outputs of the new model were presented. Comparisons were made between the results generated by the new model with those generated by the previous model. Comparisons were also made between the results of the new model and the experimental data.

CHAPTER 6 CONCLUSIONS AND RECOMMENDATIONS

In this thesis, the experiments that were performed to investigate the boundary conditions of the bench top testing apparatus and to validate the performance of a numerical model were outlined and detailed. The results of these experiments and the corresponding influence on the development of a new numerical model were presented. A numerical model was constructed that predicts the time to second-degree burns when steel shim and Kevlar®/PBI specimens are tested in a standard bench top testing apparatus. The details of this new model were presented and different variables as predicted by the model were shown, including the most important, the second-degree burn time predictions. The performance of the new model was compared with the previous model using experimental data and the differences were discussed.

6.1 Conclusions

The following conclusions can be made from this study:

- A two-dimensional treatment of the radiation heat transfer as well as a localized treatment of the convection heat transfer significantly improved the accuracy of this model in comparison to the previous model that treated this problem one-dimensionally, when a material is tested that displays large spatial variations in temperature (e.g., steel shim stock).

- In materials that display less of a variation in temperature (i.e. Kevlar®/PBI), the new model still demonstrates an improvement in performance over the previous model, however the improvement is less pronounced.

- The new model effectively treated the boundary conditions involved in the bench top testing of thermal protective fabrics and captured a fine enough resolution of the physics involved to produce results that were within the scatter of experimental data.

- The previous model, although it treated the boundary conditions as one-dimensional, is a very efficient tool when testing fabrics where there are not significant spatial variations in temperature on the unexposed side of the fabric that faces the copper disc test sensor.

6.2 Recommendations

The following are recommendations for the implementation of this work:

- As mentioned earlier, there were many possible reasons hypothesized for the inaccuracy of the predicted heat transfer when using larger air gap sizes in the previous model. However, this research was focused on one of these possibilities, namely, the treatment of the heat transfer within the air gap. Therefore, future work could be performed to investigate the other possible causes such as: moisture transfer within the air gap, the participation of the combustion products as a coupling mechanism between the radiation and convection heat transfer, as well as the influence of the dynamic air gap during the bench top tests.

- The model developed here and the corresponding experimental data used a bench top apparatus that contained a horizontal air gap. However, most of the air spaces present between people and clothing are vertical in orientation. Therefore, a study involving a similar apparatus modified to produce a vertical enclosure would provide useful information.

6.3 Caution

- The testing of certain materials as part of this research project are not endorsements for these produces, nor should the performance data contained within be used a method for the selection of materials in the use of actual fire safety garments. The experimental information was only used to create and validate a numerical model and the purpose of this data should not be extended.

REFERENCES

---

1. International Organization for Standardization, "ISO 9151 Protective Clothing Against Heat and Flame - Determination of Heat Transmission on Exposure to Flame", Geneva, Switzerland, 1995.

2. Torvi, D.A., "Heat Transfer in Thin Fibrous Materials Under High Heat Flux Conditions", PhD Thesis, University of Alberta, Edmonton, AB, 1997.

3. American Society for Testing and Materials, "ASTM F 1930 Standard Test Method for Evaluation of Flame Resistant Clothing for Protection Against Flash Fire Simulations Using an Instrumented Manikin", West Conshohocken, PA, 2000.

4. Elkins, W. and Thompson, J.G., "Instrumented Thermal Manikin", Acurex Corporation, Aerotherm Division Report AD-781 176, 1973.

5. Dale, J.D., Crown, E.M., Ackerman, M.Y., Leung, E., and Rigakis, K.B., "Instrumented Mannequin Evaluation of Thermal Protective Clothing" Performance of Protective Clothing: Fourth Volume, ASTM STP 1133, James P. McBriarty and Norman W. Henry, eds., American Society for Testing and Materials, West Conshohocken, PA, 1992, pp. 717-733.

6. Behnke, W.P., "Predicting Flash Fire Protection of Clothing From Laboratory Tests Using Second-Degree Burn to Rate Performance", Fire and Materials, Vol. 8, 1984, pp. 57-63.

7. American Society for Testing Materials, "ASTM D 4108-87 Standard Test Method for Thermal Protective Performance of Materials and Clothing By Open-Flame Method", West Conshohocken, PA, 1987.

8. Canadian General Standards Board, "CAN/CGSB-155.1 – M88 Fire Fighters' Protective Clothing for Protection Against Heat and Flame", Ottawa, 1988.

9. Stoll, A.M., Chianta, M.A., and Munroe, L.R., "Flame Contact Studies", Journal of Heat Transfer, Vol. 86, 1964, pp. 449-456.

10. Incropera, F.P., and DeWitt, D.P., Fundamentals of Heat and Mass Transfer, 4th Edition, John Wiley and Sons, Toronto, Ontario, 1996, p. 509.

11. Goldstein, R.J., and Volino, R.J., "Onset and Development of Natural Convection Above a Suddenly Heated Horizontal Surface", Journal of Heat Transfer, Vol. 117, 1995, pp. 808-821.

12. Catton, I., "Natural Convection in Enclosures", Proceedings, 6th International Heat Transfer Conference, Vol. 6, 1978, pp. 13-31.

13. Stoll, A.M., and Chianta, M.A., "Method and Rating System for Evaluation of Thermal Protection", Aerospace Medicine, Vol. 40, 1969, pp.1232-1238.

14. Henriques, F.C., Jr. and, "Studies of Thermal Injuries I. The Conduction of Heat to and Through Skin and the Temperatures Attained Therein. A Theoretical and Experimental Investigation", The American Journal of Pathology, Vol. 23, 1947, pp. 531-549.

15. Moritz, A.R. and Henriques, F.C., Jr., "Studies of Thermal Injuries V. The Relative Importance of Time and Surface Temperature in the Causation of Cutaneous Burns", The American Journal of Pathology, Vol. 23, 1947, pp. 695-720.

16. "Anatomy of the Skin", University of Maryland Medicine, Accessed: July 2003, http://www.umm.edu/dermatology-info/anatomy.htm.

17. Kim, I.Y., Lee, C., Li, P., Corner, B.D., and Paquette, S., "Investigation of Air Gaps Entrapped in Protective Clothing Systems", Fire and Materials, Vol. 26, 2002, pp. 121-126.

18. Maveety, J.G., and Leith, J.R., "Heat Transfer in Rayleigh-Bernard Convection with Air in Moderate Size Containers", International Journal of Heat and Mass Transfer, Vol. 41, 1997, pp. 785-796.

19. Emery, A.F., and Lee, J.W., "The Effects of Property Variations on Natural Convection in a Square Enclosure", Journal of Heat Transfer, Vol. 121, 1999, pp. 57-62.

20. Oosthuizen, P.H., "Convection in a Cubical Enclosure with a Partially Heated Lower Surface and Cooled Side Walls", Proceedings, The 13th International Symposium of Transport Phenomena, Victoria, 2002, pp. 333-337.

21. Hollands, K.G.T., Raithby, G.D., and Konicek, L., "Correlation Equation for Free Convection Heat Transfer in Horizontal Layers of Air and Water", International Journal of Heat and Mass Transfer, Vol. 18, 1975, pp. 879-884.

22. Ewer, J., Galea, E.R., Patel, M.K., Taylor, S., Knight, B., and Petridis, M., "Smartfire: An Intelligent CFD Based Fire Model", Journal of Fire Protection Engineering, Volume 10, Number 1, 1999, pp.13-27.

23. McGrattan, K.B., Baum, H.R., Rehm, R.G., Hamins, A., Forney, G.P., Floyd, J.E., Hostikka, S., Prasad, K., “Fire Dynamics Simulator (Version 3) – Technical Reference Guide”, NISTIR 6783, 2002 Edition.
[Online: http://fire.nist.gov/fds]

24. Drysdale, D., “An Introduction to Fire Dynamics”, Second Edition, John Wiley & Sons, West Sussex, England, 1998, pp. 52-53.

25. Sawcyn, C.M.J., and Torvi, D.A., “Flow Visualization in Air Spaces Between Protective Fabrics and Sensors in Protective Clothing Tests”, Proceedings, The 13th International Symposium of Transport Phenomena, Victoria, 2002, pp. 197-202.

26. Chapman, A.J., Heat Transfer, Fourth Edition, Macmillan Publishing Company, New York, 1987, p. 510.

27. Modest, M.F., Radiative Heat Transfer, McGraw-Hill, Inc., New York, 1993.

28. Jakob, M., Heat Transfer, Volume II, John Wiley & Sons, New York, 1957.

APPENDICES

The Fortran 77 programs used to implement the new heat transfer model have been provided in their entirety. Appendix 1 is the program used to model the heat transfer when the specimen tested is steel shim stock. Appendix 2 is the program used to model the heat transfer when the specimen is Kevlar®/PBI.

APPENDIX 1 – The Steel Shim Stock Model

```
C-----------------------------------------------------------------
      program Copper_Disk_Shim
C
C     This program calculates the thermal response
C     of a copper calorimeter that is subject to a
C     convective and radiative heat flux. Losses from the
C     calorimeter are also accounted for.
C
C     The heat fluxes are calculated across an air gap that
C     has the temperatures measured experimentally for a steel
C     shim as the boundary conditions for the 'bottom plate'.
C     These boundary conditions are implemented using 7 elements
C     in this program.
C
C     Define Variables
      implicit none
      REAL Qrad, Qconv, Qloss, Qnet, DELTA, TIME, TEMP, Cop_DENS,
     * Tamb, SPHT, GAP, R0, Cop_Mass, A0, T_RISE, Texp, THICK, E0,
     * Qr10, SQ1, E1, A1, T1, RES1, F10, T2, A2big, A2, RES2,
     * SQ2, E2, Qr20, F20, T3, A3big, A3, RES3, SQ3, E3, Qr30,
     * F30, T4, A4big, A4, RES4, SQ4, E4, Qr40, F40,
     * T5, A5big, A5, RES5, SQ5, E5, Qr50, F50,
     * T6, A6big, A6, RES6, SQ6, E6, Qr60, F60,
     * T7, A7big, A7, RES7, SQ7, E7, Qr70, F70,
     * Tbot, Ttop, Tair, BETA, KIN_VIS, THER_DIFF, THER_COND, g,
     * RAY, AA, BB, Nu, CONV, FACTOR, F12to0, F123to0, F1234to0,
     * F12345to0, F123456to0, F1234567to0,
     * RAD, CONVEC, LOSS, DUMMY, STOLL_CRIT, STOLL_TIME, RATIO,
     * RATIO2
C
C     Qrad = radiation heat flux [W]
C     RAD = radiation heat flux [kW/m2]
C     Qconv = convective heat flux [W]
C     CONVEC = convective heat flux [kW/m2]
C     CONV = convection coefficient [W/m2K]
C     Qloss = heat loss from disk [W]
C     LOSS = heat loss from disk [kW/m2]
C     Qnet = net heat transfer rate to disk [W]
C     DELTA = time step for quasi-steady state idealogy [s]
C     Texp = exposure time [s]
C     TIME = real (current) time for exposure [s]
C     TEMP = temperature of the copper disk [K]
C     Cop_DENS = density of copper [kg/m3]
C     SPHT = specific heat of copper [J/kg*K]
C     THICK = thickness of copper disk [m]
C     Cop_Mass = mass of copper disk [kg]
C     A0 = area of copper disk sensor [m^2]
C     R0 = radius of copper disk sensor [m]
C     E0 = emissivity of copper disk sensor
C     Cop_Mass = mass of copper disk sensor [kg]
C     FACTOR = needed for subroutine of view factor
```

```
C       STOLL_TIME = time to reach Stoll Criterion
C       STOLL_CRIT = Stoll criterion temperature @ TIME
C       DUMMY = variable used for logical test (loop)
C       GAP = size of the air gap [m]
C       Tamb = ambient temperature of the surroundings [K]
C       SQ'X' = size of the element number 'X'(square)
C       F'X'0 = view factor from element 'X' to disk
C       A'X' = area of element 'X'
C       E'X' = emissivity of element 'X'
C       RES'X' = resistance to thermal radiation of element 'X'
C       T'X' = temperature of element 'X' @ TIME (current)
C       Qr'X'0 = radiation heat flux from element 'X' to disk [W]
C       RATIO = used to transition from 4 elements to 5 elements
C               for the 'localized convection treatment
C       RATIO2 = used to transition from 5 elements to 6 elements
C               for the 'localized convection treatment
C       Tair = temperature of the air in the gap [K]
C       BETA = variable for calculating Rayleigh number [1/K]
C       KIN_VIS = kinematic viscosity of the air in gap
C       THER_DIFF = thermal diffusivity of the air in gap
C       THER_COND = thermal conductivity of the air in gap
C       g = acceleration due to gravity [m/s2]
C       RAY = Rayleigh number
C       AA and BB = are arguments within the Rayleigh equation
C       Nu = Nusselt number
C       T_RISE = calculated temperature rise of disk for time step
C
C       Open output file
        open(unit=10,file="copper.txt",status="unknown")
C
        TIME = 0.0
        STOLL_TIME = 0.0
        STOLL_CRIT = 0.0
        DUMMY = 0.0
        Texp = 10.0
        DELTA = 0.01
        GAP = 0.00635
        Tamb = 300.0
        TEMP = 300.0
        THICK = 0.016
        Cop_DENS = 8954
        R0 = 0.02
        A0 = 3.1415926*R0**2.0
        E0 = 0.95
        Cop_Mass = Cop_DENS*A0*THICK
C
C       Set the size of the elements.
C       Find the view factors for the elements using subrout. FACTOR
C       Also, solve for a few of the elements' variables that do not
C       change with time.
C
C       Element 1
C
        SQ1 = 0.00914
        F10 = FACTOR(GAP, R0, SQ1)
```

```
      A1 = SQ1**2.0
      E1 = 0.95
      RES1 = ((1.0-E1)/(A1*E1))+(1.0/(A1*F10))+((1.0-E0)/(A0*E0))
C
C     Element 2
C
      SQ2 = 0.02032
      F12to0 = FACTOR(GAP, R0, SQ2)
      A2big = SQ2**2.0
      A2 = A2big - A1
      F20 = ((F12to0*A2big)-(F10*A1))/A2
      E2 = 0.95
      RES2 = ((1.0-E2)/(A2*E2))+(1.0/(A2*F20))+((1.0-E0)/(A0*E0))
C
C     Element 3
C
      SQ3 = 0.02794
      F123to0 = FACTOR(GAP, R0, SQ3)
      A3big = SQ3**2.0
      A3 = A3big - A2big
      F30 = ((F123to0*A3big)-(F12to0*A2big))/A3
      E3 = 0.95
      RES3 = ((1.0-E3)/(A3*E3))+(1.0/(A3*F30))+((1.0-E0)/(A0*E0))
C
C     Element 4
C
      SQ4 = 0.0381
      F1234to0 = FACTOR(GAP, R0, SQ4)
      A4big = SQ4**2.0
      A4 = A4big - A3big
      F40 = ((F1234to0*A4big)-(F123to0*A3big))/A4
      E4 = 0.95
      RES4 = ((1.0-E4)/(A4*E4))+(1.0/(A4*F40))+((1.0-E0)/(A0*E0))
C
C     Element 5
C
      SQ5 = 0.04064
      F12345to0 = FACTOR(GAP, R0, SQ5)
      A5big = SQ5**2.0
      A5 = A5big - A4big
      F50 = ((F12345to0*A5big)-(F1234to0*A4big))/A5
      E5 = 0.95
      RES5 = ((1.0-E5)/(A5*E5))+(1.0/(A5*F50))+((1.0-E0)/(A0*E0))
C
C     Element 6
C
      SQ6 = 0.06858
      F123456to0 = FACTOR(GAP, R0, SQ6)
      A6big = SQ6**2.0
      A6 = A6big - A5big
      F60 = ((F123456to0*A6big)-(F12345to0*A5big))/A6
      E6 = 0.95
      RES6 = ((1.0-E6)/(A6*E6))+(1.0/(A6*F60))+((1.0-E0)/(A0*E0))
C
C     Element 7
```

```
C
        SQ7 = 0.152
        F1234567to0 = FACTOR(GAP, R0, SQ7)
        A7big = SQ7**2.0
        A7 = A7big - A6big
        F70 = ((F1234567to0*A7big)-(F123456to0*A6big))/A7
        E7 = 0.95
        RES7 = ((1.0-E7)/(A7*E7))+(1.0/(A7*F70))+((1.0-E0)/(A0*E0))
C
C       Loop program for 10 second exposure time
C
        Do while (TIME.LT.Texp)
C
C       Check to see if Stoll criterion temp has been exceeded
C
        STOLL_CRIT = (8.871465*TIME**0.2905449) + Tamb
              IF (DUMMY.EQ.0.0) THEN
                 IF (TEMP.GT.STOLL_CRIT) THEN
                    STOLL_TIME = TIME - DELTA
                    DUMMY = 1.0
                 END IF
              END IF
C
C       Calculate the radiative heat transfer (W)
C
C       Radiation from Element 1 to Sensor
C
        T1 = 0.00123*TIME**6.0 - 0.03607*TIME**5.0
     *       + 0.25516*TIME**4.0
     *       + 2.37744*TIME**3.0 - 47.32422*TIME**2.0
     *       + 276.63187*TIME + 337.00138
        IF (T1.LT.300.0)THEN
                 T1 = 300.1
        END IF
        Qr10 = 5.67E-08*(T1**4.0-TEMP**4.0)/RES1
C
C       Radiation from Element 2 to Sensor
C
        T2 = - 0.00204*TIME**6.0 + 0.06367*TIME**5.0
     *       - 0.87656*TIME**4.0
     *       + 8.08782*TIME**3.0 - 58.3936*TIME**2.0
     *       + 276.63011*TIME + 333.4756
        IF (T2.LT.300.0)THEN
                 T2 = 300.1
        END IF
        Qr20 = 5.67E-08*(T2**4.0-TEMP**4.0)/RES2
C
C       Radiation from Element 3 to Sensor
C
        T3 = 0.00015*TIME**6.0 - 0.00216*TIME**5.0
     *       - 0.15039*TIME**4.0
     *       + 4.57216*TIME**3.0 - 51.6256*TIME**2.0
     *       + 272.44876*TIME + 337.30534
        IF (T3.LT.300.0)THEN
                 T3 = 300.1
```

```
      END IF
      Qr30 = 5.67E-08*(T3**4.0-TEMP**4.0)/RES3
C
C     Radiation from Element 4 to Sensor
C
      T4 = - 0.00446*TIME**6.0 + 0.14686*TIME**5.0
     *     - 1.92364*TIME**4.0
     *     + 13.49826*TIME**3.0 - 62.73657*TIME**2.0
     *     + 225.99407*TIME + 325.02562
      IF (T4.LT.300.0)THEN
               T4 = 300.1
      END IF
      Qr40 = 5.67E-08*(T4**4.0-TEMP**4.0)/RES4
C
C     Radiation from Element 5 to Sensor
C
      T5 = - 0.00145*TIME**6.0 + 0.05581*TIME**5.0
     *     - 0.86526*TIME**4.0
     *     + 7.18194*TIME**3.0 - 38.36509*TIME**2.0
     *     + 156.58948*TIME + 325.69998
      IF (T5.LT.300.0)THEN
               T5 = 300.1
      END IF
      Qr50 = 5.67E-08*(T5**4.0-TEMP**4.0)/RES5
C
C     Radiation from Element 6 to Sensor
C
      T6 = - 0.00306*TIME**6.0 + 0.10148*TIME**5.0
     *     - 1.31201*TIME**4.0
     *     + 8.4874*TIME**3.0 - 30.85513*TIME**2.0
     *     + 81.10245*TIME + 310.96402
      IF (T6.LT.300.0)THEN
               T6 = 300.1
      END IF
      Qr60 = 5.67E-08*(T6**4.0-TEMP**4.0)/RES6
C
C     Radiation from Element 7 to Sensor
C
      T7 = - 0.000072*TIME**6.0 + 0.001516*TIME**5.0
     *     - 0.010812*TIME**4.0 + 0.024653*TIME**3.0
     *     + 0.11539*TIME**2.0 + 2.56912*TIME + 298.29636
      IF (T7.LT.300.0)THEN
               T7 = 300.1
      END IF
      Qr70 = 5.67E-08*(T7**4.0-TEMP**4.0)/RES7
C
      Qrad = Qr10 + Qr20 + Qr30 + Qr40 + Qr50 + Qr60 + Qr70
      RAD = Qrad / (A0*1000.0)
C
C     Calculate the convective heat transfer (W)
C
C         Determine the 'local area' of convection
C
          IF (GAP.LT.0.0061)THEN
              RATIO = 1.0 - ((.0061 - GAP)/0.0061)
```

```
              Tbot = (T1*A1 + T2*A2 + T3*A3 + T4*A4
     *        + RATIO*T5*A5)/((A5big - A4big)*RATIO + A4big)
              Ttop = (TEMP*A0 + Tamb*((A5big - A4big)*RATIO
     *        + A4big - A0))/((A5big - A4big)*RATIO + A4big)
          ELSE IF (GAP.LT.0.0091)THEN
              RATIO2 = 1.0 - ((.0091 - GAP)/0.003)
              Tbot = (T1*A1 + T2*A2 + T3*A3 + T4*A4 + T5*A5
     *        + RATIO2*T6*A6)/((A6big - A5big)*RATIO2 + A5big)
              Ttop = (TEMP*A0 + Tamb*((A6big - A5big)*RATIO2
     *        + A5big - A0))/((A6big - A5big)*RATIO2 + A5big)
          ELSE
              Tbot = (T1*A1 + T2*A2 + T3*A3 + T4*A4 + T5*A5
     *                 + T6*A6)/A6big
              Ttop = (TEMP*A0 + Tamb*(A6big - A0))/A6big
          END IF
C
C    Now finish the calculation for convection using correlation
C
      Tair = (Tbot + Ttop)/2.0
      BETA = 1.0 / Tair
      KIN_VIS = (0.00007*Tair**2.0 + 0.0607*Tair
     *  - 9.0061)/1000000.0
      THER_DIFF = (0.00006*Tair**2.0 + 0.1266*Tair
     *  - 22.005)/1000000.0
      THER_COND = (-0.0000266*Tair**2.0 + 0.0914735*Tair +
     *           1.4192599)/1000.0
      g = 9.81
      RAY = g*BETA*(Tbot-Ttop)*GAP**3.0/(KIN_VIS*THER_DIFF)
      AA = 1.0 - 1708.0 / RAY
      IF (AA.LT.0.0) THEN
          AA = 0.0
      END IF
      BB = ((RAY/5830.0)**(1.0/3.0))-1.0
      IF (BB.LT.0.0) THEN
          BB = 0.0
      END IF
      Nu = 1.0 + 1.44 * AA + BB
      CONV = THER_COND * Nu / GAP
      Qconv = CONV * A0 * (Tbot - TEMP)
      CONVEC = Qconv / (A0*1000.0)
C
C     Calculate the heat losses (W)
C
      Qloss = 25.0*A0*(TEMP-Tamb)
      LOSS = Qloss / (A0*1000.0)
C
C     Calculate the net heat transfer (W)
C
      Qnet = Qrad + Qconv - Qloss
C
C     Calculate temperature rise of copper disk sensor
C     assuming quasi-steady state lumped capacitance.
C
      SPHT = 0.000000135*TEMP**3.0 - 0.000286776*TEMP**2.0
     * + 0.27996649*TEMP + 322.83
```

```
      T_RISE = Qnet*DELTA/(Cop_Mass*SPHT)
      TEMP = TEMP + T_RISE
C
C     Increment to the next time step
C
      TIME = TIME + DELTA
C
C     Output desired variables
C
      write(10,*) TIME, TEMP, RAD, CONVEC, LOSS
      Print*, STOLL_TIME
C
      end do
C
C     This is the end of the main loop.
C
C
C
      END
C
C     End of main program
C
C------------------------------------------------------------------
C
C     subroutine to calculate view factor from sq to circ given
C     GAP, Ro, Sq
C
      real function FACTOR(Gap, Ro, Sq)
C
      implicit none
      integer i, j
      real C, B, F, TOTAL, Gap, Ro, Sq,
     * W(16), X(16), Y(16)
C
C     GAP = air gap spacing [m]
C     Ro = radius of copper disk [m]
C     SQ = side of square
C     C = variable used for view factor
C     B = "                           "
C     F = "                           "
C     Total = used for Gaussian Quads
C     Factor = view factor
C     W, X, and Y = Guass points and weights
C
C     Numerical Integration
C
C     Using 16 Gauss Points
C
      W(1) = 0.02715246
      W(2) = 0.06225352
      W(3) = 0.09515851
      W(4) = 0.12462897
      W(5) = 0.14959599
      W(6) = 0.16915652
      W(7) = 0.18260342
```

```
      W(8) = 0.18945061
      W(9) = W(8)
      W(10) = W(7)
      W(11) = W(6)
      W(12) = W(5)
      W(13) = W(4)
      W(14) = W(3)
      W(15) = W(2)
      W(16) = W(1)
C
      X(1) = -0.98940093
      X(2) = -0.94457502
      X(3) = -0.86563120
      X(4) = -0.75540441
      X(5) = -0.61787624
      X(6) = -0.45801678
      X(7) = -0.28160355
      X(8) = -0.09501251
      X(9) = -X(8)
      X(10) = -X(7)
      X(11) = -X(6)
      X(12) = -X(5)
      X(13) = -X(4)
      X(14) = -X(3)
      X(15) = -X(2)
      X(16) = -X(1)
C
      do i=1,16
         Y(i) = X(i)
      end do
C
      B = Ro/GAP
      TOTAL = 0.0
C
      do i=1,16
         do j=1,16
           C =((SQ**2.0)*((X(i)**2.0)+(Y(j)**2.0)))**0.5/(2.0*GAP)
           F = 1.0 - (1.0 + C**2.0 - B**2.0) /
     *     ((C**4.0 + 2*(C**2.0)*(1.0 - B**2.0)+
     *     (1 + B**2.0)**2.0)**0.5)
           TOTAL = TOTAL + W(i)*W(j)*F
         end do
      end do
C
      FACTOR = TOTAL/8.0
C
C     function return
C
      return
C
      end function FACTOR
```

APPENDIX 2 – The Kevlar®/PBI Fabric Model

```
C------------------------------------------------------------------
      program Copper_Disk_Fabric
C
C      This program calculates the thermal response
C      of a copper calorimeter that is subject to a
C      convective and radiative heat flux. Losses from the
C      calorimeter are also accounted for.
C
C      The heat fluxes are calculated across an air gap that
C      has the temperatures measured exp. for a Kevlar/PBI
C      fabric sample as the boundary conditions for the 'bottom
C      plate'.
C      These boundary conditions are implemented using 5 elements
C      in this program.
C
C      Define Variables
       implicit none
       REAL Qrad, Qconv, Qloss, Qnet, DELTA, TIME, TEMP, Cop_DENS,
     * Tamb, SPHT, GAP, R0, Cop_Mass, A0, T_RISE, Texp, THICK, E0,
     * Qr10, SQ1, E1, A1, T1, RES1, F10, T2, A2big, A2, RES2,
     * SQ2, E2, Qr20, F20, T3, A3big, A3, RES3, SQ3, E3, Qr30,
     * F30, T4, A4big, A4, RES4, SQ4, E4, Qr40, F40,
     * T5, A5big, A5, RES5, SQ5, E5, Qr50, F50,
     * Tbot, Ttop, Tair, BETA, KIN_VIS, THER_DIFF, THER_COND, g,
     * RAY, AA, BB, Nu, CONV, FACTOR, F12to0, F123to0, F1234to0,
     * F12345to0,
     * RAD, CONVEC, LOSS, DUMMY, STOLL_CRIT, STOLL_TIME, RATIO,
     * RATIO2
C
C      Qrad = radiation heat flux [W]
C      RAD = radiation heat flux [kW/m2]
C      Qconv = convective heat flux [W]
C      CONVEC = convective heat flux [kW/m2]
C      CONV = Convection coefficient [W/m2K]
C      Qloss = heat loss from disk [W]
C      LOSS = heat loss from disk [kW/m2]
C      Qnet = net heat transfer rate to disk [W]
C      DELTA = time step for quasi-steady state idealogy [s]
C      Texp = exposure time [s]
C      TIME = real (current) time for exposure [s]
C      TEMP = temperature of the copper disk [K]
C      Cop_DENS = density of copper [kg/m3]
C      SPHT = specific heat of copper [J/kg*K]
C      THICK = thickness of copper disk [m]
C      Cop_Mass = mass of copper disk [kg]
C      A0 = area of copper disk sensor [m^2]
C      R0 = radius of copper disk sensor [m]
C      E0 = emissivity of copper disk sensor
C      Cop_Mass = mass of copper disk sensor [kg]
C      FACTOR = needed for subroutine of view factor
C      STOLL_TIME = time to reach Stoll Criterion
```

```
C       STOLL_CRIT = Stoll criterion temperature @ TIME
C       DUMMY = variable used for logical test (loop)
C       GAP = size of the air gap [m]
C       Tamb = ambient temperature of the surroundings [K]
C       SQ'X' = size of the element number 'X'(square)
C       F'X'0 = view factor from element 'X' to disk
C       A'X' = area of element 'X'
C       E'X' = emissivity of element 'X'
C       RES'X' = resistance to thermal radiation of element 'X'
C       T'X' = temperature of element 'X' @ TIME (current)
C       Qr'X'0 = radiation heat flux from element 'X' to disk [W]
C       RATIO = used to transition from 4 elements to 5 elements
C               for the 'localized convection treatment
C       RATIO2 = used to transition from 5 elements to 6 elements
C               for the 'localized convection treatment
C       Tair = temperature of the air in the gap [K]
C       BETA = variable for calculating Rayleigh number [1/K]
C       KIN_VIS = kinematic viscosity of the air in gap
C       THER_DIFF = thermal diffusivity of the air in gap
C       THER_COND = thermal conductivity of the air in gap
C       g = acceleration due to gravity [m/s2]
C       RAY = Rayleigh number
C       AA and BB = are arguments within the Rayleigh equation
C       Nu = Nusselt number
C       T_RISE = calculated temp rise of disk for time step [K]
C
C       Open output file
        open(unit=10,file="copper.txt",status="unknown")
C
        TIME = 0.0
        STOLL_TIME = 0.0
        STOLL_CRIT = 0.0
        DUMMY = 0.0
        Texp = 10.0
        DELTA = 0.01
        GAP = 0.00635
        Tamb = 300.0
        TEMP = 300.0
        THICK = 0.0016
        Cop_DENS = 8954
        R0 = 0.02
        A0 = 3.1415926*R0**2.0
        E0 = 0.95
        Cop_Mass = Cop_DENS*A0*THICK
C
C       Set element sizes.
C       Find the view factors for the elements using subrout FACTOR
C       Also, solve for a few of the elements' variables that do not
C       change with time.
C
C       Element 1
C
        SQ1 = 0.00762
        F10 = FACTOR(GAP, R0, SQ1)
        A1 = SQ1**2.0
```

```
      E1 = 0.95
      RES1 = ((1.0-E1)/(A1*E1))+(1.0/(A1*F10))+((1.0-E0)/(A0*E0))
C
C     Element 2
C
      SQ2 = 0.0254
      F12to0 = FACTOR(GAP, R0, SQ2)
      A2big = SQ2**2.0
      A2 = A2big - A1
      F20 = ((F12to0*A2big)-(F10*A1))/A2
      E2 = 0.95
      RES2 = ((1.0-E2)/(A2*E2))+(1.0/(A2*F20))+((1.0-E0)/(A0*E0))
C
C     Element 3
C
      SQ3 = 0.0381
      F123to0 = FACTOR(GAP, R0, SQ3)
      A3big = SQ3**2.0
      A3 = A3big - A2big
      F30 = ((F123to0*A3big)-(F12to0*A2big))/A3
      E3 = 0.95
      RES3 = ((1.0-E3)/(A3*E3))+(1.0/(A3*F30))+((1.0-E0)/(A0*E0))
C
C     Element 4
C
      SQ4 = 0.05842
      F1234to0 = FACTOR(GAP, R0, SQ4)
      A4big = SQ4**2.0
      A4 = A4big - A3big
      F40 = ((F1234to0*A4big)-(F123to0*A3big))/A4
      E4 = 0.95
      RES4 = ((1.0-E4)/(A4*E4))+(1.0/(A4*F40))+((1.0-E0)/(A0*E0))
C
C     Element 5
C
      SQ5 = 0.15
      F12345to0 = FACTOR(GAP, R0, SQ5)
      A5big = SQ5**2.0
      A5 = A5big - A4big
      F50 = ((F12345to0*A5big)-(F1234to0*A4big))/A5
      E5 = 0.95
      RES5 = ((1.0-E5)/(A5*E5))+(1.0/(A5*F50))+((1.0-E0)/(A0*E0))
C
C     Loop program for 10 second exposure
C
      Do while (TIME.LT.Texp)
C
C     Check to see if Stoll criterion temp has been exceeded
C
      STOLL_CRIT = (8.871465*TIME**0.2905449) + Tamb
            IF (DUMMY.EQ.0.0) THEN
               IF (TEMP.GT.STOLL_CRIT) THEN
                  STOLL_TIME = TIME - DELTA
                  DUMMY = 1.0
               END IF
```

```
            END IF
C     Calculate the radiative heat transfer (W)
C
C     Radiation from Element 1 to Sensor
C
      T1 = 0.000345*TIME**6.0 - 0.058541*TIME**5.0
     *     + 1.516127*TIME**4.0
     *     - 15.002625*TIME**3.0 + 55.591655*TIME**2.0
     *     + 31.965361*TIME + 314.66620
      IF (T1.LT.300.0)THEN
               T1 = 300.1
      END IF
      Qr10 = 5.67E-08*(T1**4.0-TEMP**4.0)/RES1
C
C     Radiation from Element 2 to Sensor
C
      T2 = -0.002089*TIME**6.0 + 0.023761*TIME**5.0
     *      + 0.479060*TIME**4.0
     *      - 9.217917*TIME**3.0 + 43.902354*TIME**2.0
     *      + 27.315820*TIME + 311.093450
      IF (T2.LT.300.0)THEN
               T2 = 300.1
      END IF
      Qr20 = 5.67E-08*(T2**4.0-TEMP**4.0)/RES2
C
C     Radiation from Element 3 to Sensor
C
      T3 = -0.004591*TIME**6.0 + 0.116970*TIME**5.0
     *      - 0.833308*TIME**4.0
     *      - 0.674475*TIME**3.0 + 20.087094*TIME**2.0
     *      + 38.742460*TIME + 310.137574
      IF (T3.LT.300.0)THEN
               T3 = 300.1
      END IF
      Qr30 = 5.67E-08*(T3**4.0-TEMP**4.0)/RES3
C
C     Radiation from Element 4 to Sensor
C
      T4 = -0.00197*TIME**6.0 + 0.05118*TIME**5.0
     *      - 0.45233*TIME**4.0
     *      + 1.38204*TIME**3.0 - 0.08867*TIME**2.0
     *      + 26.96393*TIME + 302.62067
      IF (T4.LT.300.0)THEN
               T4 = 300.1
      END IF
      Qr40 = 5.67E-08*(T4**4.0-TEMP**4.0)/RES4
C
C     Radiation from Element 5 to Sensor
C
      T5 = -0.000316*TIME**6.0 + 0.006985*TIME**5.0
     *      - 0.027440*TIME**4.0
     *      - 0.288770*TIME**3.0 + 1.718788*TIME**2.0
     *      + 5.258292*TIME + 299.135645
      IF (T5.LT.300.0)THEN
               T5 = 300.1
```

```
      END IF
      Qr50 = 5.67E-08*(T5**4.0-TEMP**4.0)/RES5
C
      Qrad = Qr10 + Qr20 + Qr30 + Qr40 + Qr50
      RAD = Qrad / (A0*1000.0)
C
C     Calculate the convective heat transfer (W)
C
C         Determine the 'area' of convection
C
          IF (GAP.LT.0.0061)THEN
              RATIO = 1.0 - ((.0061 - GAP)/0.0061)
              Tbot = (T1*A1 + T2*A2 + T3*A3
     *        + RATIO*T4*A4)/((A4big - A3big)*RATIO + A3big)
              Ttop = (TEMP*A0 + Tamb*((A4big - A3big)*RATIO
     *        + A3big - A0))/((A4big - A3big)*RATIO + A3big)
          ELSE IF (GAP.LT.0.0091)THEN
              RATIO2 = 1.0 - ((.0091 - GAP)/0.003)
              Tbot = (T1*A1 + T2*A2 + T3*A3 + T4*A4
     *        + RATIO2*T5*A5)/((A5big - A4big)*RATIO2 + A4big)
              Ttop = (TEMP*A0 + Tamb*((A5big - A4big)*RATIO2
     *        + A4big - A0))/((A5big - A4big)*RATIO2 + A4big)
          ELSE
              Tbot = (T1*A1 + T2*A2 + T3*A3 + T4*A4 + T5*A5)
     *            /A5big
              Ttop = (TEMP*A0 + Tamb*(A5big - A0))/A5big
          END IF
C
C    Now finish the calculation for convection using correlation
C
      Tair = (Tbot + Ttop)/2.0
      BETA = 1.0 / Tair
      KIN_VIS = (0.00007*Tair**2.0 + 0.0607*Tair
     *        - 9.0061)/1000000.0
      THER_DIFF = (0.00006*Tair**2.0 + 0.1266*Tair
     *        - 22.005)/1000000.0
      THER_COND = (-0.0000266*Tair**2.0 + 0.0914735*Tair +
     *          1.4192599)/1000.0
      g = 9.81
      RAY = g*BETA*(Tbot-Ttop)*GAP**3.0/(KIN_VIS*THER_DIFF)
      AA = 1.0 - 1708.0 / RAY
      IF (AA.LT.0.0) THEN
          AA = 0.0
      END IF
      BB = ((RAY/5830.0)**(1.0/3.0))-1.0
      IF (BB.LT.0.0) THEN
          BB = 0.0
      END IF
      Nu = 1.0 + 1.44 * AA + BB
      CONV = THER_COND * Nu / GAP
      Qconv = CONV * A0 * (Tbot - TEMP)
      CONVEC = Qconv / (A0*1000.0)
C
C     Calculate the heat losses (W)
C
```

```
          Qloss = 25.0*A0*(TEMP-Tamb)
          LOSS = Qloss / (A0*1000.0)
C
C         Calculate the net heat transfer (W)
C
          Qnet = Qrad + Qconv - Qloss
C
C         Calculate temperature rise of copper disk sensor
C         assuming quasi-steady state lumped capacitance.
C
          SPHT = 0.000000135*TEMP**3.0 - 0.000286776*TEMP**2.0
     *    + 0.27996649*TEMP + 322.83
          T_RISE = Qnet*DELTA/(Cop_Mass*SPHT)
          TEMP = TEMP + T_RISE
C
C         Increment to the next time step
C
          TIME = TIME + DELTA
C
C         Output desired variables
C
          write(10,*) TIME, TEMP, RAD, CONVEC, LOSS
          Print*, STOLL_TIME
C
          end do
C
C         This is the end of the main loop.
C
C
C
          END
C
C         End of main program
C
C-----------------------------------------------------------------
C
C         FACTOR subroutine to calculate view factor is identical to
C         the FACTOR subroutine used for the shim model shown in
C         Appendix 1.
C
```